ANALYSIS, DESIGN AND OPTIMIZATION OF OFFSHORE POWER SYSTEM NETWORK

PARIKSHIT YADAV

NATIONAL UNIVERSITY OF SINGAPORE

2013

ANALYSIS, DESIGN AND OPTIMIZATION OF OFFSHORE POWER SYSTEM NETWORK

PARIKSHIT YADAV
(B.Tech (Hons.), MNIT, Jaipur, INDIA)

A THESIS SUBMITTED FOR THE DEGREE OF

DOCTOR OF PHILOSOPHY

DEPARTMENT OF ELECTRICAL AND COMPUTER ENGINEERING

NATIONAL UNIVERSITY OF SINGAPORE

2013

DECLARATION

I hereby declare that this thesis is my original work and it has been written by me in its entirety. I have duly acknowledged all the sources of information which have been used in the thesis.

This thesis has also not been submitted for any degree in any university previously.

PARIKSHIT YADAV
28th March, 2013

CONTENTS

SUMMARY

The rise in greenhouse gas emissions has forced the industries to rethink and change their operating philosophy and strategies to reduce the impact on the environment by adopting greener practices and technologies. International Maritime Organization (IMO) has envisioned eliminating or reducing to the barest minimum, all the adverse environmental impacts from the ships. The stringent emission legislation and the price of fuel oil has increased the demand for safer, secure and energy efficient marine vessels. The main objective of this thesis is to find solutions, which can significantly reduce emissions, enhance the efficiency and safety of marine vessels. In this thesis, Keppel's B280 Semi-submersible oil rig platform is considered as the case study of the marine vessel.

Optimization plays an important role in finding solutions to achieve "SAFE, SECURE AND EFFICIENT SHIPPING ON CLEANER OCEANS". The problem of reducing emissions, enhancing the efficiency and safety of marine vessels is formulated as non-convex optimization problems. The formulated non-convex optimization problems are hard to solve using iterative numerical optimization methods such as Newton's method, Sequential Quadratic Programming (SQP), Gradient descent etc. The iterative numerical optimization methods are very fast and need less computational time, however, these methods are highly sensitive to starting points and frequently converge to a local optimum solution or diverge altogether. Metaheuristic algorithms eradicate some of the afore-mentioned difficulties and are quickly replacing the classical methods in solving practical problems. During the last decades, several metaheuristic algorithms have been proposed. However, the performance and efficiency of most of the metaheuristic algorithms depend on the extent of balance between diversification and intensification during the course of the search. Proper balance between these two characteristics results in enhanced performance

of the algorithm. In order to overcome this problem, a robust and self-tuned algorithm must be developed which is almost-parameter-free search algorithm and converges very quickly, and needs lower iterations.

In this thesis, a new variant of the Harmony Search (HS) algorithm is proposed that maintains a proper balance between diversification and intensification throughout the search process by automatically selecting the proper pitch adjustment strategy based on its Harmony Memory. The performance of the proposed Intelligent Tuned Harmony Search (ITHS) algorithm is investigated and compared with eight state-of-the-art HS variants over 17 benchmark functions. Furthermore, to investigate the robustness of the proposed algorithm at higher dimensions, a scalability study is also performed. Finally, the numerical results obtained reflect the superiority of the proposed ITHS algorithm in terms of accuracy, convergence speed, and robustness when compared with other state-of-the-art HS variants. The developed optimization problem is used to find the solutions of different formulated optimization problems.

The next objective is to develop solutions to reduce emissions, enhance efficiency and safety of marine vessels. To exploit the opportunity to save fuel and maintenance costs, the multiple power generating components must be operated as optimal as possible for every load demand. The first essential task for optimal scheduling of the generators task is to develop an accurate model of the specific fuel consumption curve. In this thesis, the specific fuel consumption curve is modeled using cubic spline interpolation. The specific fuel consumption curve is used to formulate the constrained optimization problem. The objective of the formulated optimization problem is to optimally schedule the diesel generators to ensure minimum fuel consumption for different loading conditions. The formulated optimization problem is solved using ITHS algorithm.

The bulk of the power consumption of the marine vessel is dependent on the thruster propulsion load. Therefore, the power demanded for propulsion must be optimized to improve the efficiency of the vessel. The power demanded by the propulsion system is mainly governed by the Dynamic Positioning (DP) system. The main purpose of a positioning control system is to make sure that a vessel maintains a specified position and compass heading, unaffected by the disturbances acting on it. In DP system, the thrust allocator is used to distribute the desired generalized forces computed by the motion controller among the thrusters. However, in order to ensure safe operation of the vessel despite the thruster failure, the vessel is equipped with redundant thruster configuration and therefore is over-actuated as per the guidelines of **IMO** (International Maritime Organization) **MSC** (Maritime Safety Committee) Circ.645 and **IMCA** (International Marine Contractors Association) M 103. For over-actuated vessels, the solution to the thrust allocation problem can be found by formulating it as an optimization problem. In this thesis, the over-actuated control allocation problem is solved with an objective to minimize power consumption. The developed ITHS algorithm is used for solving the non-convex thrust allocation problem. The optimal thruster allocation using ITHS reduces power consumption of the rig as compared to other optimization algorithms.

The power consumed by the marine vessel depends on the thrust generated by the thrusters and the efficiency of the electrical propulsion system controlling the thrusters. However, most of the optimization based approaches only focus on minimizing the power demanded by the thrusters and ignore the efficiency of the electrical propulsion system. However, during lower demand (calm weather conditions), if all thrusters are operating simultaneously then the electrical propulsion system of the thrusters are lightly loaded and operate in inefficient regions. Therefore, one should distribute the maximum load amongst some of the thrusters while keeping others idle. In this thesis, an energy-efficient thrust

allocation approach is proposed and formulated as an optimization problem, with an objective to minimize the total power consumption by ensuring that the electrical propulsion system operates in the efficient region. The optimal thruster allocation using ITHS reduces the power consumption of the rig as compared to other optimization algorithms. Furthermore, the total power consumption for energy-efficient thrust allocation approach is lower as compared to conventional thrust allocation approach for all the considered algorithms. It proves that the proposed approach is effective in reducing the power consumption of the semi-submersible oil rig platform.

Another important aspect that is of concern is the harmonic distortions in marine vessels. Harmonic distortion in the electrical power system is an important factor for safe and reliable operation of the marine vessels, as it adversely affects the electric and electronic sub-systems. Therefore, marine regulating bodies have imposed stringent limits on voltage total harmonic distortion and individual harmonic distortion at the point of common coupling. In this thesis, a Voltage Harmonic compliant Energy-Efficient thrust allocation problem is formulated to enhance the efficiency and also ensure that the electric propulsion system meets the harmonic limits as per marine standards. The formulated optimization problem is solved using the ITHS algorithm. After meeting the harmonic limits, the total power consumption for the oil rig platform using ITHS algorithm is lower compared to other optimization algorithms. The major advantage of the proposed approaches is that, there is no need of additional hardware integration and the proposed approaches can be integrated in the existing system by just changing the algorithms of the DP software. Therefore, the proposed solutions can be applied to both new and old vessels.

ACKNOWLEDGEMENTS

LIST OF FIGURES

LIST OF TABLES

CHAPTER 1. INTRODUCTION

1.1   Background

Shipping plays a very important and vital role in today's global society. Seaborne transport services the global demand for food, energy, raw materials and finished products. Apart from trade and transportation, various other tasks are performed by special ships. These include offshore service activities, infrastructure development (such as cable laying, pipe laying and dredging), fishing, exploration and research, towing services, etc [1]. Therefore, shipping is truly the lynchpin of the global economy. Due to close connection to trade, international shipping also plays a vital role in facilitation of trade as the most cost-effective means of transport.

Shipping is responsible for transporting almost 90% of world trade which has doubled in the past 25 years and corresponds to 3.3% of the global CO_2 emissions. International Maritime Organization (IMO) projects that CO_2 emissions from international maritime activity are expected to rise by10-26% by 2020 and by 126-218 % by 2050 [1, 2]. The demand for global shipping brings with it a host of environmental related problems and therefore, shipping emissions have been recognized as a growing problem for environmental policy makers [3]. Another important concern for shipping industry is safe and reliable operation of the marine vessels. During, the last few decades, the concept of diesel-electric propulsion has emerged as a key technology in providing **"SAFE, SECURE AND EFFICIENT SHIPPING ON CLEANER OCEANS".**

Diesel-electric propulsion decouples the speed of the diesel engine from that of the propeller and offers the possibility to operate the diesel engines at their optimum operational point, resulting in lower emissions and lower fuel consumption as compared to conventional diesel-engine based direct drive system. In addition, diesel-electric propulsion

1

provides other benefits, such as increased safety, survivability, maneuverability, precise and smooth speed control, reduced machinery space, low operational and maintenance costs, increased design flexibility and capability to reduce noise [4].

1.2   Diesel Electric Propulsion System

The diesel-electric propulsion system is powered via an on-board power pool consisting typically of 6-8 diesel generators. In a diesel-electric propulsion system, the diesel engines are normally medium to high-speed engines. The diesel generators are connected to the switchboard to form the high voltage busbar. The switchboard is usually distributed or split in two, three, or four sections, in order to obtain the redundancy requirements of the vessel [5, 6]. As per the application guidelines from **NORSOK** (Norsk Sokkels Konkuranseposisjon), the switchboard voltage levels for the main distribution system are as follows :

- 11kV: Medium voltage generation and distribution. Should be used when total installed generator capacity exceeds 20MW. Should be used for motors from 400kW and above.

- 6.6kV: Medium voltage generation and distribution. Should be used when total installed generator capacity is between 4-20MW. Should be used for motors from 300kW and above.

- 690V: Low voltage generation and distribution. Should be used when total installed generator capacity is below 4MW. Should be used for consumers below 400kW and as primary voltage for converters for drilling motors.

- For utility distribution lower voltage is used, e.g. 400/230V.

The electric power from the switchboard is transferred into different forms of energy. The majority of the power onboard is used for propulsion. The electrical motors are used to convert electrical energy into mechanical energy used by propellers. Induction motors are

the most commonly used for propulsion. However, synchronous motors may also be used for high power applications. The thrust produced is controlled either by constant speed and controllable pitch propeller design, variable speed fixed pitch propeller design, or in rare cases with a combination of speed and pitch control. Variable speed fixed pitch propeller design has significantly simpler mechanical underwater construction with reduced low-thrust losses compared to controllable pitch propeller [6]. In case of variable speed fixed pitch propeller design, the thrust is controlled by varying the speed of the propeller using variable frequency drive.

1.3   Marine Control Structure

Marine control system has been of special interest since last century. The various complexities and coupled behavior demands for automatic control system for marine vessels. Automatic control system is widely used for controlling the heading, heave control, way-point tracking control, fin and rudder-roll damping, dynamic positioning (DP), thruster assisted position mooring (PM) etc. [4].

Increasing industrial and social development on a global scale has led to unprecedented demand for energy, the vast majority of which continues to be met through the exploitation of the world's finite reserves of fossil fuels. This motivates exploration and exploitation at continuously increasing water depths. For deeper depths conventional mooring systems, like a jack-up barge or an anchored rig, structure cannot be used rather DP system and thruster assisted position mooring system are used to keep the marine vessel in the fixed position. DP system automatically controls the position and heading of the marine vessel subjected to environmental and external forces, using large rating azimuth thrusters fitted at its pontoon level [7, 8]. DP and PM systems are used on different types of vessels, ranging from shuttle tankers, semi-submersibles, offshore service vessels, construction

vessels and cruise vessels, etc. [9]. The block diagram of a control system of a typical marine vessel is shown in Fig.1.1.
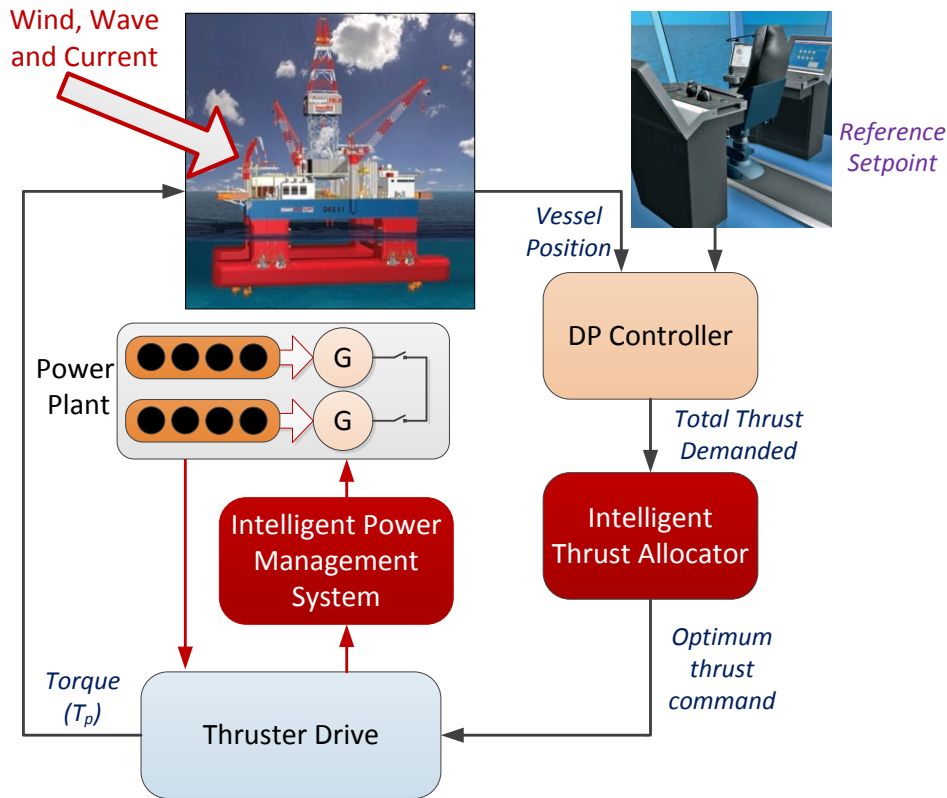
Fig.1.1. Overview of an automatic ship control system with a high level controller.

The reference set point may be either to keep the vessel in the fixed position with a fixed heading or follow a particular trajectory (Tracking control). The vessel is subjected to different environmental disturbances and these disturbances constitute of disturbances due to waves, current and wind. The environmental disturbances deviate the vessel from the desired set point. The vessels position is measured or estimated using different kinds of sensors and algorithms and sent to the DP controller. The DP controller produces desired surge force (F_X) , sway force (F_Y) and yaw moment (M_Z) required to keep the vessel at the desired set point. The thrust allocator needs to determine the magnitude and direction of the thrust required for each thruster to create a force and moment equilibrium. However,

there exist multiple solutions for the thrust-allocation problem because, the marine vessels are over-actuated as per the guidelines of guidelines of IMO MSC Circ.645 and IMCA M 103 [10, 11]. Therefore, the solution to the thrust allocation problem can be found by formulating it as an optimization problem, with an objective to minimize power consumption, drag, tear/wear and other costs related the control variables, subjected to the constraints such as thruster position constraints and other operational constraints [12, 13]. The solution of the thrust allocation algorithm is fed as reference input to the thruster drives. The thruster drive ensures that the actuators produce the desired thrust. The power required by the thruster drives is demanded from the marine power plant. A typical marine vessel is powered via an on-board power pool consisting typically of 6-8 diesel generators. Therefore, power management system is required for optimal scheduling of the generators. The thrust allocator and power management system play and significant role in the control of the marine vessel.

1.4   Case Study of the Marine Vessel

In this thesis, Keppel's B280 Semi-submersible oil rig platform is considered as the case study of the marine vessel. The oil rig is powered by a pool of eight Wärtsilä 16V26A diesel generators each of 4960 kW power rating. The eight generators are connected in ring configuration to form the 11 kV busbar. The 11 kV busbar supplies the load to the eight thruster motors, located at the pontoon level of the oil rig platform and other auxiliary loads [14]. Fig. 1.2 shows the schematic of the main power installations in a Keppel B280 semi-submersible oil rig platform with electrical propulsion in a Single Line Diagram (SLD) [15]. The vessel is a four column stabilized semi-submersible oil rig platform. Four rectangular shaped stability columns, and two pontoons provide the buoyancy. The thruster layout of the oil rig platform is shown in Fig. 1.3.
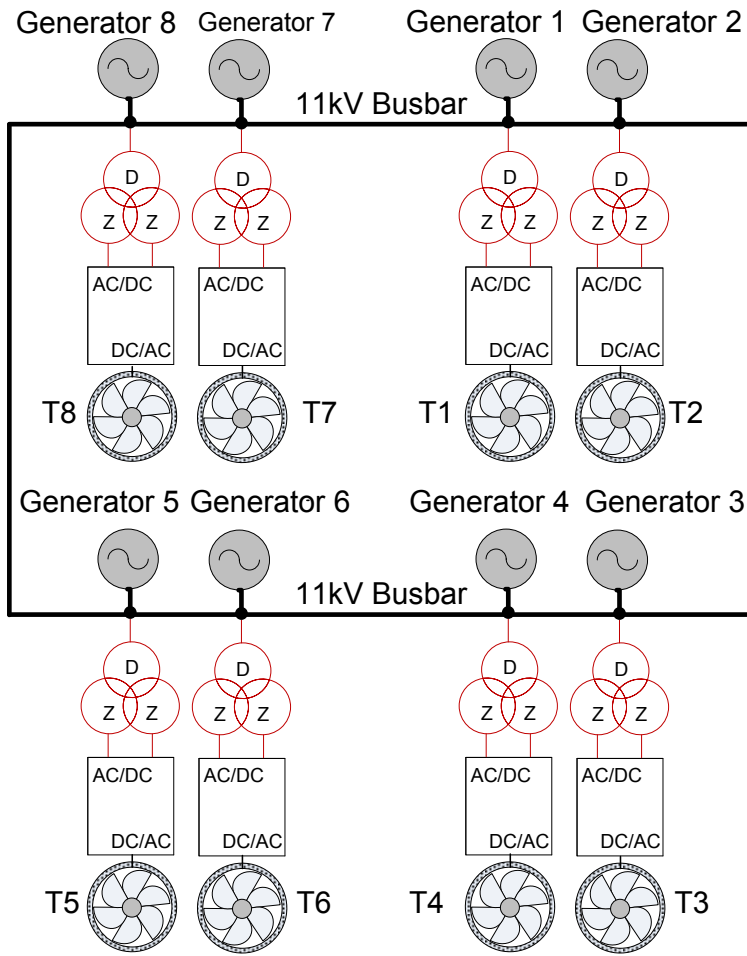
Fig. 1.2. SLD of the electrical propulsion system of the Keppel's B280
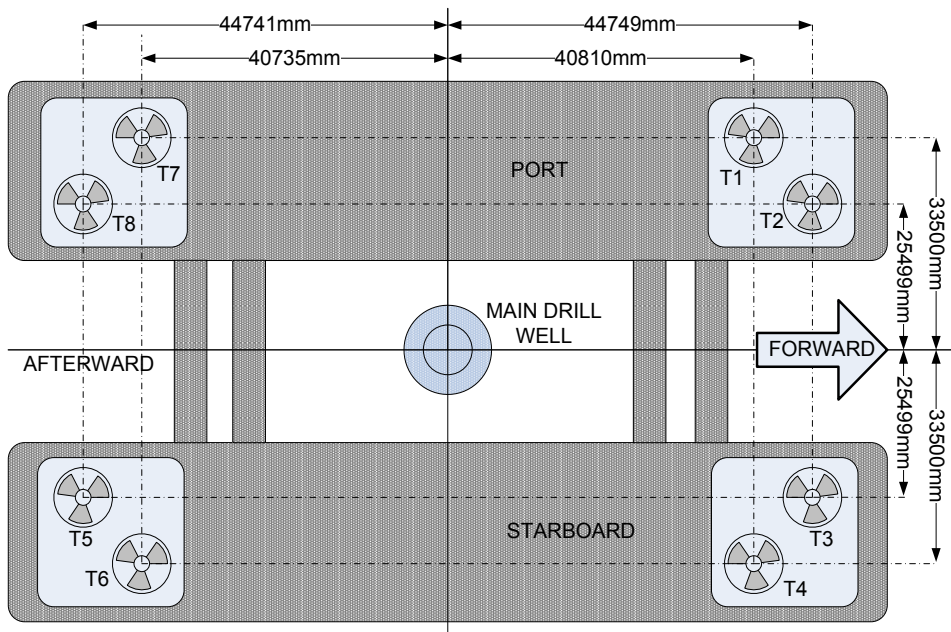
Fig. 1.3. Thruster layout of Keppel's B280 and corresponding dimensions

1.5   Motivation and Problem Statement

Industrial Revolution led to the use of machinery and factories for mass production with a sole objective to enhance the productivity and profits. However, on the contrary industrial revolution also led to multifold increase in the greenhouse gas emissions. The rise in greenhouse gas emissions has forced the industries to rethink and change their operating philosophy and strategies to reduce the impact on the environment by adopting greener practices and technologies. IMO has envisioned eliminating or reducing to the barest minimum, all the adverse environmental impacts from the ships. In addition to the strong environmental concerns, the sky-rocketing fuel prices have changed the competitive landscape. Over, the last ten years, the price of fuel oil has increased by six times and in Singapore, the world's largest bunkering port, the price of fuel oil has increased by 45 % in the last two years [16]. The price of fuel now represents around 50% or more of vessel operating costs. The stringent emission legislation and the price of fuel oil has increased the demand for safer, secure and energy efficient marine vessels. In this thesis, some of the issues identified have been related to the marine control structure which can significantly reduce the emissions, enhance the efficiency and safety of marine vessels.

> **Issue 1: Optimal Scheduling of the Diesel Generators in Semi-submersible Oil Rig Platforms**
>
> To exploit the opportunity to save fuel and maintenance costs, the multiple power generating components must be operated as optimal as possible for every load demand. The oil rig is powered by a pool of eight Wärtsilä 16V26A diesel generators each of 4960 kW power rating. The load requirements of the rig are governed by the disturbances, which are stochastic in nature and most of the time the demanded load is less than 50% of the full load [17, 18]. Therefore, generators

operate in the inefficient zone if all the generators are switched ON.

The optimum generation scheduling of available generators to minimize the total fuel consumption while satisfying the load demand and operational constraints plays an important role in improving the power density and efficiency of the oil rig. Over the past few years, a number of approaches have been developed, to improve the efficiency and reduce fuel consumption of marine vessels [17-22].

The fuel consumption of diesel generators is generally governed by the specific fuel consumption curves, which characteristically don't differ for different manufacturers [23]. The key feature for this discourse is that lightly loaded generators are much less efficient than more heavily loaded units. Moreover, the increase in specific fuel consumption with a decrease in load tends to be much larger below about 50% load than above 50% load [23-25]. Therefore, one should distribute the maximum load for some of generators and keep others idle.

The first essential task for optimal scheduling of the generators task is to develop an accurate model of the specific fuel consumption curve. The challenge is to use the nonlinear specific fuel consumption curve for formulation of the optimization problem with an objective to minimize fuel consumption of the diesel generators under different loading conditions. The nonlinear specific fuel consumption curve makes the optimization problem more complex with multiple minima and therefore there is a need of robust optimization technique.

- ➤ **Issue 2: Development of Optimal Thrust Allocation for Semi-submersible Oil Rig Platforms**

Increasing industrial and social developments on a global scale has led to unprecedented demand for energy, the vast majority of which continues to be met through the exploitation of the world's finite reserves of fossil fuels. This motivates exploration and exploitation at continuously increasing water depths. However, offshore drilling units for deeper water depths such as semi-submersible drilling rig face unique challenge. During drilling, when the drill pipe casing is connected to the oil well, if the rig is displaced due to environmental disturbances, the drill case can collapse or fracture, resulting in oil spills and therefore huge financial losses. Since the depth of the seabed is more than 1,000 ft, conventional mooring systems, like a jack-up barge or an anchored rig, structure cannot be used rather DP system and thruster assisted position mooring system are used to keep the oil rig platform at the fixed position. DP system automatically controls the position and heading of the oil rig subjected to environmental and external forces, using large rating azimuth thrusters fitted at its pontoon level [7, 8].

In this thesis, a semi-submersible oil rig platform equipped with eight azimuth thrusters is considered as a case study for marine vessels. For vessels that are operating to DP class 2 or 3 standards, the vessel should be left with sufficient power and thrusters to maintain position after worst case failure. Therefore, the semi-submersible oil rig is equipped with redundant thruster configuration and is over-actuated as per the guidelines of IMO MSC Circ.645 and IMCA M 103 [10, 11]. Azimuth thrusters fitted at oil rig platform's pontoon level can produce forces in different directions leading to an over-actuated control problem that can be formulated as an optimization problem, in order to minimize power consumption,

drag, tear/wear and other costs related to the use of control, subject to constraints such as actuator position limitations [12, 13]. The thrust allocator tries to minimize the power consumption and takes forbidden/spoil zones into account. Forbidden/spoil zones are used to avoid thruster-thruster interactions, which reduce the efficiency of the thrusters [26]. The control allocation problem formulated for oil rig equipped with azimuth thrusters is a *non-convex optimization problem* due to thrust direction constraints on azimuth thrusters [13].

In general, a non-convex constrained optimization problem is hard to solve using state-of-the-art iterative numerical optimization. Many methods, such as the linear or quadratic programming have been applied to solve thruster allocation problem [9, 13, 27-35]. Classical optimization methods like sequential quadratic programming (SQP) have proved to be feasible method to solve non-convex thruster allocation problem, but these methods are highly sensitive to starting points and frequently converge to local optimum solution or diverge altogether. Therefore, conventional methods fail to find the optimum solution for the thrust allocation problem and often get trapped in local minima. Therefore, the challenge is to develop optimal thrust allocation methodology to reduce fuel consumption of the oil rig platform and find the solution of the formulated optimization problem using a robust optimization technique.

➢ **Issue 3: Development of an Energy-Efficient Thrust allocation for Semi-submersible Oil Rig Platforms**

The power consumed by the oil rig platform depends on the thrust generated by the azimuth thrusters and the efficiency of the electrical propulsion system controlling the azimuth thruster. However, most of the optimization based approaches only focus on minimizing the power demanded by the thrusters and ignore the efficiency of the electrical propulsion system. The thrust generated by an azimuth thruster is controlled by an electrical propulsion system and the efficiency of the lightly loaded electrical propulsion system is much less, than that of a more heavily loaded system. The load demanded during station keeping depends on the total environmental loads acting on the platform. During lower demand (calm weather conditions), if all the azimuth thrusters are operating then the electrical propulsion system of the azimuth thrusters are lightly loaded and operate in less efficient region. Therefore, one would distribute the maximum load for some of the azimuth thrusters and keep others idle. However, in conventional thrust allocation approach, since the efficiency of the electrical propulsion system is ignored, the thrusters may even operate in the inefficient region during lower load demand and increase the total power consumption of the oil rig platform. Since, efficiency greatly influences the power consumption of the system. Therefore, energy efficient systems have potential to reduce the power consumption of the system and have been widely used in different areas [36-43]. The challenge is to develop energy-efficient thrust allocation approach with an objective to minimize the total power consumption by ensuring that the electrical propulsion system operates in the efficient region and is subjected to force and moment constraints to ensure fixed position of the oil rig platform.

> **Issue 4: Meeting Harmonic Limits in the Semi-submersible Oil Rig Platforms**

Due to rapid deployment of power electronic systems, in marine vessels for propulsion, power distribution, auxiliaries, sonar, and radar [44], the harmonic distortion of the electrical power system tends to increase and power quality deteriorates. Harmonic distortion in the electrical power system is an important factor for safe and reliable operation of the marine vessels, as it adversely affects the electric and electronic subsystems. Any failure or malfunction of sub-systems such as propulsion or navigation systems can result in an accident at sea or close inshore with serious consequences [45-47]. Therefore, marine regulating bodies have imposed stringent limits on voltage total harmonic distortion and individual harmonic distortion at the point of common coupling.

Several harmonic mitigation techniques have been proposed for high power industry applications, to mitigate the harmonic current and voltage distortion introduced by variable speed drives [48, 49]. However, major high-power drive manufacturers around the world are increasingly using multi-pulse rectifier systems in their drives for harmonic mitigation [50-52]. Multi-pulse rectifier system has several advantages, such as less complexity, high reliability, lower volume, and minimal resonance interaction problem within the power distribution system [53]. In this thesis, a DP class 2 semi-submersible oil rig platform equipped with 8 azimuth thrusters is considered as a case study of marine vessel. Fig. 1.2 shows the schematic of the main power installations in a Keppel B280 semi-submersible oil rig platform with electrical propulsion in a Single Line Diagram (SLD) [15, 54]. Each thruster system uses a 12-pulse rectifier system, powered by a phase shifting transformer with two secondary windings. In the 12-pulse rectifier system, the relative phase shift of 30° in the two secondary windings with respect to primary

winding is achieved either by the vector group Dd11.75d0.75 or Dd11.25d0.275 [55].The vector group Dd11.75d0.75 produces a phase shift of $-7.5°, +22.5°$ and Dd11.25d0.25 produces a phase shift of $-22.5° + 7.5°$. As shown in Fig.1.2, the thruster system T1, T3, T5, and T7 use phase-shifting transformer of vector group Dd11.75d0.75 and thruster system T2, T4, T6, and T8 use phase-shifting transformer of vector group Dd11.25d0.25. Therefore, the primary of the each transformer has harmonics of the order of $12n \pm 1$. Furthermore, the two vector groups Dd11.75d0.75 and Dd11.25d0.25 have a relative phase shift of 15° and forms a quasi-24 pulse rectifier system at 11kV busbar. The harmonics at the busbar can further be reduced to the order of $24n \pm 1$ provided the load demanded by the azimuth thrusters of vector group Dd11.75d0.75 and Dd11.75d0.75 is the same. In a semi-submersible oil rig platform, loading of the each azimuth thruster is controlled by a DP system. The DP system uses thrust allocator to determine the magnitude and direction of thrust required for each azimuth thruster to create force and moment equilibrium. Several thrust allocation approaches have been successfully tested on marine vessels [9, 13, 29-32, 54, 56-61]. The conventional thrust allocation approaches only focus on minimizing the power demanded by the thrusters. Therefore, the load demanded by the azimuth thrusters of vector group Dd11.75d0.75 and vector group Dd11.75d0.75 may not be the same and hence leads to higher voltage Total Harmonic Distortion (V_{THD}^{Bus}) and Individual Harmonic Distortion (V_h^{Bus}) at 11 kV busbar.

The V_{THD}^{Bus} and V_h^{Bus} at 11 kV busbar can be limited by (a) Switching more generators (reduces source reactance), (b) Reducing the loading of the thruster motors and (c) Equaling the load demanded by the azimuth thrusters of vector group Dd11.75d0.75 and vector group Dd11.75d0.75. However, switching extra generator and reducing

the loading of the thruster motors would be energy inefficient. Similarly, reducing the loading of the thruster motors would also lead to higher power consumption. The option (c) doesn't ensure the V_{THD}^{Bus} and V_h^{Bus} at 11 kV busbar are within the limits set by them therefore, there is a tradeoff between the requirements of low power consumption of the oil rig platform and low THD. The best solution to this tradeoff is the optimization of power consumption of the oil rig platform with THD constraints. The V_{THD}^{Bus} and V_h^{Bus} at 11 kV busbar can be reduced by intelligently controlling the loads of each azimuth thruster. The challenge is to develop Voltage Harmonic Distortion compliant Energy-Efficient Thrust allocation for Semi-submersible Oil Rig Platforms and find its solution using robust optimization algorithms.

➢ **Issue 5: Design of an Intelligent, Robust and Fast Optimization Algorithm**

The optimization problems formulated in the above issues are non-convex in nature. The formulated non-convex constrained optimization problems are hard to solve using classical optimization methods such as Newton's method, Sequential Quadratic Programming (SQP), Gradient descent etc. The classical optimization methods are very fast and need less computational time, however, these methods are highly sensitive to starting points and frequently converge to a local optimum solution or diverge altogether.

There are two kinds of classical optimization techniques: direct search method and gradient search method. In the direct search method, only the objective function and constraints are used for the search process, whereas in the gradient search method, the first order and/or second order derivatives are used for the search process. Direct search methods are very slow because many function iterations are required,

whereas gradient search methods are faster, but they are inefficient for discontinuous and non-differentiable functions. Furthermore, both methods seek local optima, thus starting the search in the vicinity of a local optima causes them to miss the global optima.

Metaheuristic algorithms eradicate some of the afore-mentioned difficulties and are quickly replacing the classical methods in solving practical optimization problems. Metaheuristic algorithms typically intend to find a good solution to an optimization problem by 'trial-and-error' in a reasonable amount of computational time. During the last few decades, several metaheuristic algorithms have been proposed. These algorithms include Genetic Programming, Evolutionary Programming, Evolutionary Strategies, Genetic Algorithms, Differential Evolution, Harmony Search algorithm, Ant Colony Optimization, Particle Swarm Optimization, and Bee Algorithms [62-65].

The Harmony Search algorithm is one of the recently developed optimization algorithms. The Harmony Search algorithm, developed by Geem et al. [66] in 2001, is inspired by the music improvisation process. In the music improvisation process, the musician searches for a harmony and continues to adjust the pitches of the instruments to achieve a better state of harmony. The effort to find harmony in music is analogous to finding optimality in an optimization process. In other words, a musician's improvisation process can be compared with the search process in optimization. The pitch of each musical instrument determines the aesthetic quality, just as the objective function value is determined by the set of values assigned to each decision variable.

The simplicity and effectiveness of the HS algorithm has led to its application to optimization problems in different areas [7, 67-107]. The HS algorithm is good at

identifying the high performance regions of the solution space in a reasonable time but has difficulty performing a local search for numerical applications. To improve the performance of the HS algorithm, several variants of HS have been proposed [91, 93, 94, 108]. However, their effectiveness in dealing with diverse problems is still unsatisfactory. The performances of these variants mainly depend on the selection of different parameter values of the algorithm. Improper selection of the parameter values often leads to a lack of balance between diversification and intensification. The tuning of the parameters itself becomes another optimization problem.

The performance and efficiency of most of the metaheuristic algorithms depend on the extent of balance between diversification and intensification during the course of the search. Intensification (exploitation) is the ability of an algorithm to exploit the search space in the vicinity of the current good solution using the information already collected, while diversification (exploration) helps the algorithm explore the new regions of a large search space quickly and allows dissemination of the new information into the population. Proper balance between these two characteristics results in enhanced performance of the algorithm [109, 110]. In order to overcome this, the more robust and self-tuned algorithm must be developed which is almost-parameter-free and converges very quickly, and needs lower iterations.

1.6   Contribution of the Thesis

➢ **Development of an Intelligent Tuned Harmony Search Algorithm for Optimization**

Based on the idea of balanced intensification and diversification, a new harmony search variant is proposed which borrows the concepts from the decision making based on despotism, in which one dominant forms the group and makes the decision on behalf of that group. The pitch adjustment strategy adopted by the formed group helps the algorithm in maintaining a proper balance between intensification and diversification within the bounded search space of the formed group. Meanwhile, the individuals who are not part of the dominant group follow the path of rebellion. This pitch adjustment strategy helps the algorithm search for a better solution than that of the worst individual in the Harmony Memory. Therefore, it enhances the explorative behavior of the algorithm.

The performance of the proposed ITHS algorithm is influenced by a few other parameters, such as harmony memory size (HMS) and harmony memory considering rate (HMCR). The effects of varying these parameters on the performance of ITHS algorithm is also analyzed in detail. The final parameters of HMCR and HMS are chosen based on the analysis. The analysis also demonstrated that the proposed algorithm is capable of maintaining a proper balance between intensification and diversification even with a lower population size.

To evaluate the performance of the proposed ITHS algorithm comprehensively, it is compared with eight state-of-the-art HS variants over seventeen benchmark functions with different characteristics. The numerical results obtained reflect the superiority of the proposed ITHS algorithm in terms of accuracy, convergence speed, and robustness when compared with other state-of-the-art HS variants.

Therefore, an intelligent group formation and a novel harmony improvisation scheme help the search progress with a better balance between intensification and diversification when compared with other variants of HS and other metaheuristic algorithms. Another added advantage of the proposed algorithm is that there is no need to tune the parameters of the proposed algorithm, thereby leading to an intelligent tuned harmony search algorithm. The developed ITHS algorithm is further used for finding the optimal solution for different optimization problem. The details of the above stated contribution are explained in Chapter 2.

➢ **Optimal Scheduling of the Diesel Generators in Semi-submersible Oil Rig Platforms**

As discussed in previous section that accurate modeling of the specific fuel consumption is significant for optimal scheduling of the generators. Therefore, the specific fuel consumption curve is modeled using cubic spline interpolation. The specific fuel consumption curve is used to formulate the constrained optimization problem. The objective of the formulated optimization problem is to optimally schedule the diesel generators to ensure minimum fuel consumption for different loading conditions. The formulated optimization problem is solved using ITHS algorithm. The details of the above stated contribution are explained in Chapter 3.

➢ **Optimal Thrust Allocation for Semisubmersible Oil Rig Platforms**

For vessels that are operating to DP class 2 or 3 standards, the vessel should be left with sufficient power and thrusters to maintain position after worst case failure. Therefore, the semi-submersible oil rig is equipped with redundant thruster configuration and is over-actuated as per the guidelines of IMO MSC Circ.645 and

IMCA M 103. Azimuth thrusters fitted at oil rig platform's pontoon level can produce forces in different directions leading to an over-actuated control problem that can be formulated as an optimization problem. The objective of the formulated optimization problem is to minimize the power consumption. In addition, the optimization problem also takes forbidden/spoil zones into account. In the formulated constraint optimization problem the error between the demanded generalized force (τ) and generalized force jointly produced by the actuators must be close to zero to keep the vessel at the desired position. In order to satisfy the constraints of the formulated optimization problem, a novel constraint handling method based on Superiority of Feasible Solutions (SF) is proposed. The details of the above stated contribution are explained in Chapter 4.

➢ **Energy Efficient Thrust Allocation approach for Semi-submersible Oil Rig Platforms**

The power consumed by the oil rig platform depends on the thrust generated by the thrusters and the efficiency of the electrical propulsion system. A detailed model to compute the efficiency of the electrical propulsion system is developed and the numerical results obtained are compared with experimental test results.

The thrust allocation approach is modified and the developed efficiency model is used for calculation of the power consumed by the oil rig platform. The energy-efficient thrust allocation approach is developed and formulated as an optimization problem, with an objective to minimize the total power consumption by ensuring that the electrical propulsion system operates in the efficient region and is subjected to force and moment constraints to ensure fixed position of the oil rig platform. The details of the above stated contribution are explained in Chapter 5.

➢ **Voltage Harmonic Distortion compliant Energy-Efficient Thrust allocation for Semi-submersible Oil Rig Platforms**

In a quasi-24 pulse rectifier system, the harmonics at the busbar are of the order of $24n \pm 1$ provided the load demanded by the vector group Dd11.75d0.75 and Dd11.25d0.25 are the same. In conventional thrust allocation approach the load demanded by the azimuth thrusters of vector group Dd11.75d0.75 and Dd11.75d0.75 may not be the same. This leads to higher voltage Total Harmonic Distortion (V_{THD}^{Bus}) and Individual Harmonic Distortion (V_h^{Bus}) at busbar. In order to overcome this problem a Harmonic compliant Energy-Efficient Thrust allocation approach is developed to meet the harmonic limits, with an objective to minimize the power consumption of the semi-submersible oil rig platform. In addition, to the constraints imposed by the conventional thrust allocation problem, the constraints imposed on V_{THD}^{Bus} and V_h^{Bus} have also been incorporated in the optimization problem. The detailed model to calculate V_{THD}^{Bus} and V_h^{Bus} at busbar is also developed. The details of the above stated contribution are explained in Chapter 6.

1.7 Overview of the Thesis

Based on above descriptions, this thesis is organized as

Chapter 2 provides an overview of classical HS algorithm and its recently developed state-of-the-art HS variants. The details of the proposed Intelligent Tuned Harmony Search (ITHS) algorithm are also presented in this Chapter. However, the performance of the

proposed ITHS algorithm is influenced by other parameters, such as the harmony memory size (HMS) and the harmony memory considering rate (HMCR). The effects that varying these parameters have on the performance of the ITHS algorithm is also analysed in detail. The performance of the proposed ITHS algorithm is investigated and compared with eight state-of-the-art HS variants over seventeen benchmark functions. Furthermore, to investigate the robustness of the proposed algorithm at higher dimensions, a scalability study is also performed.

Chapter 3 focuses on the optimal scheduling of the generators to reduce the fuel consumption in the oil rig platform. This Chapter also provides the details of SFC curve modeling using cubic spline interpolation.

Chapter 4 provides an overview of the three degrees of freedom (3-DOF) thrust allocation. The insight into these principles will help the reader in understanding the motivation for following an engineering approach for optimal thrust allocation in an over-actuated marine vessel. The details and drawbacks of the Lagrange multiplier method conventionally used for the thrust allocation in the case study marine vessel are also discussed. The thrust allocator tries to minimize the power consumption and takes forbidden/spoil zones into account. The details of the formulated optimization problem are presented. The optimization problem formulated is subjected to both equality and inequality constraints. Therefore, a novel constraint handling method based on Superiority of Feasible Solutions (SF) is proposed.

Chapter 5 focuses on development of a detailed model to calculate the power consumption of the electrical propulsion system. In this chapter, the energy-efficient thrust allocation

approach is developed with an objective to minimize the total power consumption by ensuring that the electrical propulsion system operates in the efficient region. In addition the optimization problem also includes the force and moment constraints to ensure fixed position of the oil rig platform.

Chapter 6 focuses on development of a detailed mathematical model to calculate V_{THD}^{Bus} and V_h^{Bus} at 11 kV busbar. In this Chapter, the details of the Voltage Harmonic Distortion compliant Energy-Efficient Thrust allocation approach are presented. The proposed approach ensures that the V_{THD}^{Bus} and V_h^{Bus} at 11 kV busbar are within the limits, by intelligently controlling the load demanded by the azimuth thrusters of vector group Dd11.75d0.75 and vector group Dd11.75d0.75.

Chapter 7 concludes the main issues studied in the thesis. Future work is also discussed.

CHAPTER 2. AN INTELLIGENT TUNED HARMONY SEARCH ALGORITHM FOR OPTIMIZATION

2.1 Introduction

In mathematics and computer science, optimization refers to a process of selecting or finding the best element from a set of available alternatives. Every process has the potential to be optimized, and indeed, many challenging problems in science, engineering, economics, and business can be formulated as optimization problems. The objective of a formulated optimization problem can be the minimization of time, cost, and risk or the maximization of profit, quality, and efficiency.

In this thesis several issues highlighted in Chapter 1 have been formulated as optimization problems. The formulated non-convex constrained optimization problem are hard to solve using iterative numerical optimization methods such as Newton's method, Sequential Quadratic Programming (SQP), Gradient descent etc. Therefore, to find the optimum solution an Intelligent Tuned Harmony Search (ITHS) algorithm is developed in this Chapter.

The rest of the Chapter is arranged as follows: Section 2.2 provides an overview of classical HS algorithm and its recently developed state-of-the-art HS variants. The details of the proposed ITHS algorithm are presented in Section 2.3. The proposed ITHS algorithm is compared with other sub-population based approaches in Section 2.4. The impacts of varying parameters on the performance of the ITHS algorithm are demonstrated in Section 2.5. In Section 2.6, the classical benchmark problems are considered, and the numerical results obtained using the proposed algorithm are compared with other state-of-the-art variants of HS. Furthermore, to investigate the robustness of the proposed algorithm, the shifted, shifted-rotated and hybrid composite benchmark problems are investigated. In order to demonstrate the performance of the proposed method at higher dimensions, a

scalability study is also conducted, and the numerical results obtained are compared with other variants of the HS algorithm. Finally, the research findings and the contributions of the proposed algorithm are discussed in Section 2.7.

2.2   Harmony Search and Other Variants

In this section, an engineering approach is introduced that is used in the design and development of an algorithm inspired by the musical process of searching for a perfect state of harmony. A brief overview of the classical HS algorithm and other variants are provided.

2.2.1   Harmony Search Algorithm

A metaheuristic algorithm, mimicking the improvisation process of music players has been recently developed and named Harmony Search [66]. The HS algorithm has been very successful for a wide variety of optimization problems, presenting several advantages with respect to traditional optimization techniques [109, 111]. The HS algorithm imposes fewer mathematical requirements and does not require specific initial value settings of the decision variables. Because the HS algorithm is based on stochastic random searches, the derivative information is also not necessary. In the HS algorithm, musicians search for a perfect state of harmony determined by aesthetic estimation, as the optimization algorithms search for a best state (i.e., global optimum) determined by an objective function. Each musician corresponds to a decision variable; a musical instrument's pitch range corresponds to a range of values for the decision variables; musical harmony at a certain time corresponds to a solution vector at certain iteration; and an audience's aesthetics correspond to the objective function. Just as musical harmony is incrementally improved, a solution vector is also improved iteration by iteration.

To understand the design principle of the HS algorithm, let us first idealize the improvisation process adopted by a skilled musician. When a musician is improvising, he

or she has three possible choices: (1) playing any famous tune exactly from his or her memory, (2) playing something similar to the aforementioned tune (thus adjusting the pitch slightly) or (3) composing new or random notes. In this section, various steps of the HS algorithm and a description of how the HS is designed and applied are presented.

Step 1: Initialize the optimization problem and algorithm parameters

To apply HS, the problem should be formulated in the optimization environment, having an objective function and constraints as shown in (2.1).

$$Minimize \ (or \ Maximize) f(\vec{x})$$
$$subject \ to \ x_i \in X_i \ , i = 1,2,3, \ldots., N$$

(2.1)

where $f(\vec{x})$ is the objective function with $\vec{x}$ as the solution vector composed of decision variables x_i, and X_i is the set of a possible range of values for each decision variable x_i and $(_Lx_i \leq x_i \leq _Ux_i)$ where $_Lx_i$ and $_Ux_i$ are the lower and upper bounds for each decision variable, respectively. In addition, the values of different parameters of the HS algorithm are also specified in this step. These parameters include harmony memory size (HMS), harmony memory considering rate ($HMCR$), pitch-adjusting rate (PAR) and the maximum number of improvisations or iterations ($Maxiter$).

Step 2: Initialize the harmony memory (HM)

The initial HM consists of a HMS number of randomly generated solution vectors for the optimisation problem under consideration. Each component of the solution vector in HM is initialised using the uniformly distributed random number between the lower and upper bounds of the corresponding decision variable $[_Lx_i, _Ux_i]$, where $1 \leq i \leq N$. The ith component of the jth solution vector is given by (2.2)

$$x_i^j = \ _Lx_i + (_Ux_i - _Lx_i) \ rand[0,1]$$

(2.2)

where $j = 1, 2, 3 \ldots, HMS$ and $rand\,[0, 1]$ is a uniformly distributed random number between 0 and 1. Each row of the HM consists of a randomly generated solution vector for the formulated optimisation problem, and the objective function value for the jth solution vector is denoted by $f(\vec{x^j})$. The HM matrix formed is governed by Eqs. (2.3-2.4).

$$HM(j, 1 : N) = \vec{x^j} \qquad (2.3)$$

$$HM(j, N + 1) = f(\vec{x^j}) \qquad (2.4)$$

The HM with the size of $HMS \times (N + 1)$ can be represented by a matrix, as shown in (2.5).

$$HM = \begin{bmatrix} x_1^1 & x_2^1 & x_3^1 & \ldots \ldots \ldots \ldots & x_N^1 & f(\vec{x^1}) \\ x_1^2 & x_2^2 & x_3^2 & \ldots \ldots \ldots \ldots & x_N^2 & f(\vec{x^2}) \\ x_1^3 & x_2^3 & x_3^3 & \ldots \ldots \ldots \ldots & x_N^3 & f(\vec{x^3}) \\ . & . & . & & . & . \\ . & . & . & & . & . \\ & & & . & & \\ x_1^{HMS} & x_2^{HMS} & x_3^{HMS} & \ldots \ldots \ldots \ldots & x_N^{HMS} & f(\vec{x^{HMS}}) \end{bmatrix} \qquad (2.5)$$

Step 3: Improvise a new harmony from the HM

After defining the HM as shown in (2.5) for the optimization problem, the improvisation of the HM is performed by generating a new harmony vector $\vec{x'} = (x_1' \quad x_2' \quad x_3' \quad \ldots \ldots \ldots \ldots x_N')$. Each component of the new harmony vector is generated using (2.6).

$$x_i' \leftarrow \begin{cases} x_i' \in HM(i) & with\ probability\ HMCR \\ x_i' \in X_i & with\ probability\ (1 - HMCR) \end{cases} \qquad (2.6)$$

where $HM(i)$ is the ith column of the HM, $HMCR$ is defined as the probability of selecting a component from the HM members, and $(1 - HMCR)$ is, therefore, the probability of generating a component randomly from the possible range of values. If x_i' is generated from the HM, then it is further modified or mutated according to PAR. PAR determines the probability of a candidate from the HM mutating, and $(1 - PAR)$ is the probability of no mutation. The pitch adjustment for the selected x_i' is given by (2.7).

$$x_i' \leftarrow \begin{cases} x_i' \pm rand[0,1].bw & with\ probability\ PAR \\ x_i' & with\ probability\ (1 - PAR) \end{cases} \qquad (2.7)$$

where $rand$ $[0,1]$ is the randomly generated number between 0 and 1 and bw is the pitch bandwidth.

Step 4: Update the HM

The newly generated harmony vector $(\mathbf{x}')$ is evaluated in terms of the objective function value. If the objective function value for the new harmony vector is better than the objective function value for the worst harmony in the HM, then the new harmony is included in the HM , and the existing worst harmony is excluded from the HM.

Step 5: Go to step 3 until termination criterion is reached.

The iteration process in Steps 3 and 4 of the corresponding independent run of the optimization problem are repeated until the termination criterion $(Maxiter)$ is not satisfied. Finally, the best solution is selected from the final HM and is considered the best solution to the formulated optimisation problem for the corresponding independent run.

2.2.2 Harmony Search Variants

The HS is good at identifying the high performance regions of the solution space in a reasonable time but has difficulty performing a local search for numerical applications. The parameters HMCR, PAR and bw, introduced in Step 3, help the algorithm find globally and locally improved solutions [109, 111].

The performance of the HS algorithm can be improved by fine-tuning the values of PAR and bw. The choice of a small PAR value with a large bw value can cause the algorithm performance to deteriorate and increase the computational time needed to find the optimum solution. Initially, the value of the parameter bw must be large to increase the diversification of the search. However, in final iterations the algorithm must focus more on intensification; therefore, a small bw value is preferred. To improve the performance of the HS algorithm and to eliminate the drawbacks that occur with fixed values of PAR and bw, Mahdavi *et al*. [112] proposed an improved harmony search (IHS) algorithm that dynamically updates the PAR and bw values with the number of iterations. IHS algorithm has exactly the same steps as those in the classical HS algorithm with the exception of Step 3, where the value of parameter PAR is linearly increased and the value of parameter bw is exponentially decreased with the number of iterations. The mathematical expressions for PAR and bw are given by (2.8-2.9), respectively.

$$PAR(iter) = PAR_{min} + (PAR_{max} - PAR_{min}) \cdot \left(\frac{iter}{Maxiter} \right) \qquad (2.8)$$

where PAR_{min} is the minimum pitch adjustment rate, PAR_{max} is the maximum pitch adjustment rate, $iter$ is current iteration and $Maxiter$ is the maximum number of iterations.

$$bw(iter) = bw_{max} \cdot exp\left[\left\{\ln\left(\frac{bw_{min}}{bw_{max}}\right)\right\} \cdot \left(\frac{iter}{Maxiter}\right)\right] \qquad (2.9)$$

where bw_{min} is the minimum bandwidth and bw_{max} is the maximum bandwidth. However, the choice of minimum and maximum bandwidth greatly influences the performance of the proposed IHS algorithm.

Inspired by the concept of swarm intelligence as proposed in Particle Swarm Optimization (PSO) [113], a new variant of the HS algorithm was proposed by Omran and Mahadavi [114]. The new approach, called the global-best harmony search (GHS) algorithm, directly adopts the current best pitch from the harmony memory to simplify the pitch adjustment step. Therefore, the limitation of determining the minimum and maximum values of the parameter *bw* as proposed in the IHS algorithm is overcome by replacing the *bw* parameter altogether and adding a social dimension to the HS algorithm. The GHS algorithm has exactly the same steps as the IHS algorithm with the exception of Step 3. The pitch adjustment for the selected x'_j is given by (2.10).

$$bx'_i \leftarrow \begin{cases} x_k^{best}, \text{with probability } PAR \\ x'_i, \text{with probability } (1 - PAR) \end{cases} \qquad (2.10)$$

where $best$ is the index of the best harmony in the HM and k is $rand\ [0, N]$, a uniformly distributed random number between 0 and N. However, due to the pitch adjustment procedure adopted by the GHS algorithm, all the solution vectors have a tendency to move towards the current best solution vector despite their actual quality of the objective function, as shown in Fig 2.1. Therefore, the proposed pitch adjustment may reduce the diversification of the search and cause the performance of the GHS algorithm to deteriorate.
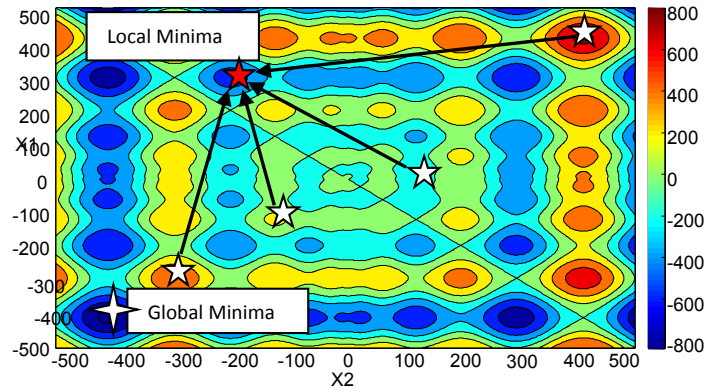
*Fig. 2.1 Pitch adjustment mechanism for the 2-D multimodal problem with variables X1 and X2
in GHS, where HMS = 5, HMCR =1 and PAR = 1*

Based on the idea that the better harmony vector has a higher selection probability and new harmonies are generated in each iteration, Cheng *et al* [70] developed another improved HS algorithm called modified HS (MHS), which is found to be more efficient than the basic HS algorithm for slope stability. Inspired by the GHS algorithm, Quan-Ke Pan *et al*. proposed a self-adaptive GHS (SGHS) algorithm [94]. Unlike the GHS algorithm, the SGHS algorithm employs a new improvisation scheme and an adaptive parameter tuning method. The SGHS algorithm does not require a precise setting of specific values for the critical parameters $HMCR$, PAR and bw in accordance with problem's characteristic and complexity. These parameters are self-adapted by a learning mechanism or dynamically decreased with an iteration counter.

The performance of the metaheuristic algorithms can be improved with the technique of multiple interacting sub-populations. Based on this approach, Quan-Ke Pan *et al*. proposed a local-best harmony search algorithm with dynamic sub-populations (DLHS) [91]. In the DLHS algorithm, the whole *HM* is divided into many small-sized sub-HMs, and the independent evolution is performed on each sub-HM. To maintain population diversity, the small-sized sub-HMs are re-grouped frequently with a re-grouping schedule to exchange information amongst the solutions.

Chia-Ming Wang and Yin-Fu Huang [115] introduced a Self-Adaptive Harmony Search (SAHS) algorithm where the pitch adjustment is based on the consciousness (Harmony Memory). SAHS eliminates the selection of both PAR and bw parameter values, and there is no need to tune the control parameters. More precisely, the new harmony vector is generated according to the maximum and minimum values of the decision variables in the HM. The SAHS algorithm has exactly the same steps as those of the classical HS algorithm with the exception of Step 3, where the value of the parameter PAR is linearly decreased with the number of iterations as shown in (2.11).

$$PAR(iter) = PAR_{max} - (PAR_{max} - PAR_{min}).\left(\frac{iter}{Maxiter}\right) \qquad (2.11)$$

where PAR_{min} is the minimum pitch adjustment rate and its value is fixed to 0, PAR_{max} is the maximum pitch adjustment rate and its value is fixed to 1, $iter$ is iteration and $Maxiter$ is the maximum number of iterations. If x_i' is generated from the HM, then it is further modified or mutated according to the value of the parameter PAR. The pitch adjustment for the selected x_i' from the HM is given by (2.12).

$$x_i' \leftarrow \begin{cases} x_i' + \left(\max(HM)^i - x_i'\right).rand[0,1] \\ \qquad with\ probability\ 0.5.PAR \\ x_i' + \left(\min(HM)^i - x_i'\right).rand[0,1] \\ \qquad with\ probability\ 0.5.PAR \\ x_i' \qquad with\ probability\ (1-PAR) \end{cases} \qquad (2.12)$$

where $\min(HM)^i$ and $\max(HM)^i$ denote the lowest and the highest values of the ith variable in the *HM, respectively*, and $rand$ $[(0, 1)$ is a uniform number in the $(0, 1)]$ range. From (2.12), it is evident that diversification and intensification of the search are controlled by the difference between $\min(HM)^i$ and $\max(HM)^i$. The initial area of exploration of the search is large due to a significant difference between $\min(HM)^i$ and $\max(HM)^i$.

Therefore, the SAHS algorithm focuses more on the diversification of the search. Because the difference between $\min(HM)^i$ and $\max(HM)^i$ decreases gradually, the SAHS algorithm progressively makes finer adjustments to the solution vector and hence focuses more on the intensification of the search. It is clear that the pitch adjustment through this mechanism would not violate the boundary constraint of the decision variables. Fig. 2.2 shows the initial area of exploration of the SAHS algorithm. The figure shows that the diversification of the solution vectors is bounded by $\min(HM)^i$ and $\max(HM)^i$. If the optimal solution lies outside the area of exploration, then the SAHS algorithm would miss the global minima. In addition, the proposed SAHS needs many iterations to converge.
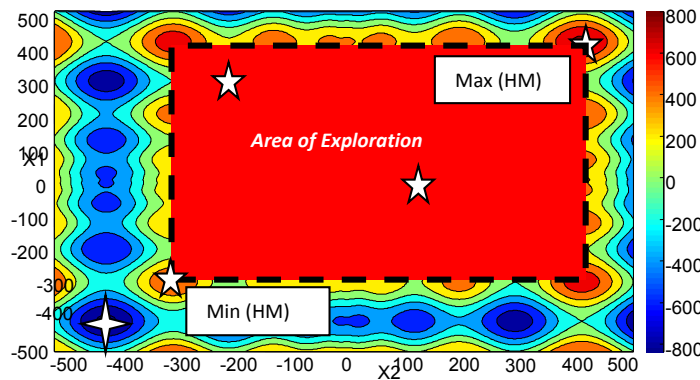
Fig. 2.2 Pitch adjustment mechanism for the 2-D multimodal problem with variables X1 and X2 in SAHS, where HMS = 5, HMCR =1 and PAR =1

Recently, Swagatam Das *et al*. proposed an explorative HS (EHS) algorithm [116]. In the EHS algorithm, the limitation of tuning the parameter *bw* in the IHS algorithm is eliminated by making it proportional to the current population variance. The proposed technique enhances the explorative power of the algorithm and, together with the exploitative behaviour due to selection, can provide a better balance of both diversification and intensification. Therefore, EHS performs well on a wide variety of objective functions. However, the enhanced explorative power of EHS leads to the slower convergence of the

algorithm, similar to SAHS. Therefore, the computational time required to find the optimal solution is quite long.

2.3 Proposed Method

The effectiveness of the metaheuristic algorithms is governed by two major components: diversification and intensification. These components are also referred to as exploration and exploitation [65, 109, 110, 117, 118]. Intensification involves a local search in the vicinity of current best solution, while diversification involves the algorithm exploring the global search space. The proper balance between these two components influences the overall efficiency and performance of the algorithm. If the algorithm focuses too much on intensification, then only a fraction of the search space may be explored. Therefore, the probability of the algorithm becoming trapped in local optima is higher. On the contrary, if the algorithm focuses too much on diversification, then it converges very slowly. Therefore, the computational time required to find the optimal solution is quite long. Maintaining the optimal balance between intensification and diversification is itself an optimisation problem. Therefore, simple intensification and diversification techniques are not sufficient.

Inspired by the decision-making theory, a new variant of harmony search is proposed in this Chapter. This search intelligently controls the intensification and diversification based on its consciousness or previous experience. The decision making is based on despotism, where one dominant makes and executes the decision. In the proposed method, the Harmony Memory is treated like an organisation. The first step is to identify a leader (dominant) as the representative of the organisation. The leader is chosen based on the objective function value of each solution vector of the population and is represented by (2.13).

$$\overrightarrow{x^{best}} = HM(best, 1:N) \qquad\qquad (2.13)$$

where *best* is the index of the best harmony in the *HM*. Therefore, $\overrightarrow{x^{best}}$ is assigned the responsibility of a leader and is responsible for further search and decision making. It is known that multiple interacting sub-populations enhance the balance between diversification and intensification in the metaheuristic search. Therefore, to have a proper balance between diversification and intensification, the $\overrightarrow{x^{best}}$ that was chosen divides the Harmony Memory into two groups (sub-populations), say Group A and Group B, as explained in Table 2.1.

Table 2.1. Procedure of Group Formation

$HM^{mean} = mean\big(HM(N+1)\big);$

$for\ j = 1:HMS$

$if\ (HM(j, N+1) \le\ mean(HM(N+1))$

$HM(j, 1:N) \in Group\ A$

$else\ HM(j, 1:N) \in Group\ B$

$end\ if$

$end\ for$

Group A consists of all the solution vectors or populations whose objective function value is less than or equal to HM^{mean}, and Group B consists of the rest. HM^{mean} is the mean of the objective function's value of the whole HM. Table 2.2 demonstrates the division of the initial Harmony Memory into Group A and Group B for a five-dimension problem. Group A is responsible for both intensification and diversification, whereas Group B is responsible only for diversification. The proposed ITHS algorithm dynamically updates the value of parameter PAR with the number of iterations as shown in (2.14).

$$PAR(iter) = PAR_{max} - (PAR_{max} - PAR_{min}) \cdot \left(\frac{iter}{Maxiter}\right) \qquad (2.14)$$

where PAR_{min} is the minimum pitch adjustment rate and its value is fixed to 0, PAR_{max} is the maximum pitch adjustment rate and its value is fixed to 1, $iter$ is iteration and $Maxiter$ is the maximum number of iterations. Because the value of the parameter PAR is updated in a similar manner as that of the SAHS algorithm, the values of minimum pitch adjustment rate (PAR_{min}) and maximum pitch adjustment rate (PAR_{max}) are fixed to 0 and 1, respectively. Chia-Ming Wang and Yin-Fu Huang [115], suggested that the value of the parameter PAR should be decreased with time to prevent overshoot and oscillations, whereas the value of parameter bw should be large initially. This suggestion would help the algorithm to diversify the search space of the solution vectors and prevent the solution from getting trapped in local minima. However, PAR should be decreased gradually to fine-tune the solution vectors, forcing the algorithm to focus more on intensification in the final iterations. Therefore, it seems reasonable that decreasing the value of the parameter PAR and bw with iterations could fine-tune the final solutions.

The Harmony Memory improvisation for the selected x_i' is determined by the group to which it belongs. The pitch adjustment for the selected x_i' is given by (2.15).

$$x_i' \leftarrow \begin{cases} x_i^{Best} - \left(x_i^{Best} - x_i' \right) . rand[0,1] \\ \qquad with\ probability\ 0.5.PAR \\ x_i^{Best} + \left(x_i^{worst} - x_i' \right) . rand[0,1] \\ \qquad with\ probability\ 0.5.PAR \\ x_i'\ with\ probability\ (1 - PAR) \end{cases} \qquad (2.15)$$

where x_i^{Best} and x_i^{Worst} denote the ith variable of the best and the worst solution vectors, respectively, from the HM evaluated in terms of the objective function from the previous

iteration's experience. Therefore, the pitch adjustment is based on the consciousness (Harmony Memory) of the search.

In the early stage, there is a need for optimum balance between intensification and diversification. The pitch adjustment strategy adopted in Group A takes care of both the intensification and diversification of the search. The term $x_i^{Best} - (x_i^{Best} - x_i')\cdot rand[0,1]$ allows the selected x_i' to search between itself and x_i^{Best} in the search space. Here, the search is governed by the attractiveness of the objective function of x_i^{Best}. Therefore, this pitch adjustment strategy is mainly responsible for the intensification of the search.

The other term, $x_i^{Best} + (x_i^{worst} - x_i')\cdot rand[0,1]$, is responsible for the diversification of the search. If the selected x_i' is closer to x_i^{worst}, then the term $(x_i^{worst} - x_i')$ is smaller. Therefore, the value of $x_i^{Best} + (x_i^{worst} - x_i')\cdot rand[0,1]$ is close to x_i^{Best}, and the selected x_i' is forced to move closer to x_i^{Best}. However, if the selected x_i' is far from x_i^{worst}, then the value is forced to move farther from x_i^{Best}. Therefore, this pitch adjustment strategy mainly governs the diversification of the search. The pitch adjustment strategy adopted in Group A helps the algorithm in maintaining a proper balance between intensification and diversification.

The search space of Group A is bounded by x_i^{Best} and x_i^{worst} and therefore, there is a probability that the proposed ITHS algorithm may converge to a local optimum solution if the optimum solution lies outside the defined boundary of Group A. This case would be similar to that of the SAHS algorithm as shown in Fig. 2.2 except that the SAHS algorithm is bounded by $\min(HM)^i$ and $\max(HM)^i$. To overcome this bounding, it is necessary to enhance the diversification of the proposed ITHS algorithm. Therefore, Group B is formed, and if the selected x_i' belongs to Group B, it is responsible for enhancing the diversification

of the search. The selected x_i' randomly selects the decision variable from the solution vector corresponding to $\overrightarrow{x^{best}}$ and starts the search in its neighbourhood. The pitch adjustment strategy adopted in Group B is similar to that of a rebellion. The pitch adjustment for the selected x_i' is given by (2.16).

$$x_i' \leftarrow \begin{cases} x_i' + (x_m^{Best} - x_i').rand[0,1] \\ where\ m =\ int(1 + (N-1)*rand) \end{cases} \tag{2.16}$$

However, the pitch adjustment in (2.16) is a debatable modification. As in many engineering problems, there may be vast differences in search ranges from one dimension to another. Although a bound checking criterion follows this step, it leads to inefficient use of iterations in such problems. A novel method is proposed to modify x_m^{Best} that ensures that each decision variable x_i is in its range $[_Lx_i,\ _Ux_i]$, where $_Lx_i$ and $_Ux_i$ are the lower and upper bounds of the ith decision variable, respectively. Because x_m^{Best} is in the range of $[_Lx_m,\ _Ux_m]$, it can be expressed by (2.17), where Δ_m is between 0 and 1. Similarly, $(x_m^{Best})'$ can be expressed by (2.18).

$$x_m^{Best} =\ _Lx_m + (_Ux_m -_Lx_m)\Delta_m \tag{2.17}$$

$$(x_m^{Best})' =\ _Lx_i + (_Ux_i -_Lx_i)\Delta_m \tag{2.18}$$

Using (2.17) and (2.18), $(x_m^{Best})'$ can be expressed as in (2.19).

$$(x_m^{Best})' =\ _Lx_i + (_Ux_i -_Lx_i)\frac{\left(x_m^{Best} -\ _Lx_m\right)}{\left(_Ux_m -_Lx_m\right)} \tag{2.19}$$

When the lower bound of each dimension is equal to 0, then the expression for $(x_m^{Best})'$ in (2.19) can be simplified and rewritten as in (2.20).

$$(x_m^{Best})' = ({}_U x_i / {}_U x_m) \, x_m^{Best}$$

(2.20)

To demonstrate the search behaviour of the proposed ITHS algorithm, the sphere function

of 30 dimensions is considered, and an *HMS* of 10 is used. Fig. 2.3 shows the variation in

the size of Group A for the sphere function of 30 dimensions over 50,000 iterations. It is

evident from Fig. 2.4 that, throughout the search, the size of the group varies between 2

and 8. Whenever the size of Group A is less than 5, Group B is more actively involved in

the search process, and whenever the size of Group A is more than 5, Group A is more

actively involved in the search process. The proposed technique of maintaining the balance

between diversification and intensification intuitively forces the difference between

HM^{Best} and HM^{mean} to decrease with iterations. It is evident from Fig. 2.3 that the

difference gradually approaches zero. Therefore, the proposed algorithm is successful in

maintaining the optimal balance between intensification and diversification throughout the

search process. The detailed pseudo code explaining the various steps involved in the ITHS

algorithm is shown in Table 2.3 for easier implementation and understanding of the

proposed algorithm.
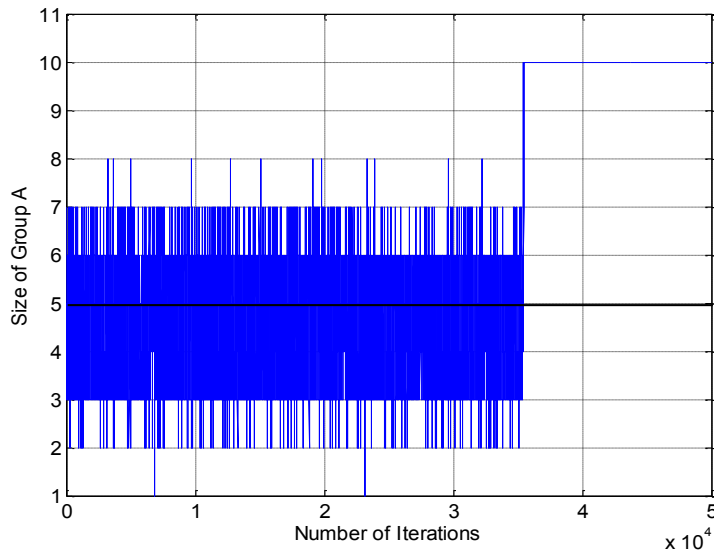
Fig. 2.3   Variation of the size of Group A in ITHS with iterations
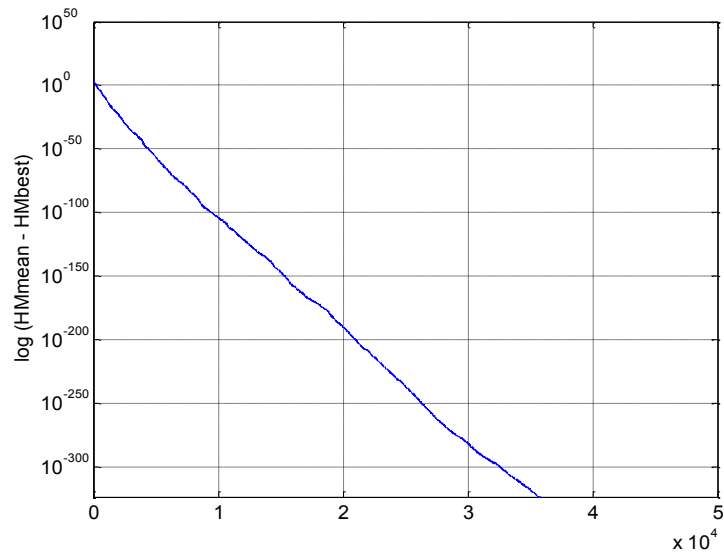
Fig. 2.4 Variation in the difference of HMmean and HMbest in ITHS with iterations

Table 2.2. Formation of group using ITHS for a 5-dimension problem

x_1	x_2	x_3	x_4	x_5	$f(x)$	Group
16.26866	97.68213	-5.15299	99.07627	62.0034	23493.55	B
22.1677	*59.19047*	*-15.5752*	*9.933763*	*-66.3032*	*8732.305*	*A*(BEST)*
26.61441	32.22113	13.64259	59.68605	-72.2944	10721.55	A
-72.7814	-38.6562	23.06349	-24.8935	62.17859	11809.22	A
39.89253	-49.3713	-8.06111	-11.614	92.52417	12789.53	A
-43.823	-70.5507	73.40084	15.47508	75.90527	18286.63	B
91.74061	-65.7189	-80.7651	-15.8434	-48.7132	21882.31	B
97.12966	59.42995	11.54855	11.56542	24.50162	13833.55	A
11.02824	-6.76834	77.93064	-41.2959	-79.0907	14201.3	A
91.32978	74.20154	-80.5355	1.485601	-38.0521	21783.13	B

Table 2.3. Pseudo code for ITHS algorithm.

Step1: Initialize ITHS Parameters
f(x): Objective Function
N: Number of Variables

$_L x_i$: Lower Bound; $_U x_i$: Upper Bound;

HMS: Harmony Memory Size=10; HMCR: Harmony Memory Consideration Rate=0.99
PAR_{min} = 0; PAR_{max} = 1; Maxiter = Maximum Number of Iterations=50,000
Step2: Initialize Harmony Memory (HM)
Find best and worst harmony vectors for the HM
Step3: Improvise Harmony Memory (HM)
$while(not\ Maxiter)$
$\qquad for\ i = 1$ to number of decision variables N do
$\qquad\qquad if\ rand[0,1] \leq HMCR$ /* *(memory consideration)* */
$\qquad\qquad d = int(1 + (HMS - 1).rand[0,1])$
$\qquad\qquad x_i' = HM(d,i);$

$$PAR(iter) = PAR_{max} - (PAR_{max} - PAR_{min}).\left(\frac{iter}{Maxiter}\right)$$

$\qquad\qquad\qquad if\ rand[0,1] \leq PAR(iter)$ /* *(pitch adjustment)* */
$\qquad\qquad\qquad HM^{mean} = mean(HM(N + 1));$
$\qquad\qquad\qquad\quad if(HM(d, N + 1) \leq mean(HM(N + 1)))$
$\qquad\qquad\qquad\quad$ /* *(Group A, Both Intensification and Diversification)* */
$\qquad\qquad\qquad\qquad if\ rand[0,1] \leq 0.5$
$\qquad\qquad\qquad\qquad y_i = x_i^{Best} - (x_i^{Best} - x_i').rand[0,1]$
$\qquad\qquad\qquad\qquad\ else$
$\qquad\qquad\qquad\qquad\quad y_i = x_i^{Best} + (x_i^{worst} - x_i').rand[0,1]$
$\qquad\qquad\qquad\qquad\ end\ if$
$\qquad\qquad\qquad\quad else$
$\qquad\qquad\qquad\quad$ /* *(Group B, Only Diversification)* */
$\qquad\qquad\qquad\qquad m = int(1 + (N - 1) * rand[0,1])$
$\qquad\qquad\qquad\qquad x_m^{Best} = x_m^{Best} * {_U x_i} \Big/ {_U x_m}$
$\qquad\qquad\qquad\qquad y_i = x_i' + (x_m^{Best} - x_i').rand[0,1]$
$\qquad\qquad\qquad\quad end\ if$

$\qquad\qquad\qquad\qquad if\ \left({_L x_i} \leq y_i \leq {_U x_i} \right)$
$\qquad\qquad\qquad\qquad x_i' = y_i$
$\qquad\qquad\qquad\qquad end\ if$
$\qquad\qquad\qquad end\ if$
$\qquad\qquad else$ /* *(random selection)* */
$\qquad\qquad x_i' = {_L x_i} + ({_U x_i} - {_L x_i}).rand[0,1]$
$\qquad\qquad end\ if$
$\qquad end\ for$
$\qquad$ **Step.4: Update Harmony Memory**
$\qquad$ Calculate the fitness of new harmony vector.
$\qquad if\ (f(\vec{x'}) \leq f\left(\overrightarrow{x^{worst}}\right)$
$\qquad \overrightarrow{x^{worst}} = \vec{x'}$
$\qquad end\ if$
Find best and worst harmony vectors for the *HM*
$end\ while$
Solution= $f\left(\overrightarrow{x^{Best}}\right)$
$end\ procedure$

40

2.4   Comparison with other sub-population based algorithms

Metaheuristic algorithms often get trapped in local minima due to a lack of balance between diversification and intensification. The metaheuristic algorithms are often 'cursed by dimensionality', and therefore, the probability of finding the solution in the vicinity of the global optimum decreases exponentially as the dimensionality of the search space increases [119].

To improve the performance of the search, a co-operative and co-evolutionary genetic algorithm (CCGA) was proposed [120]. In co-operative and co-evolutionary algorithms, the search space is partitioned into lower dimensional sub-spaces, and multiple populations evolve to find the final solution. Based on a similar technique, co-operative PSO (CPSO) was proposed [119]. In the case of CPSO, instead of using a single PSO population to find the optimal N-dimension solution vector, the solution vector is split into its constituent components and assigned to multiple PSO populations. Each PSO population optimises a single component of the solution vector. Hence, solving a single component is equivalent to solving the one-dimensional (1-D) optimisation problem [110, 119]. The fitness function is evaluated by combining solutions found by each of the PSOs representing the smaller sub-spaces. In the proposed ITHS algorithm, the whole population is partitioned into sub-populations, and each sub-population solves the original optimisation method and not the one-dimensional (1-D) optimisation problem. Therefore, the proposed approach is entirely different than CPSO and other co-operative and co-evolutionary algorithms.

Another approach to maintain proper balance between diversification and intensification and further enhance the performance of a metaheuristic algorithm is based on the technique of multiple interacting sub-populations. Inspired by this technique, Dynamic Multi Swarm PSO (DMS-PSO) was proposed [121]. In DMS-PSO, the swarm population is divided into

smaller size swarms, and each swarm uses its own members to search for a better area in the search space. To increase the diversity of the search, a randomised re-grouping schedule is introduced after a certain number of generations. In this way, the good information obtained by each swarm is exchanged among the swarms. Therefore, DMS-PSO gives better performance on multimodal problems than some other PSO variants, but the local search performance is not very good. The local search capability of DMS-PSO is further enhanced by hybridising it with the Quasi-Newton method and the Harmony Search [122, 123].

In the case of DMS-PSO, the sub-populations evolve in parallel. Each sub-population generates a new solution vector, and its objective function value is compared with the objective function value of the worst solution vector of the corresponding sub-population. In case of the proposed ITHS algorithm, there are two sub-populations that cooperate and generate only one new solution vector, which are compared with the worst solution vector of the whole population, not the sub-population.

The sub-population formation technique proposed in the ITHS algorithm is different from that of DMS-PSO. In the ITHS algorithm, the division of whole population into two groups, Group A and Group B, is carried out based on HM^{mean}. The solution vectors, whose objective function value is less than HM^{mean}, belong to Group A, and the rest belong to Group B. This strategy leads to dynamic sub-population size. In DMS-PSO, the whole population is divided into sub-populations randomly, and unlike ITHS, the sub-population size is constant. In addition to intelligent sub-population formulation, the novel harmony improvisation scheme performed by each group is unique. Group A is responsible for both intensification and diversification, whereas Group B is responsible for diversification only. In DMS-PSO, the search strategy adopted by each group is the same.

Based on the technique of multiple interacting sub-populations adopted in DMS-PSO, several other variants of GA and PSO have been proposed [110, 117, 118, 124]. However, in the case of the HS algorithm, except for the DLHS algorithm, no other variant of HS algorithm has proposed a sub-population based approach for optimisation. The intelligent group formation and novel harmony improvisation scheme adopted by the proposed ITHS algorithm are different from the other sub-population approaches adopted by GA, PSO and HS algorithms.

2.5 Impact of control parameters variation on the performance of ITHS

The evolution of the solution for the proposed algorithm over generations is affected by two important parameters: harmony memory size (HMS), and harmony memory considering rate ($HMCR$). To determine the impact of these two control parameters on the performance of the ITHS algorithm, the full factorial experiments for ITHS algorithm are conducted for the eight basic benchmark problems [114, 125]. These benchmark problems are summarised in Table 2.4. It is evident that sphere, Schwefel's Problem 2.22, Rosenbrock and rotated hyper-ellipsoid are unimodal, while Schwefel's Problem 2.26, Rastrigin, Ackley and Griewank are difficult multimodal functions where the number of local optima increases exponentially with the problem dimension. The camelback function is a low-dimensional function with only a few local optima. There are more complex benchmark problems proposed in [126]. However, the full factorial experiments for those are omitted to save space and also in considering that they display a similar trend.

Table.2.4. Benchmark Problems

Function	Function range	$(\vec{x})$	f_{min}^*
Sphere $f_1(\vec{x}) = \sum_{i=1}^{N} x_i^2$	$-100 \leq x_i \leq 100$	0	0
SCHWEFEL'S Problem 2.22 $f_2(\vec{x}) = \sum_{i=1}^{N} |x_i| + \prod_{i=1}^{N} |x_i|$	$-10 \leq x_i \leq 10$	0	0
ROSENBROCK $f_3(\vec{x}) = \sum_{i=1}^{N} (100(x_{i+1} - x_i^2)^2 + (x_i - 1)^2$	$-30 \leq x_i \leq 30$	$(1,1,.....1)$	0
ROTATED HYPER- ELLIPSOID $f_4(\vec{x}) = \sum_{i=1}^{N} \left(\sum_{j=1}^{i} x_j \right)^2$	$-100 \leq x_i \leq 100$	0	0
GENERALISED SWEFEL'S PROBLEM 2.26 $f_5(\vec{x}) = -\sum_{i=1}^{N} \left(x_i \sin(\sqrt{|x_i|}) \right)$	$-512 \leq x_i \leq 512$	$(420.9687, .., 420.9687)$	-418.982887*N
RASTRIGIN $f_6(\vec{x}) = \sum_{i=1}^{N} (x_i^2 - 10 \cos(2\pi x_i) + 10)$	$-5.12 \leq x_i \leq 5.12$	0	0
ACKLEY $f_7(\vec{x}) = -20 \exp \left(-0.2 \sqrt{\frac{1}{N} \sum_{i=1}^{N} \cos(2\pi x_i)} \right)$ $- \exp \left(\frac{1}{N} \sum_{i=1}^{N} \cos(2\pi x_i) \right)$ $+ 20 + e$	$-32 \leq x_i \leq 32$	0	0
GRIEWANK $f_8(\vec{x}) = \frac{1}{4000} \sum_{i=1}^{N} x_i^2 - \prod_{i=1}^{N} \cos \left(\frac{x_i}{\sqrt{i}} \right) + 1$	$-600 \leq x_i \leq 600$	0	0
SIX- HUMP CAMEL- BACK $f_9(\vec{x}) = 4x_1^2 - 2.1x_1^4 + \frac{1}{3}x_1^6 + x_1 x_2 - 4x_2^2 - 4x_2^4$	$-5 \leq x_i \leq 5$	$(0.08983, 0.7126)$	-1.0316285

In the full factorial experiment, the values of PAR_{max} and PAR_{min} are set to 1 and 0, respectively. Each problem is run for 30 independent replications, and each replication is allowed to run for 50,000 evaluations of the objective function (*Maxiter* = 50,000). The

variation of the mean fitness value with variation in *HMCR* and *HMS* for each problem is

shown in Figs. (2.5) - (2.13), and the variation of the best fitness value with variation in

HMCR and *HMS* for each problem is shown in Tables 2.5-2.13. Fig. (2.5) - (2.13) show

that a small *HMCR* value causes deterioration in the performance of the ITHS algorithm

because, for small values of *HMCR*, only a few elite harmonies are selected, and the ITHS

algorithm behaves closer to a random search. Therefore, the proposed algorithm is forced

to focus more on diversification and less on intensification. This unbalance causes the

performance of the ITHS algorithm to deteriorate. It is evident from the experiments that

the benchmark problems have the minimum value for an *HMCR* of 0.99 for different *HMS*.

Therefore, *HMCR* is chosen as 0.99. Similarly, based on the experiments, the other

parameter, *HMS* is chosen near 10 for 30 dimensions, and in the case of lower dimensions,

such as the Camel-back function, an appropriate value of *HMS* is approximately 50.
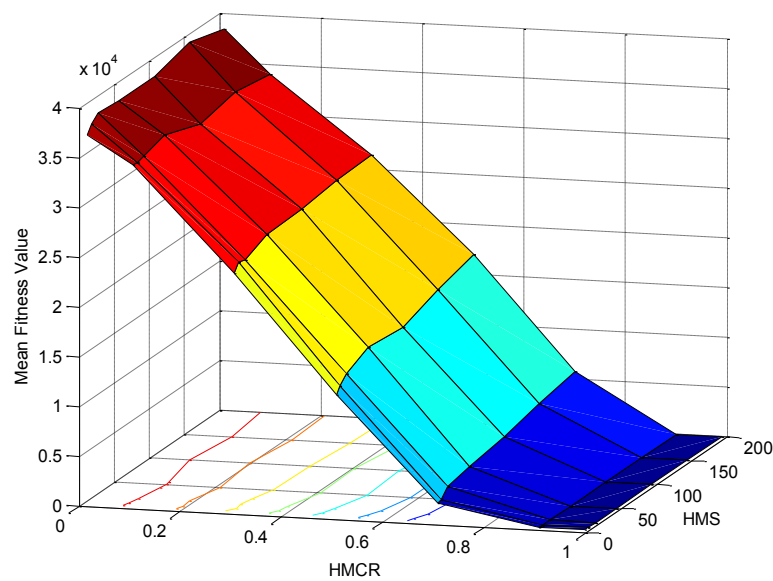
*Fig. 2.5 Variation of the Mean Fitness Value with change in HMS and HMCR for Sphere's
Function*
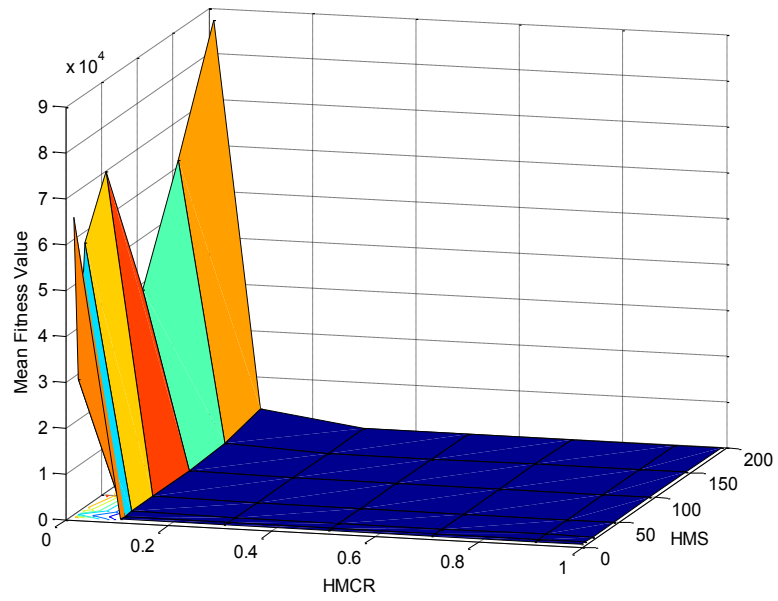
Fig. 2.6 Variation of the Mean Fitness Value with change in HMS and HMCR for Schwefel's Problem 2.22
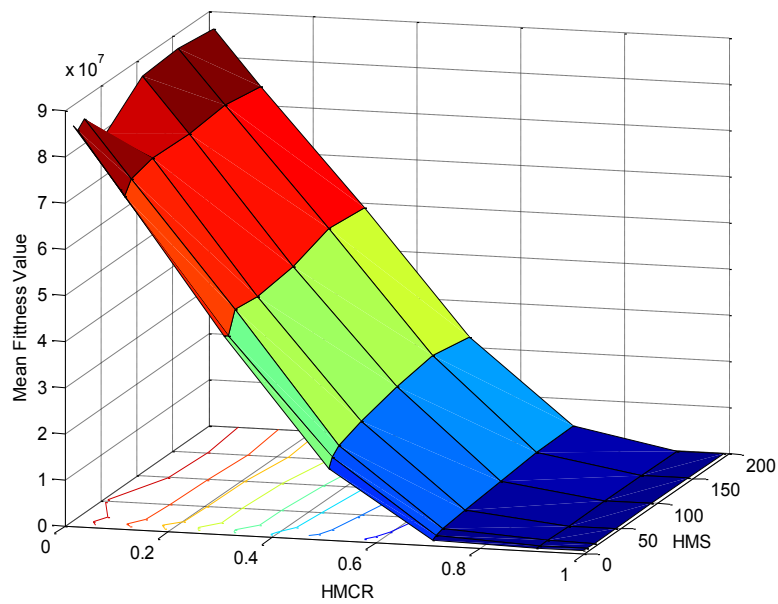
Fig. 2.7 Variation of the Mean Fitness Value with change in HMS and HMCR for Rosenbrock Function
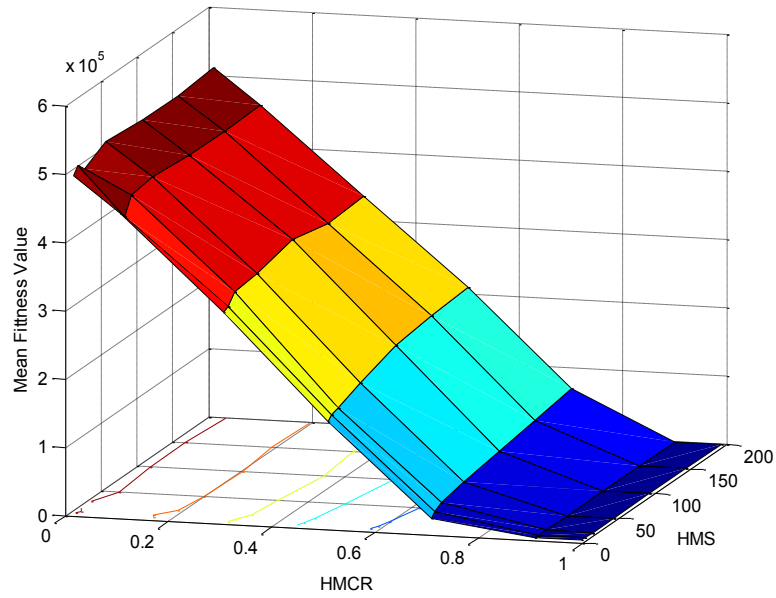
Fig. 2.8 Variation of the Mean Fitness Value with change in HMS and HMCR for Rotated Hyper-Ellipsoid Function
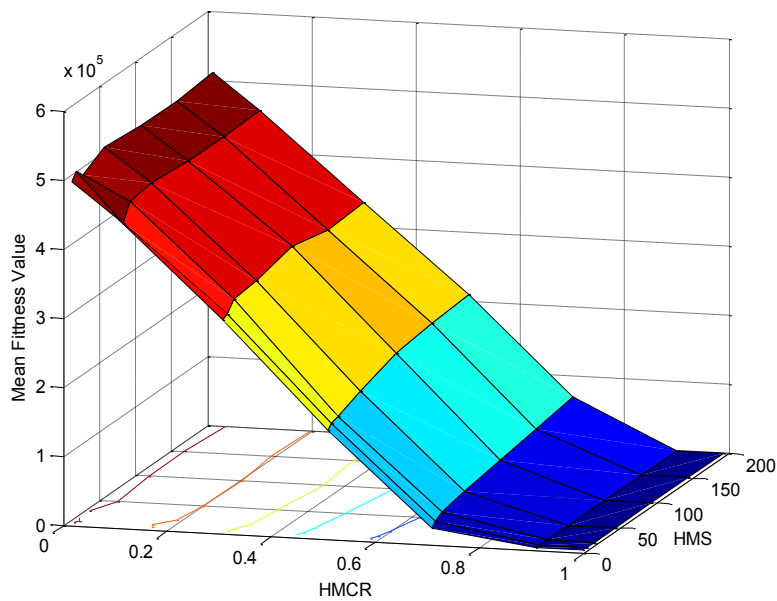
Fig. 2.9 Variation of the Mean Fitness Value with change in HMS and HMCR for Generalised Schwefel's 2.26 Problem
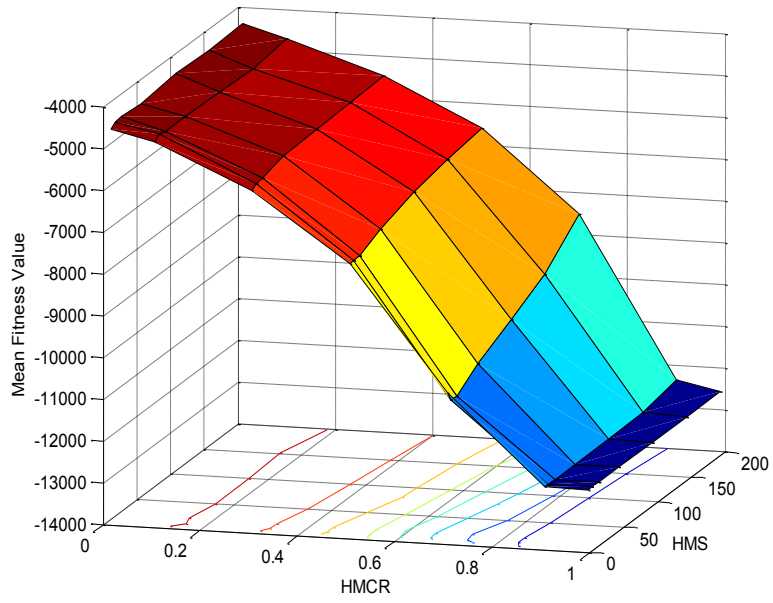
Fig. 2.10 Variation of the Mean Fitness Value with change in HMS and HMCR for Rastrigin Function
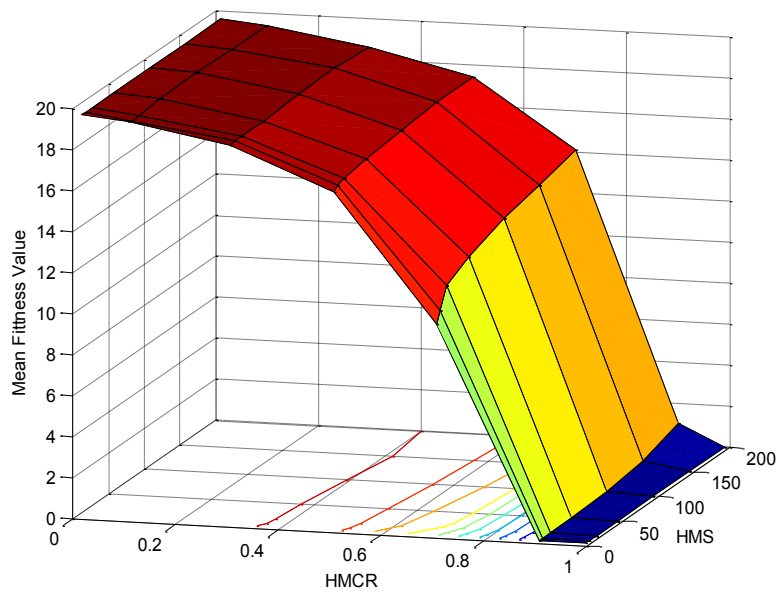
Fig. 2.11 Variation of the Mean Fitness Value with change in HMS and HMCR for Ackley's Function
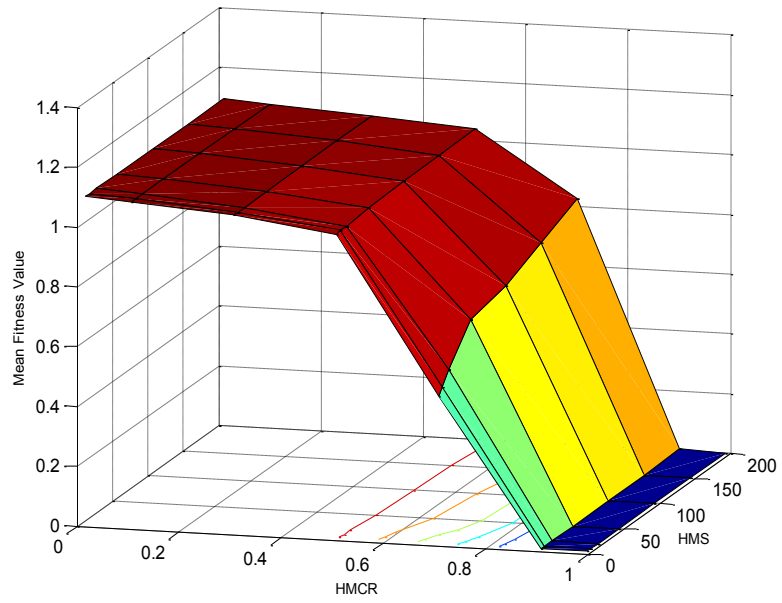
Fig. 2.12 Variation of the Mean Fitness Value with change in HMS and HMCR for Griewank Function
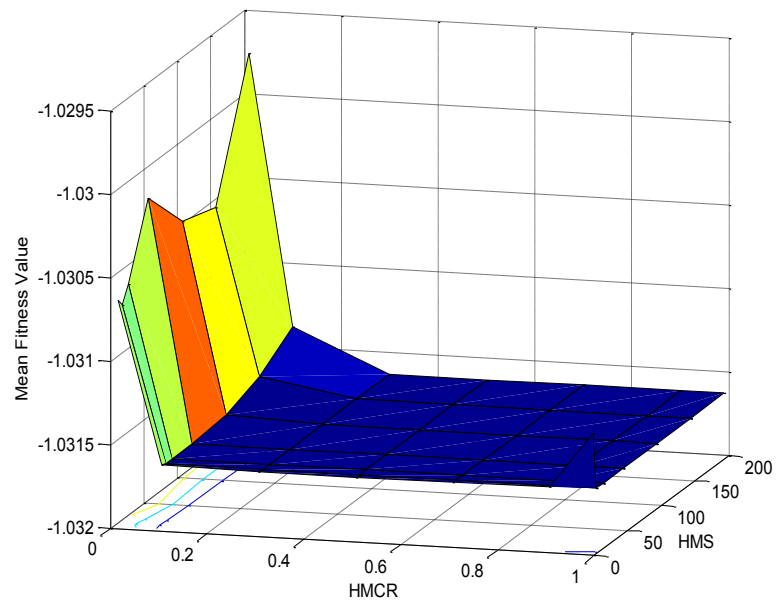
Fig. 2.13 Variation of the Mean Fitness Value with change in HMS and HMCR for Six-Hump Camel-Back Problem

Table 2.5. Variation of the best fitness value with change in HMS and HMCR for Sphere function for 30 dimensions

HMS/MCR	0.01	0.1	0.3	0.5	0.7	0.9	0.99
5	30146.12	28626.43	17019.68	8071.49	875.8423	5.72E-14	2.65E-26
10	**30216.23**	**26321.12**	**19327.23**	**8451.346**	**1230.969**	**1.09E-24**	**0**
20	31050.65	27210.16	19836.72	7704.213	1401.84	1.72E-14	2.14E-257
50	27042.05	25897.72	18690.78	11634.97	2014.708	2.54E-06	1.21E-125
100	31496.07	26147.22	21598.16	9978.096	2132.289	0.022972	6.13E-67
150	32541.33	29805.38	20158.04	11584.95	3373.607	0.375183	2.29E-46
200	32519.54	24504.97	21276.12	12790.59	3656.718	2.176077	4.73E-33

Table 2.6. Variation of the best fitness value with change in HMS and HMCR for Schwefel's 2.22 problem function for 30 dimensions

HMS/MCR	0.01	0.1	0.3	0.5	0.7	0.9	0.99
5	565.9439	86.44238	55.20005	33.39627	8.013138	8.52E-14	2.16E-78
10	**283.3457**	**76.16044**	**52.75796**	**33.81736**	**9.082007**	**1.09E-15**	**6.48E-240**
20	109.8083	83.12504	45.41498	37.78317	9.081136	2.02E-09	4.19E-155
50	137.985	83.70902	59.31394	36.43178	12.14067	0.000183	8.07E-74
100	102.2644	77.78469	51.37094	38.60828	14.91388	0.0177	5.11E-40
150	91.83527	89.13665	55.61793	42.03531	19.15127	0.115334	2.07E-27
200	100.7887	97.89458	61.35284	43.58073	19.96318	0.281818	7.54E-20

Table 2.7. Variation of the best fitness value with change in HMS and HMCR for Rosenbrock function for 30 dimensions

HMS/MCR	0.01	0.1	0.3	0.5	0.7	0.9	0.99
5	4.62E+07	4.89E+07	2.54E+07	7.66E+06	222285.8	0.002979	1.36E-28
10	**5.61E+07**	**4.85E+07**	**2.14E+07**	**1.08E+07**	**163709.7**	**0.000881**	**3.37E-29**
20	4.61E+07	5.22E+07	2.98E+07	8.96E+06	6.15E+05	1.66E-01	3.49E-29
50	3.53E+07	4.21E+07	2.94E+07	1.25E+07	1.03E+06	4.283971	1.92E-25
100	6.38E+07	4.38E+07	7.76E+06	1.12E+07	9.90E+05	29.23	1.64E-19
150	5.82E+07	4.60E+07	3.74E+07	1.18E+07	1.87E+06	42.75723	2.06E-17
200	5.24E+07	5.17E+07	2.61E+07	1.18E+07	1.47E+06	59.2817	1.63E-10

Table 2.8. Variation of the best fitness value with change in HMS and HMCR for Rotated hyper-ellipsoid function for 30 dimensions

HMS/MCR	0.01	0.1	0.3	0.5	0.7	0.9	0.99
5	371569.1	355130.3	257144.4	99042.65	8608.957	9.21E-16	5.58E-33
10	**366027.6**	**303921.7**	**235018**	**83678.87**	**12862.67**	**4.01E-21**	**1.0E-323**
20	426140.3	349818.7	251649.2	112502.9	15209.52	7.27E-12	2.35E-244
50	424853.5	351552.3	264148	145752.2	22649.56	0.000531	3.92E-116
100	410095.4	356996.2	265683.8	165522.2	30947.97	0.251013	2.20E-62
150	388134.4	359247.2	238809.8	168263	38470.77	8.989585	4.56E-42
200	430558.1	326150.5	233216.6	146824.8	46680.24	27.89128	4.80E-31

Table 2.9. Variation of the best fitness value with change in HMS and HMCR for Generalised Schwefel's 2.26 problem for 30 dimensions

HMS/MCR	0.01	0.1	0.3	0.5	0.7	0.9	0.99
5	-5331.54	-5514.11	-7201.77	-8366.18	-11584.6	-12569.5	-12569.48662
10	**-5435.87**	**-5137.01**	**-6351.72**	**-8508.03**	**-11675.2**	**-12569.5**	**-12569.48662**
20	-4899.66	-5275.11	-6550.39	-8056.19	-11459.8	-12569.5	-12569.48662
50	-5073.79	-5707.65	-6359.66	-8236.43	-10914.1	-12569.5	-12569.48662
100	-5069.98	-5471.83	-6154.05	-7634.21	-10474.1	-12568.1	-12569.48662
150	-4975.54	-5702.48	-6273.88	-7529.52	-10336.7	-12555.3	-12569.48662
200	-4773.12	-5154.11	-6179.17	-7176.16	-9558.88	-12459.6	-12569.48662

Table 2.10. Variation of the best fitness value with change in HMS and HMCR for Rastring function for 30 dimensions

HMS/MCR	0.01	0.1	0.3	0.5	0.7	0.9	0.99
5	287.2145	275.3805	217.9923	174.7384	74.10332	3.33E-09	5.68E-14
10	294.8756	227.474	239.1263	173.947	74.81008	0	0
20	288.987	280.9263	226.1824	156.852	77.56722	1.44E-11	0
50	291.3894	275.436	223.6022	179.8345	82.72398	0.001	0
100	290.4023	295.5742	253.7818	156.9901	103.0483	0.154786	0
150	296.2344	289.7747	243.594	179.7869	102.8341	2.628527	0
200	281.0936	286.9399	249.3018	211.2535	128.9656	10.11911	0

Table 2.11. Variation of the best fitness value with change in HMS and HMCR for Ackley's function for 30 dimensions

HMS/MCR	0.01	0.1	0.3	0.5	0.7	0.9	0.99
5	1.93E+01	1.92E+01	1.79E+01	1.52E+01	8.139653	1.33E-14	2.66E-15
10	1.90E+01	1.88E+01	1.81E+01	1.52E+01	9.445229	1.45E-13	2.66E-15
20	1.92E+01	1.83E+01	1.74E+01	1.58E+01	9.05E+00	7.22E-08	2.66E-15
50	1.91E+01	1.87E+01	1.77E+01	1.56E+01	1.14E+01	7.66E-04	2.66E-15
100	1.89E+01	1.90E+01	1.72E+01	1.63E+01	1.18E+01	4.80E-02	2.66E-15
150	1.81E+01	1.89E+01	1.77E+01	1.61E+01	1.23E+01	2.55E-01	2.66E-15
200	1.86E+01	1.86E+01	1.76E+01	1.69E+01	1.25E+01	4.09E-01	2.66E-15

Table 2.12. Variation of the best fitness value with change in HMS and HMCR for Griewank function for 30 dimensions

HMS/MCR	0.01	0.1	0.3	0.5	0.7	0.9	0.99
5	1.075297	1.063868	1.037183	0.9169	0.278918	8.88E-16	0
10	1.081499	1.07219	1.042403	0.996685	0.329148	0	0
20	1.086606	1.071933	1.04479	0.9377	0.345236	3.33E-16	0
50	1.072406	1.069046	1.047329	0.950645	0.535846	1.80E-08	0
100	1.082124	1.071933	1.037429	0.993685	0.560788	2.25E-05	0
150	1.082814	1.068176	1.053766	1.002901	0.626521	0.000294	0
200	1.078155	1.063867	1.041643	1.029967	0.742405	0.001801	0

Table 2.13. Variation of the best fitness value with change in HMS and HMCR for Six-hump Camel-back problem

HMS/MCR	0.01	0.1	0.3	0.5	0.7	0.9	0.99
5	-1.03162	-1.03163	-1.03163	-1.03163	-1.03163	-1.03163	-1.03163
10	-1.03156	-1.03163	-1.03163	-1.03163	-1.03163	-1.03163	-1.03163
20	-1.0316	-1.03163	-1.03163	-1.03163	-1.03163	-1.03163	-1.03163
50	-1.03157	-1.03163	-1.03163	-1.03163	-1.03163	-1.03163	-1.03163
100	-1.03158	-1.03163	-1.03163	-1.03163	-1.03163	-1.03163	-1.03163
150	-1.03159	-1.03163	-1.03163	-1.03163	-1.03163	-1.03163	-1.03163
200	-1.03161	-1.03162	-1.03163	-1.03163	-1.03163	-1.03163	-1.03163

2.6   Results and Discussion

2.6.1   Experimental study on function optimization

To evaluate the effectiveness of the ITHS algorithm, its performance is compared with the eight state-of-the-art HS variants. The algorithms for comparison are Harmony Search (HS), Improved Harmony Search (IHS), Global Harmony Search (GHS), Modified Harmony Search (MHS), Local-best Harmony Search algorithm with dynamic sub-populations (DLHS), Self-adaptive Global best Harmony Search (SGHS), Self-Adaptive Harmony Search (SAHS) and Explorative Harmony Search (EHS).

The parameters for the HS, IHS, and GHS algorithms are kept fixed and are the same as those in [114]. For the HS algorithm, *HMS = 5, HMCR = 0.9, PAR = 0.33* and *bw = 0.01*. For the IHS algorithm, *HMS = 5, HMCR = 0.9, PAR_{min} =0.1, PAR_{min} = 0.99, bw_{min} = 0.0001* and $bw_{max} = ({}_U x_i - {}_L x_i)/20$. For the GHS algorithm, *HMS = 5, HMCR = 0.9, PAR_{min} = 0.1* and *PAR_{max} = 0.99*. The parameters for the MHS algorithm are set as those in [70] with *HMS = 2N, HMCR = 0.98, PAR = 0.1, Nhm = 0.1 × HMS, Nm1 = 500* and *Nm2 = 200*. The parameters for the SAHS algorithm are set as those in [115] with *HMS = 50, HMCR = 0.99, PAR_{min} = 0* and *PAR_{max} =1*. The parameters for the DLHS algorithm are set as those in [91] with *HMS = 9*, $bw_{max} = ({}_U x_i - {}_L x_i)/200$, *bw_{min} = 0.0001, R = 50*, and *m = 3*. The parameters for the SGHS algorithm are set as those in [94] with *HMCRm = 0.98, PARm = 0.9*, $bw_{max} = ({}_U x_i - {}_L x_i)/10$, and *bw_{min} = 0.0005*. The parameters for the EHS algorithm are set as those in [116] with *HMS=50, HMCR = 0.99, PAR = 0.33* (same as the classical HS), and $bw = k\sqrt{Var(x)}$ with *k* = 1.17. The detailed descriptions of these algorithms can be found in their corresponding references.

All functions were implemented in 30 dimensions except for the two-dimensional Camel-back function. In the experiments, each problem was run for 30 independent replications, and each replication is allowed to run for 50,000 evaluations of the objective function (*Maxiter* = 50,000) when solving 30-dimensional problems and for 100,000 evaluations of the objective function (*Maxiter* = 100,000) when solving their 50-dimensional counter parts. However, in case of the SAHS algorithm, both 30- and 50-dimension problems are run for 100,000 evaluations, and in case of EHS, both 30 and 50 dimension problems are run for 400,000 evaluations.

2.6.2 Computational Results

In this section, the benchmark problems of different characteristics are used to evaluate the performance of the proposed algorithm, and the results obtained are compared with eight state-of-the-art HS variants. These benchmark problems provide a balance of unimodal, multimodal, shifted, shifted rotated and hybrid composite problems taken from the evolutionary computation literature [114, 125]. In Case 1, the proposed ITHS is applied to the typical benchmark problems described in Table 2.14 and compared with other variants of the HS algorithm. However, these typical benchmark problems are considered too simple. Therefore, in Case 2, shifted, shifted rotated and hybrid composite benchmark problems, as shown in Table 2.14, are used to evaluate the robustness of the proposed ITHS algorithm and compared with other variants of the HS algorithm. Furthermore, to evaluate the performance and efficiency of the proposed algorithm over larger dimension problems, the scalability study is also conducted, and the numerical results obtained are compared with other variants of the HS algorithm in Case 3.

2.6.3 Case 1: Typical Benchmark Problems

The variants of the HS algorithm are applied to the typical benchmark problems as given in Table 2.14. The dimension of the benchmark problems is 30, except for the two-dimensional Camel-back problem. To evaluate the performance of an algorithm on a benchmark problem, the following performance metrics are considered: (a) the quality of the final solution and (b) the convergence speed (measured in terms of the number of evaluations/iterations) and the success rate [116].

A.   Comparison of Quality of Solution

The Average Error (AE) and the Standard Deviation (SD) of each benchmark problem are calculated for 30 independent runs. AE is computed using (2.21).

$$AE = \frac{\sum_{j=1}^{30} \left| f\left(\overrightarrow{x_{Best}^{j}}\right) - f_{min}^{*} \right|}{30} \tag{2.21}$$

where $\overrightarrow{x_{Best}^{j}}$ is the final solution vector corresponding to the jth run and $f\left(\overrightarrow{x_{Best}^{j}}\right)$ is the value of the benchmark problem corresponding to that final solution vector. The actual optimum of a particular benchmark problem is given by f_{min}^{*}. The AE, and the SD of the typical benchmark problems ($f_1 - f_9$) for various variants of HS are given in Table 2.16. To determine whether the results obtained by the ITHS algorithm are significantly different from those obtained by other variants of the HS algorithm, a nonparametric statistical test, called Wilcoxon's rank sum test (*t-test*) for independent samples [127, 128], is conducted at the 5% significance level for ITHS algorithm against the final results of other variants of the HS algorithm. The results of the *t-test* are reported in Table 2.15. In Table 2.15, a value equal to 1 or −1 indicates that the results obtained by the former algorithm are significantly better or worse than those by the later one, while a value equal to zero implies that the results obtained by the two compared algorithms are not significantly different.

It is evident from Table 2.15 that ITHS performs better than most of the HS variants over all the benchmark problems with 30 dimensions and at lower dimensions for the Camel-back problem. As shown in Table 2.15, for 7 out of 9 functions, ITHS alone achieved the mean best final accuracy, with better performance than all the competitor algorithms in a statistically significant manner (in 5% significance level). However, in two cases, f_3 and f_7, EHS outperformed ITHS. EHS also performed better than HS, IHS, GHS, MHS, SAHS, DLHS, and SGHS.

The convergence of the variants of the HS algorithm for different benchmark functions is shown in Figs. 2.14-2.22. It is evident from the Figs. 2.14-2.22 that the ITHS algorithm converges much faster when compared with other variants of the HS algorithm.

TABLE 2.14. Shifted and Shifted Rotated Benchmark Problems

Function	Function range	$(\vec{x})$	f^*_{min}
Shifted Sphere (CEC 2005 $F1$) $$f_{10}(\vec{x}) = \sum_{i=1}^{N} z_i^2 + f_{bias_1}$$ where $z = x - o$	$-100 \leq x_i \leq 100$	$o = \{o(1), o(2) ..o(n)\}$	$f_{bias_1} = -450$
Shifted Schwefel's Problem 1.22 (CEC 2005 $F2$) $$f_{11}(\vec{x}) = \sum_{i=1}^{N} \left(\sum_{j=1}^{i} z_j \right)^2 + f_{bias_2}$$ where $z = x - o$	$-10 \leq x_i \leq 10$	$o = \{o(1), o(2) ..o(n)\}$	$f_{bias_2} = -450$
Shifted Rosenbrock (CEC 2005 $F6$) $$f_{12}(\vec{x}) = \sum_{i=1}^{N} (100(z_{i+1} - x_i^2)^2 \ + (z_i - 1)^2 + f\_bias_6$$ where $z = x - o + 1$	$-30 \leq x_i \leq 30$	$o = \{o(1), o(2) ..o(n)\}$	$f_{bias_6} = 390$
Shifted Rastrigin (CEC 2005 $F9$) $$f_{13}(\vec{x}) = \sum_{i=1}^{N} (z_i^2 - 10\cos(2\pi z_i) + 10) + f\_bias_9$$ where $z = x - o$	$-5 \leq x_i \leq 5$	$o = \{o(1), o(2) ..o(n)\}$	$f\_bias_9 = 330$
Shifted Rotated High Conditional Elliptic (CEC 2005 $F3$) $$f_{14}(\vec{x}) = \sum_{i=1}^{N} (10^6)^{\frac{i-1}{N-1}} . (z_i)^2 + f\_bias_3$$ where $z = (x - o)M$; M is the linear transformation matrix	$-100 \leq x_i \leq 100$	$o = \{o(1), o(2) ..o(n)\}$	$f_{bias_3} = -450$
Shifted Rotated Griewank's function without bounds (CEC 2005 $F7$) $$f_{15}(\vec{x}) = \frac{1}{4000} \sum_{i=1}^{N} z_i^2 - \prod_{i=1}^{N} \cos\left(\frac{z_i}{\sqrt{i}}\right) + 1 + f\_bias_7$$ where $z = (x - o)M$; M is the linear transformation matrix	$-100 \leq x_i \leq 100$	$o = \{o(1), o(2) ..o(n)\}$	$f_{bias_7} = -180$
Rotated Hybrid Composition Function CF1 $f_{15}(\vec{x})$ =Marked as F16 in CEC2005 benchmark problem set.	$-5 \leq x_i \leq 5$	-	$f_{bias_{16}} = 10$
Rotated Hybrid Composition Function CF2 $f_{15}(\vec{x})$ =Marked as F18 in CEC2005 benchmark problem set.	$-5 \leq x_i \leq 5$	-	$f_{bias_{18}} = 10$

TABLE 2.15. The t-test results of comparing ITHS with the other HS algorithms

t-Test for ITHS vs.	f_1	f_2	f_3	f_4	f_5	f_6	f_7	f_8	f_9
HS	1	1	1	1	1	1	1	1	1
IHS	1	1	1	1	1	1	1	1	1
GHS	1	1	1	1	1	1	1	1	1
SAHS	1	1	1	1	1	1	1	1	1
MHS	1	1	1	1	1	1	1	1	1
DLHS	1	1	1	1	1	1	1	1	1
SGHS	1	1	1	1	1	1	1	1	1
EHS	1	1	-1	1	1	1	-1	1	1
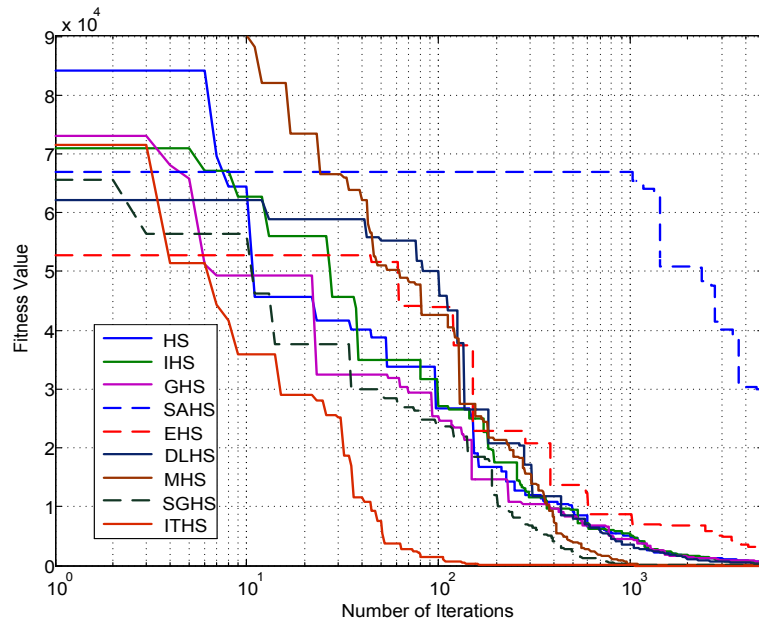
Fig. 2.14 Convergence of Sphere Function for 30 dimensions
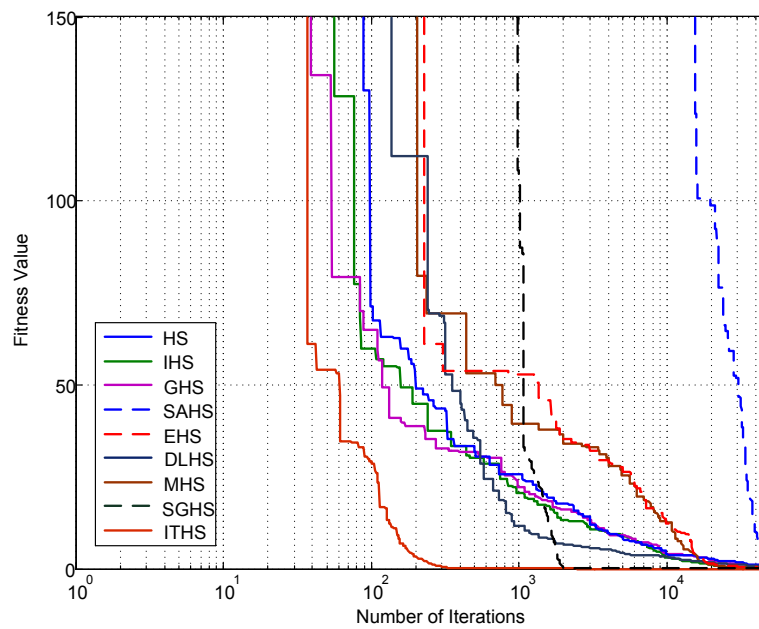
Fig. 2.15 Convergence of Schwefel's Problem 2.22 for 30 dimensions
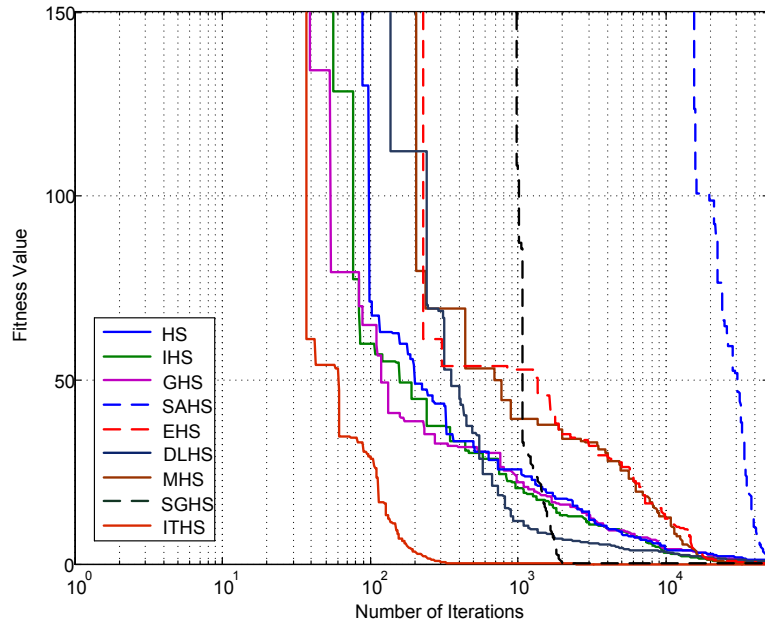
Fig. 2.16 Convergence of Schwefel's Problem 2.22 for 30 dimensions
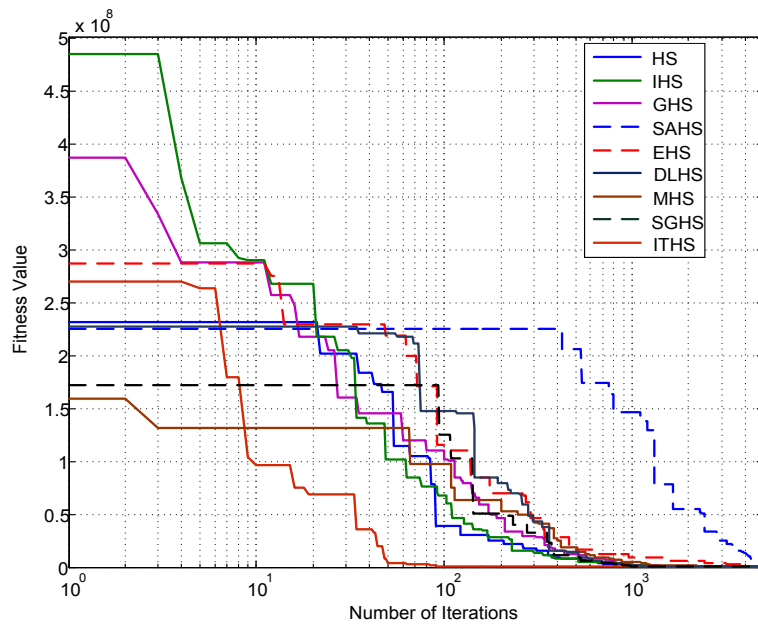
Fig. 2.17 Convergence of Rosenbrock Function for 30 dimensions
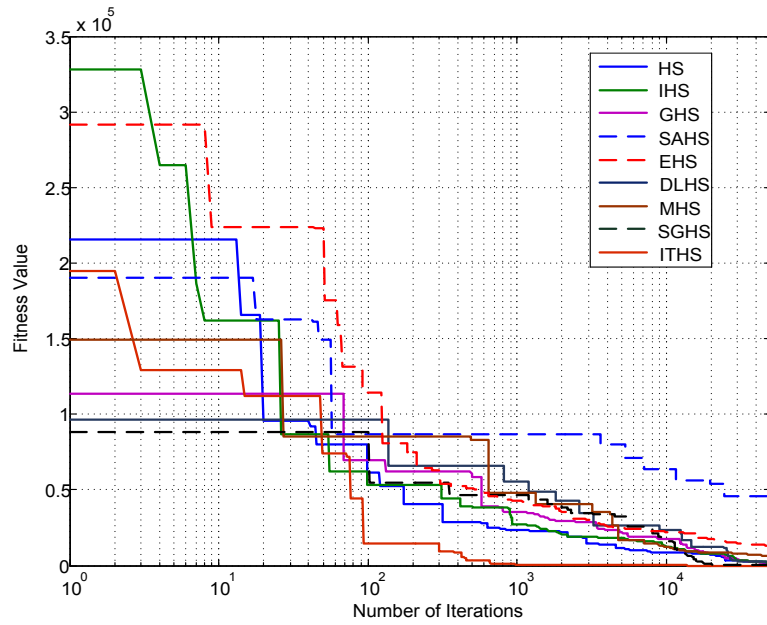
Fig. 2.18 Convergence of Rotated Hyper-Ellipsoid Function for 30 dimensions
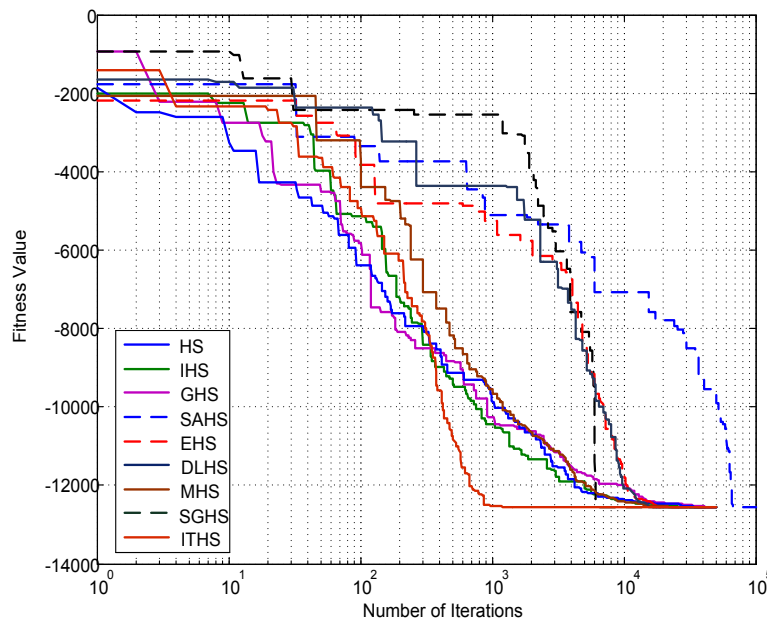
Fig. 2.19 Convergence of Generalised Schwefel's 2.26 Problem for 30 dimensions
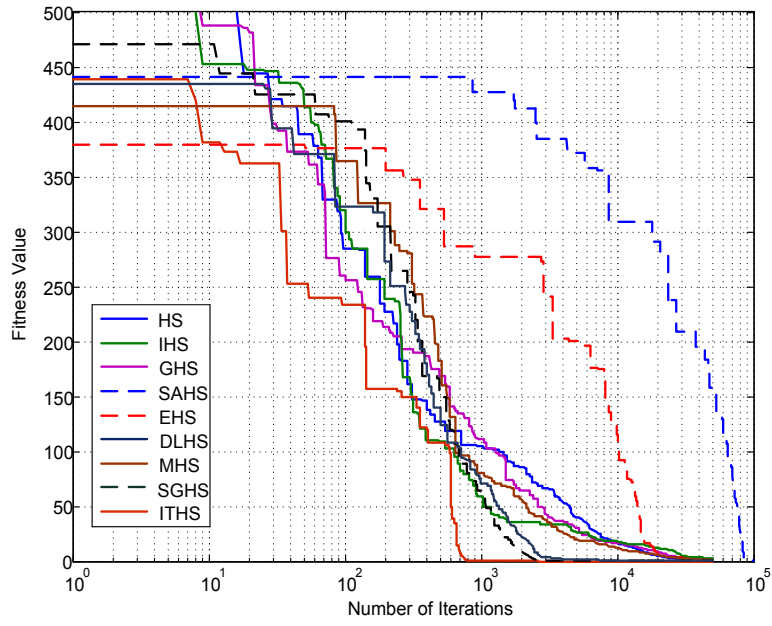
Fig. 2.20 Convergence of Rastrigin Function for 30 dimensions
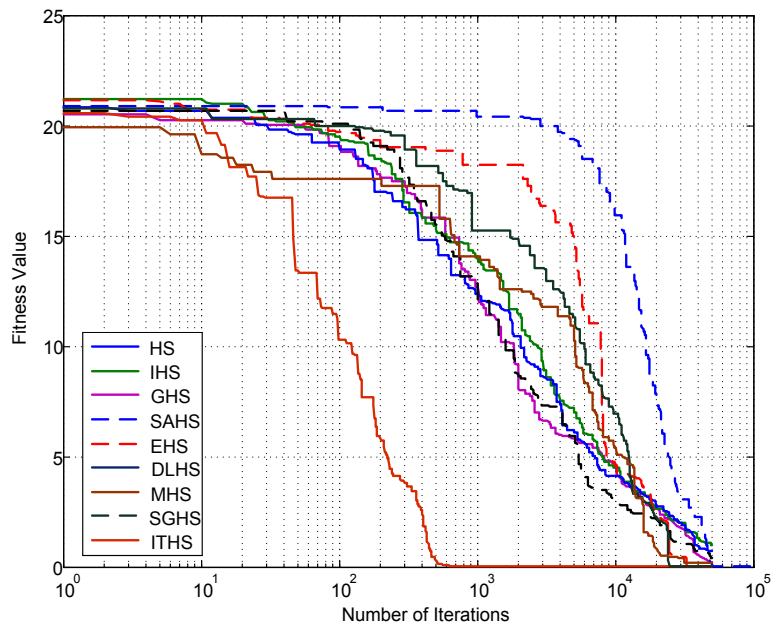
Fig. 2.21 Convergence of Ackley's Function for 30 dimensions
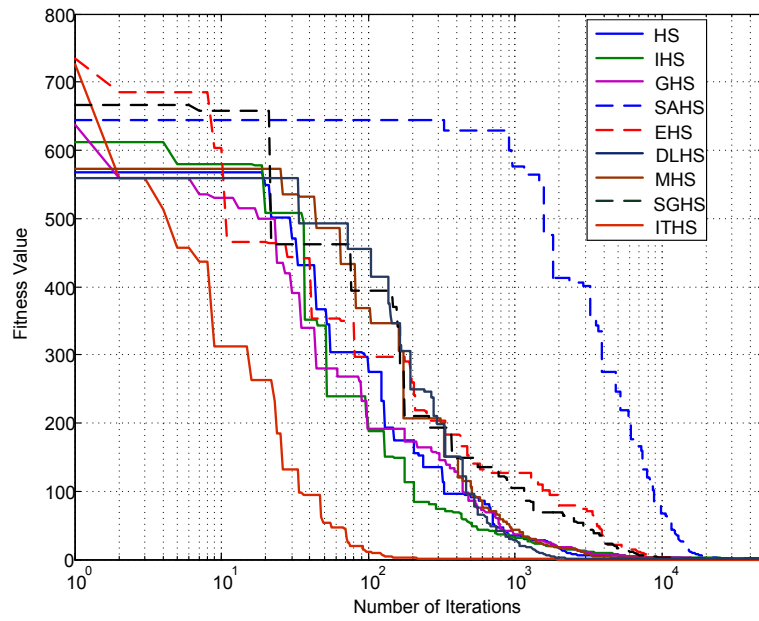
Fig. 2.22 Convergence of Griewank Function for 30 dimensions
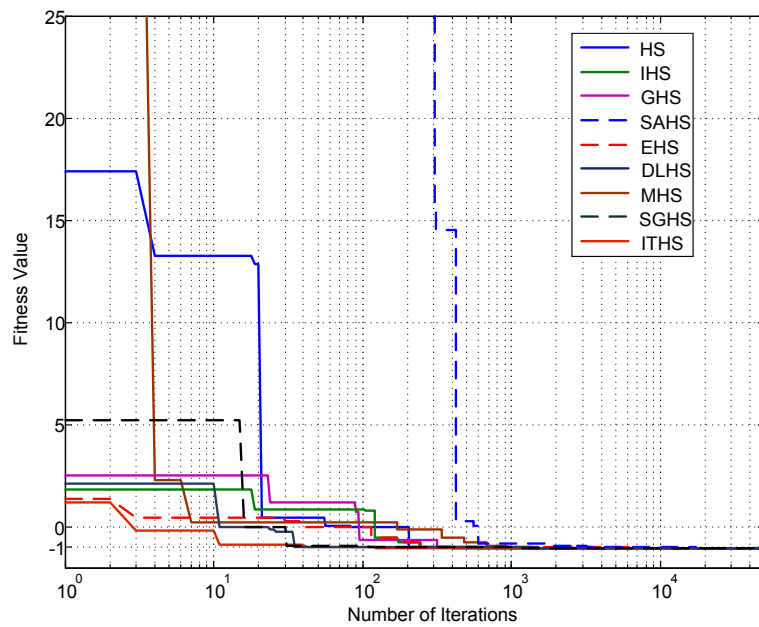
Fig. 2.23 Convergence of Camel-Back Function

B. Comparison of the Convergence Speed and Success Rate

To compare the convergence speed of different algorithms, a threshold value of the error for each benchmark problem is selected. For functions $f_1 - f_9$, this threshold is fixed at *1e-5*. For all test functions, the algorithms carry out 30 independent runs. Each algorithm is run on a function and is terminated as soon as the best error value determined by the algorithm falls below the predefined threshold (*1e-5*) or the number of iterations satisfy the termination criterion ($Maxiter$). A run is considered successful if the best error value determined by the algorithm falls below the predefined threshold (*1e-5*). In Table 2.17, the number of successful runs, mean and standard deviation of the number of iterations for each successful run are shown. A lower value of mean iterations corresponds to faster convergence of an algorithm. It is evident from Table 2.17 that the convergence of the ITHS algorithm is fastest when compared with other variants of HS algorithm. Therefore, the computational time required to find the optimal solution is minimal for the ITHS algorithm when compared with other variants of the HS algorithm. In addition, the percentage of successful runs for the ITHS algorithm is 100% for 8 of the 9 benchmark problems considered. For 7 benchmark problems, both EHS and ITHS have a 100% success rate. In the case of the Rosenbrock function (f_3), the success rate of EHS is higher when compared with that of ITHS. However, the mean number of iterations for EHS is higher than that of the ITHS algorithm. The results obtained from the experiments prove that the proposed ITHS algorithm provides higher robustness (i.e., the ability to produce similar results over repeated runs on a single problem) as well as faster convergence speed when compared with eight state-of-the-art HS variants.

2.6.4 Case 2: Shifted, Shifted Rotated and Hybrid Composite Benchmark Problems.

In this section, shifted, shifted rotated and hybrid composite benchmark problems described in Table 2.14 are evaluated for the ITHS algorithm and compared with eight state-of-the-art HS variants. The AE and SD of the benchmark problems ($f_{10} - f_{17}$) for various variants of HS algorithm are given in Table 2.18. It is evident from 2.18 that the proposed ITHS algorithm retained its position as the best performer even when applied to shifted, shifted rotated and hybrid composite benchmark problems.

2.6.5 Case 3: Scalability study

When the dimension of the functions increases from 30 to 50, the performance of the different methods considered deteriorates, as shown in Table 2.19. The Average Error (AE) and the standard deviation (SD) of the benchmark problems ($f_1 - f_9$) for 50 dimensions for various variants of HS are given in Table 2.19. It is evident from Table 19 that the proposed ITHS algorithm is still the best performer and performs better even for a wide scale of dimensions of the problem.

Table 2.16. Mean and Standard Deviation (SD) of the benchmark function optimisation results (N=30)

Function		Sphere	Schwefel's 2.22	Rosenbrock	Rotated-hyper	Schwefel's 2.26	Rastrigin	Ackley	Griewank	Camel-back
HS	AE	1.87E−04	1.72E−01	3.40E+02	4.30E+03	3.03E+01	1.39E+00	1.13E+00	1.12E+00	5.00E−07
	SD	3.20E−05	7.29E−02	2.67E+02	1.36E+03	1.20E+01	8.24E−01	4.07E−01	4.12E−02	6.934E−011
IHS	AE	7.12E−04	1.10E+00	6.24E+02	4.31E+03	3.45E+01	3.50E+00	1.89E+00	1.12E+00	5.00E−07
	SD	6.44E−04	1.81E−01	5.60E+02	1.06E+03	1.04E+01	1.18E+00	3.15E−01	4.09E−02	1.572E−12
GHS	AE	1.00E−05	7.28E−02	4.97E+01	5.15E+03	4.17E−02	8.63E−03	2.09E−02	1.02E−01	2.85E−05
	SD	2.20E−05	1.15E−01	5.92E+01	6.35E+03	5.04E−02	1.53E−02	2.17E−02	1.76E−01	1.80E−05
SAHS	AE	6.92E−07	8.53E−04	2.65E+01	5.65E+03	6.00E−01	2.48E−03	7.81E−04	8.45E−05	4.66E−03
	SD	1.10E−06	2.55E−03	5.68E−01	2.34E+03	9.86E−01	8.42E−03	4.66E−04	2.38E−04	3.93E−07
MHS	AE	2.762E−05	1.258E−02	1.32E+02	5.48E+03	1.342E−02	7.157E−02	6.025E−03	1.00E+00	5.774E−08
	SD	8.937E−06	1.887E−03	1.64E+02	2.21E+03	6.963E−05	2.520E−01	1.947E−03	3.007E−05	1.354E−08
DLHS	AE	1.299E−09	1.23E−04	2.28E+02	9.03E+02	6.79E−03	1.86E+00	1.91E+00	1.00E+00	4.65E−08
	SD	2.766E−09	2.268E−04	2.51E+02	4.66E+02	6.91E−03	1.34E+00	6.838E−01	1.166E−06	1.531E−13
SGHS	AE	1.89E−06	1.02E−04	1.51E+02	1.18E+01	4.02E−03	1.77E−02	4.84E−01	5.05E−02	5.00E−07
	SD	4.22E−05	1.70E−05	1.31E+02	7.45E+00	6.24E−03	6.75E−02	3.57E−01	3.54E−02	7.22E−07
EHS	AE	1.65E−16	2.13E−12	**9.23E-03**	2.16E-19	1.64E−02	8.15E−14	**1.56E-15**	1.27E−23	1.64E−11
	SD	6.25E−17	4.52E−13	**7.20E-04**	8.22E-18	2.79E−02	9.06E−13	**2.75E-15**	6.32E−24	4.20E−12
ITHS	AE	**3.00E-256**	**1.13E-219**	1.90E+01	**4.32E-270**	**1.34E-12**	**0**	4.91E−15	**0**	**1.76E-16**
	SD	**0**	**0**	1.32E+01	**0.00E+00**	**3.79E-12**	**0**	1.74E−15	**0**	**4.74E-16**

Table 2.17. Number of successful runs, mean number and standard deviation of iterations, required to converge to the threshold error limit over the successful runs for functions f_1 to f_9

Functions		Sphere	Schwefel's 2.22	Rosenbrock	Rotated-hyper	Schwefel's 2.26	Rastrigin	Ackley	Griewank	Camel-back
HS	SR	3	0	0	0	0	0	0	0	20
	Mean	2.143E+04	-	-	-	-	-	-	-	3.923E+02
	SD	1.071E+03	-	-	-	-	-	-	-	7.363E+02
IHS	SR	7	0	0	0	0	0	0	0	22
	Mean	1.910E+04	-	-	-	-	-	-	-	3.623E+02
	SD	9.571E+02	-	-	-	-	-	-	-	6.914E+02
GHS	SR	15	2	0	0	2	0	0	0	7
	Mean	1.160E+04	4.691E+04	-	-	2.415E+04	-	-	-	4.418E+02
	SD	1.674E+03	1.076E+03	-	-	9.520E+02	-	-	-	3.134E+02
SAHS	SR	19	5	0	0	0	3	5	4	3
	Mean	3.158E+04	5.329E+04	-	-	-	8.482E+04	6.532E+04	3.451E+04	1.223E+04
	SD	1.869E+04	3.738E+03	-	-	-	3.013E+03	6.388E+03	7.060E+03	3.725E+02
MHS	SR	16	3	0	0	3	0	3	0	25
	AE	2.054E+03	3.438E+04	-	-	2.029E+04	-	2.753E+04	-	8.464E+03
	SD	1.353E+03	1.068E+03	-	-	1.163E+03	-	4.936E+03	-	1.334E+03
DLHS	SR	25	7	0	0	4	0	0	0	26
	Mean	1.237E+04	4.371E+04	-	-	1.892E+04	-	-	-	3.183E+02
	SD	1.761E+03	5.816E+03	-	-	1.472E+03	-	-	-	5.245E+02
SGHS	SR	17	7	0	0	3	3	0	0	17
	Mean	1.868E+03	1.543E+03	-	-	6.415E+03	4.625E+03	-	-	3.146E+02
	SD	1.056E+03	9.452E+02	-	-	8.823E+02	1.533E+03	-	-	3.264E+02
EHS	SR	30	30	**19**	30	26	30	30	30	30
	Mean	2.858E+04	5.186E+04	1.327E+06	1.597E+05	2.843E+04	4.217E+04	4.868E+04	2.736E+04	4.519E+02
	SD	4.859E+03	2.563E+03	1.128E+05	4.895E+04	2.531E+03	1.340E+04	1.975E+03	1.084E+04	3.677E+02
ITHS	SR	**30**	**30**	17	**30**	**30**	**30**	**30**	**30**	**30**
	Mean	**798**	**1.0615E+03**	**1.2062E+04**	**1.0010E+04**	**1.3401E+03**	**4.0105E+03**	**1.2128E+03**	**1.0236E+03**	**234**
	SD	**112**	**122.6549**	**3.6630E+03**	**2.9890E+03**	**655.4569**	**6.1642E+03**	**451.1726**	**217.1285**	**56**

Table 2.18. Mean and Standard Deviation (SD) of error for shifted and shifted rotated benchmark functions (f₁₀ to f₁₇)

Functions		Shifted Sphere	Shifted Schwefel's 1.2	Shifted Rosenbrock	Shifted Rastrigin	Shifted rotated High conditional Elliptic function	Shifted Rotated Griewank	Rotated hybrid Composition function CF1	Rotated hybrid Composition function CF2
HS	AE	6.440E+00	3.888E+03	3.401E+03	8.710E−01	1.500E+07	4.080E+03	3.448E+02	7.739E+03
	SD	2.777E+00	1.115E+03	3.272E+03	8.086E−01	4.456E+06	5.733E+00	2.581E+02	4.192E+03
IHS	AE	4.629E−07	4.068E+03	1.731E+03	1.777E+00	1.466E+07	3.385E+03	4.738E+02	1.742E+04
	SD	1.275E−07	1.735E+03	2.951E+03	8.080E−01	6.682E+06	8.983E+01	1.828E+01	5.872E+03
GHS	AE	1.803E+03	1.889E+04	3.505E+07	6.673E+01	6.830E+07	4.075E+03	5.758E+02	1.204E+04
	SD	3.618E+02	4.538E+03	2.214E+07	9.356E+00	2.550E+07	2.127E+01	1.558E+02	1.003E+01
SAHS	AE	3.176E-04	8.175E+03	4.647E+04	1.462E+01	5.816E+06	9.163E-01	2.315E+01	1.052E+03
	SD	5.511E-04	8.941E+02	5.683E+04	3.751E+00	4.538E+05	7.971E-01	1.941E+01	1.142E+03
MHS	AE	2.701E−05	6.861E+03	2.514E+04	7.893E+00	1.849E+07	3.895E+03	4.093E+02	2.647E+03
	SD	1.086E−05	2.426E+03	1.582E+04	2.219E+00	5.311E+06	1.170E+02	1.777E+01	8.253E+02
DLHS	AE	2.443E−07	2.844E+03	3.779E+03	1.578E+00	3.194E+06	9.677E+02	2.169E+02	6.546E+02
	SD	1.331E−06	1.767E+03	4.838E+03	1.500E+00	1.720E+06	2.213E+02	1.931E+01	8.634E+01
SGHS	AE	2.700E−05	6.861E+03	2.514E+04	7.893E+00	1.849E+07	3.895E+03	1.138E+02	5.621E+02
	SD	1.086E−05	2.426E+03	1.582E+04	2.219E+00	5.311E+06	1.170E+02	8.034E+01	7.321E+01
EHS	AE	4.343E-11	1.667E-09	**4.183E-01**	1.818E-06	5.024E+01	1.007E-05	1.103E+02	4.359E+02
	SD	3.866E-12	2.943E-10	**1.7360E-02**	5.927E-07	8.008E+01	2.064E-06	2.029E+00	7.261E+01
ITHS	AE	**1.379E-253**	**4.23E-215**	2.780E+01	**4.32E-267**	**1.784E-12**	**7.655E-264**	**8.921E+01**	**1.329E+02**
	SD	**0**	**0**	2.12E+01	**0**	**8.859E-13**	**0**	**4.393E+00**	**6.166E+01**

67

Table 2.19. Mean and Standard Deviation (SD) of error for the benchmark functions (N=50)

Functions		Sphere	Schwefel's 1.2	Rosenbrock	Rotated-Hyper	Schwefel's 2.26	Rastrigin	Ackley	Griewank
HS	AE	1.9838E+02	5.4924E+00	6.182E+03	2.1353E−04	2.5888E+02	1.8948E+01	3.9473E+00	2.7121E+00
	SD	4.6205E+01	8.0736E+01	1.8262E+03	4.8059E−03	2.5853E+02	2.8401E+00	5.1082E+01	3.7346E+01
IHS	AE	1.7110E−02	3.8088E+00	5.7066E+03	2.0740E+04	3.4365E+02	2.3440E+01	4.9922E+00	2.7467E+00
	SD	4.3559E−01	6.4557E+01	2.0121E+03	4.2946E−03	3.4134E+02	3.5944E+00	1.0520E+00	3.4875E+01
GHS	AE	3.8651E+01	1.6919E+01	1.7149E+02	5.114E+04	2.8948E+02	1.0485E+01	1.1646E+03	1.0030E+00
	SD	4.0509E+01	1.5220E+01	2.0658E+02	1.7656E+04	2.2361E+02	1.5098E+01	1.0240E+03	2.9627E+03
SAHS	AE	3.0642E−03	9.7440E+02	8.5037E+01	7.3041E+04	4.3279E+04	2.2427E−01	5.8496E+04	1.3329E+04
	SD	4.169E-03	1.4145E+02	2.1323E+01	1.5697E+03	3.7670E+05	3.1756E−01	7.6511E+05	4.4163E+04
MHS	AE	6.3956E−04	8.6342E+02	1.0459E+02	1.0894E+04	4.2382E+05	2.3664E+01	1.3337E+06	1.0000E+00
	SD	1.4595E−04	1.2312E+02	3.9649E+01	2.1879E+03	4.6895E+05	3.4136E+01	1.1498E+06	0.0000E+00
DLHS	AE	6.6347E−10	9.5587E+05	3.1156E+02	3.7343E+03	3.5797E+08	3.4029E+00	8.4042E+01	1.0000E+00
	SD	7.5476E−10	5.0373E+05	4.4759E+02	1.9876E+03	3.3806E+08	3.4956E+00	1.1754E+00	2.5370E+07
SGHS	AE	3.1493E−06	2.3158E+04	4.3415E+02	3.5214E+04	1.3423E+02	2.2457E+01	5.6345E+01	6.4025E+02
	SD	2.4175E−06	6.1270E+05	2.5298E+02	3.4232E+04	1.4532E+03	1.3772E+01	4.5746E+01	4.4324E+02
EHS	AE	1.575E-12	6.139E-07	**1.166E-03**	3.280E-15	1.623E+01	4.478E-12	**2.629E+15**	5.082E+15
	SD	3.431E-12	8.696E-09	**2.585E-04**	3.560E-15	2.091E+02	1.308E-12	**2.287E+16**	5.345E+15
ITHS	AE	**2.4318E-220**	**4.0335E-153**	3.5032E+01	**4.3270E-118**	**1.3622E-7**	**9.4017E-15**	4.9653E+15	**0**
	SD	**0**	**1.3337E-152**	2.6416E+01	**1.7914E-117**	**4.2008E-12**	**2.1083E-14**	3.0375E+15	**0**

2.7   Conclusions

In this Chapter, an intelligent tuned harmony search algorithm is proposed to enhance the performance and efficiency of the HS algorithm. The proposed ITHS algorithm borrows the concepts from the decision making in a group. The self-adaptive pitch adjustment strategy adopted by the dynamic sub-populations based on the consciousness (Harmony Memory) helps the algorithm in maintaining the proper balance between diversification and intensification throughout the search process. The self-adaptive pitch adjustment strategy not only alleviates the difficulties of parameter setting but also enhances the precision of the obtained solution. However, the performance of the proposed ITHS algorithm is influenced by a few other parameters, such as harmony memory size (HMS) and harmony memory considering rate ($HMCR$). The effects of varying these parameters on the performance of the ITHS algorithm is also analysed in detail. It is evident from the numerical results of the experiments, that the benchmark problems have the minimum value for $HMCR$ of 0.99 for different values of the HMS. Therefore, $HMCR$ is chosen as 0.99. Similarly, the HMS is chosen near 10 for 30 dimensions and, in case of lower dimensions like the Camel-back function, an appropriate value of HMS is approximately 50. The proposed ITHS algorithm is evaluated for the typical benchmark problems and with eight state-of-the-art HS variants. The numerical results obtained indicate that the proposed ITHS algorithm offers better performance compared with the eight state-of-the-art HS variants. However, these typical benchmark problems are considered too simple. Therefore, shifted, shifted rotated and hybrid composite benchmark problems are used to evaluate the robustness of the proposed ITHS algorithm, and the results obtained are compared with other variants of HS. Furthermore, to evaluate the performance and efficiency of the proposed algorithm on larger dimension problems, a scalability study is also conducted, and the results are compared with other variants of HS. Finally, the numerical results reflect

the superiority of the proposed ITHS algorithm in terms of accuracy, convergence speed, and robustness when compared with other state-of-the-art HS variants. Therefore, the proposed ITHS algorithm, in contrast to other variants of the HS algorithm, has a better balance of diversification and intensification and converges to a better solution in fewer iterations. The lower number of setting parameters and fast convergence makes it an ideal method when dealing with complex engineering optimisation problems.

CHAPTER 3. OPTIMAL SCHEDULING OF THE DIESEL GENERATORS IN SEMI-SUBMERSIBLE OIL RIG PLATFORMS

3.1   Introduction

The oil rig platform is powered through an on board pool of diesel generators. Since, the load requirements of the rig are governed by disturbances, which are stochastic in nature and most of the time the load is less than 50% of the full load [17, 18]. The optimum generation scheduling of available generators to minimize the total fuel consumption while satisfying the load demand and operational constraints plays an important role in improving the power density and efficiency of the oil rig. Over the past few years, a number of approaches have been developed, to improve the efficiency and reduce the fuel consumption of marine vessels [17-22].

The fuel consumption of the diesel generators is generally governed by the specific fuel consumption curves, which characteristically don't differ for different manufacturers [23]. The key feature for this discourse is that lightly loaded generators are much less efficient than more heavily loaded units. Moreover, the increase in specific fuel consumption with a decrease in load tends to be much larger below about 50% load than above 50% load [23-25]. Therefore, one should distribute the maximum load for some of generators and keep others idle.

The accurate modeling of the fuel consumption is essential to optimally schedule the generators. Therefore, cubic spline interpolation has been used to model the SFC curve [129]. The traditional power management system (PMS) monitors the total power demand and compares it to the available supply. The system can automatically start and stop generator sets to coincide with the load changes in accordance with the pre-set load

dependent start-stop tables [18, 130].

In recent years, various methods for the optimal scheduling of the generators have been developed [131-135]. The classical optimization methods are highly sensitive to starting points and frequently converge to local optimum solution or diverge altogether. There are two kinds of classical optimization techniques: direct search method and gradient search method [62, 65, 136]. In direct search method only the objective function and constraints are used for search procedure whereas in gradient search method the first order and/or second order derivatives are used for search procedure. Direct search methods are very slow because of requirement of many function iterations whereas the gradient search methods are faster but they are inefficient on discontinuous and non-differentiable functions. Furthermore both the methods seek local optima. Thus, starting the search in the vicinity of local optima will cause us to miss the global optima [62, 65, 136]. In order to eradicate some of the above mentioned difficulties, ITHS algorithm is applied to find the optimal solution.

The rest of this Chapter is arranged in following sections. Section 3.2 provides an overview of the practical oil rig platform. The principles of modeling of specific fuel consumption curve using cubic spline interpolation are presented in Section 3.3. The insight into these principles will help the reader in understanding the motivation for following an engineering approach for optimal scheduling of the diesel generators. The optimization problem is then formulated in Section 3.4. Two case studies are considered and the results obtained from the two case studies with detailed discussions are presented in Section 3.5. Finally, the conclusions of findings are provided in Section 3.6.

3.2   The Practical Oil Rig

This section provides an overview of the semi-submersible oil rig. Deep-water drilling and floating production have become possible with Dynamic Positioning (DP) or thruster-assisted position mooring. The thrusters used for station keeping (DP operation) typically also constitutes the main propulsion in transit and maneuvering of the vessel, either all or selected units only. The main difference between the marine and a land-based electrical power system is the fact that the marine power system is an isolated system with short distances from the generated power to the consumers. Fig.1 shows the schematic of the main power installations in a Keppel B280 Semi-Submersible oil rig with electric propulsion in a *Single Line Diagram (SLD)*. The rig is powered by a pool of 8 Wärtsilä 16V26A Diesel generators each of 4860 kVA power rating. The eight generators are connected in ring configuration to form the 11kV busbar. The 11kV busbar supplies the load to the eight thruster motors, located at the pontoon level of the oil rig and other auxiliary loads. The thruster motors generate the required thrust against the environmental disturbances to keep the drill pipe casing in its intended locality.

3.3   Modeling of specific fuel consumption

Accurate modeling of SFC is an important issue in the optimal scheduling of generators with fuel consumption as optimization function. The SFC modeling made earlier has used second or higher order polynomials and exponential functions and hence suffers from higher percentage of error [18, 134]. Cubic spline interpolation on the other hand accurately models the curve with minimum residues. Table 3.1 shows the specific fuel consumption as a fraction of its full power in pu for Wärtsilä 16V26A Diesel generator [25].

.
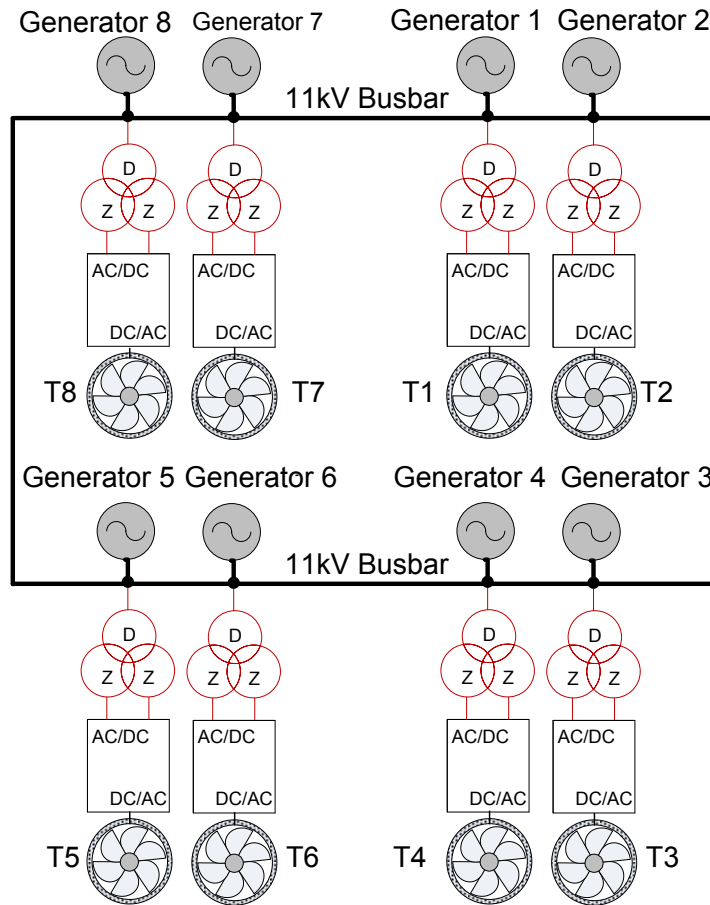
Fig. 3.1 Single Line Diagram of Thruster system.

It is evident from Table 3.1, that the data for specific fuel consumption is not available for starting (0% of the rated load) of the diesel generator. The value of the missing data can be determined by using the principle of extrapolation. Using the data from Table 3.1, the missing data using 2nd, 5th degree polynomials and Cubic spline function are entrapolated. In case of 5th degree polynomial the extrapolated value was found to be less than that at 0.25 pu load. Whereas, in reality the SFC curve for the diesel generator has the maximum specific fuel consumption at the starting. Therefore, higher degree of polynomials cannot be used for extrapolation and use of lower degree polynomials would give rise to higher error.

This problem can be overcome by use of cubic spline function. The specific fuel consumption at zero load or starting of diesel generator calculated using cubic spline is 289 g/kWh. Now, the data for the entire range from 0 pu to 1.1 pu load are available and can use interpolation techniques to find SFC accurately at any given load. Table 3.2 shows the norms of the residuals for the various methods used for curve fitting to determine the SFC. Spline interpolation is preferred over polynomial interpolation because the interpolation error can be made relatively smaller by using lower degree polynomials. Thus, avoiding the problem of Runge's phenomenon, that occurs when using higher degree polynomials. Cubic spline interpolation has been used to accurately find the SFC at any given load.

TABLE.3.1. SFC OF THE DIESEL GENERATOR AT DIFFERENT LOADS

Load (pu)	Specific Fuel Consumption (g/kWh)
0.25	233.12
0.50	201.00
0.75	192.98
0.85	195.20
0.90	195.51
1.0	196.55
1.1	199.11

TABLE.3.2. NORMS OF THE RESIDUALS FOR VARIOUS METHODS

Curve Fitting	Norms of the Residuals
Cubic Spline Interpolation	0
5th Degree polynomial	0.316
Quadratic polynomial	6.011

The mathematical (3.1)– (3.7) can be used to find the numerical value of the SFC at any given loading of the diesel generator.

For $0 \leq p_j < 0.25$

$$S(p_j) = 2.9512(p_j)^3 + 187.866(p_j)^2 + 270.67\, p_j + 289 \qquad (3.1)$$

For $0.25 \leq p_j < 0.50$

$$S(p_j) = 2.9512(p_j - 0.25)^3 + 190.08(p_j - 0.25)^2 - 176.184(p_j$$
$$- 0.25) + 233.12 \qquad (3.2)$$

For $0.50 \leq p_j < 0.75$

$$S(p_j) = 7.0041(p_j - 0.50)^3 + 192.293(p_j - 0.50)^2 - 80.591(p_j$$
$$- 0.50) + 201 \qquad (3.3)$$

For $0.75 \leq p_j < 0.85$

$$S(p_j) = -1.4424 \times 10^3 (p_j - 0.75)^3 + 197.546(p_j - 0.75)^2$$
$$+ 16.869(p_j - 0.75) + 192.98 \qquad (3.4)$$

For $0.85 \leq p_j < 0.90$

$$S(p_j) = 1.9401 \times 10^3 (p_j - 0.85)^3 + 235.158(p_j - 0.85)^2 + 13.10(p_j$$
$$- 0.25) + 195.2 \qquad (3.5)$$

For $0.90 \leq p_j < 1.0$

$$S(p_j) = 67.134(p_j - 0.90)^3 + 55.8598(p_j - 0.90)^2 + 4.1427(p_j$$
$$- 0.90) + 195.51 \qquad (3.6)$$

For $1.0 \leq p_j < 1.1$

$$S(p_j) = 67.134(p_j - 1.0)^3 + 76.0(p_j - 1.0)^2 + 17.328(p_j - 1.0)$$
$$+ 196.55 \qquad (3.7)$$

where p_j is the per unit load of generator j and $S(p_j)$ is the specific fuel consumption for

the generator j.

The specific fuel consumption curve is shown in Fig.3.2. It is evident that the SFC curve is smooth and almost linear till 0.66 as shown in section A of Fig.3.2 and non-linear between 0.66 to 1 pu load as shown in section B of Fig. 3.2.
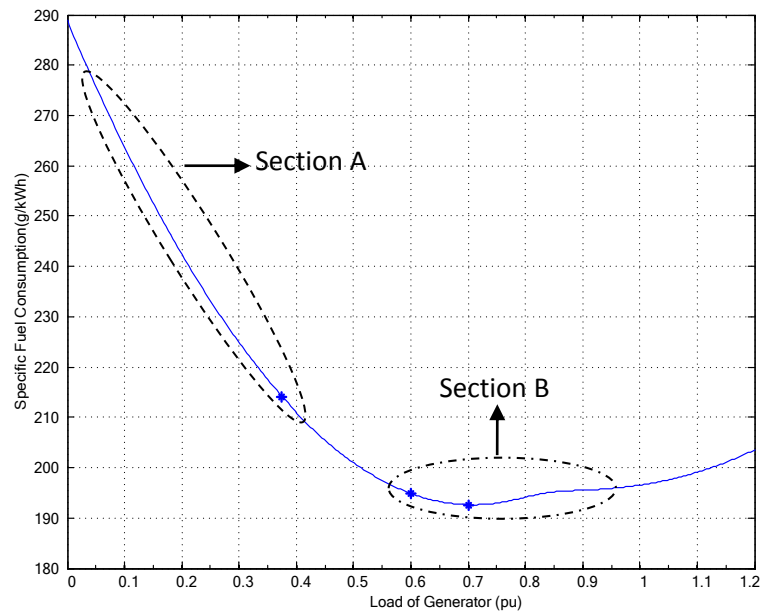
Fig. 3.2 Specific Fuel Consumption of the diesel Generator at different loads

3.4   Optimization problem formulation

The primary concern of an oil rig is to minimize the total fuel cost subjected to the operating constraints of a power system. The SFC curve in Fig.3.2 shows that the lightly loaded generators consume more fuel than more heavily loaded units. In a diesel electric system with several diesel engines it is hence an aim to keep the diesel engines loaded at their optimum operating conditions by starting and stopping generator sets dependent on the load, with an aim to keep the average loading of each running diesel engine closest possible to its optimum load point. The problem can be formulated mathematically; an oil rig with *N* number of diesel generators is being considered in this study. The rated power of each generator is given by (3.8)

$$\vec{P}^{MAX} = \left[P_1{}^{MAX}, P_2{}^{MAX}, \ldots\ldots, P_{(N-1)}{}^{MAX}, P_N{}^{MAX} \right] \tag{3.8}$$

For simplification the rating of each Generator is converted to per unit rating with the base of maximum rating generator. Let's assume that the rating of Nth generator is maximum then the rating of each generator to the base of maximum rating generator is given by (3.9).

$$\left(\vec{P}^{MAX}\right)' = \frac{\left(\vec{P}^{MAX}\right)}{\left(P_N{}^{MAX}\right)} \tag{3.9}$$

The total power demand for the oil rig at a particular instance is P_L. Let p_j denotes the power assigned to j^{th} Generator. The specific fuel consumption of Generator the jth denotes how much fuel is required to generate unit power at Generator the jth, and is denoted by $S(p_j)$ thus, the fuel consumed by the Generator j^{th} in one hour is given by (3.10)[6].

$$f(p_j) = S(p_j).p_j.\left(\vec{P}^{MAX}\right)' \tag{3.10}$$

The total fuel consumed by the oil rig in one hour is given by (3.11)

$$F(\vec{p}) = \sum_{j=1}^{N} f(p_j) = \sum_{j=1}^{N} \left[S(p_j).p_j.\left(\vec{P}^{MAX}\right)' \right] \tag{3.11}$$

The optimization problem is to minimize the total fuel consumption rate of the oil rig. Therefore, the optimization problem can be formulated as given by (3.12).

$$\text{Minimize}(F(\vec{p})) = \text{Minimize} \sum_{j=1}^{N} \left[S(p_j).p_j.\left(\vec{P}^{MAX}\right)' \right] \tag{3.12}$$

The generated power should be the same as the total load demanded by the oil rig and the generating power of each generator should lie between maximum and minimum limits. Since, the rating of each generator is in pu. The minimum limit ($_L p_j$) is 0 and the maximum limit ($_U p_j$) would be 1 pu. Hence, the main constraints of the minimization problem are given by (3.13-3.14).

The generated power should be the same as the total load demanded by the oil rig and the generating power of each generator should lie between maximum and minimum limits. Since, the rating of each generator is in pu. The minimum limit is 0 and the maximum limit would be 1 pu. Hence, the main constraints of the minimization problem are given by (3.13-3.14).

$$P_L = \sum_{j=1}^{N} p_j \cdot \left(\vec{P}^{MAX}\right)' \tag{3.13}$$

$$_LP_j \le P_j \le {_U}P_i, where, {_L}P_j = 0 \ and \ {_U}P_j = 1 \tag{3.14}$$

3.5 Results and discussions

The implementation of ITHS algorithm for optimal power generation scheduling of the diesel generators along with other conventional algorithms and evolutionary algorithms is presented in this section. The specific fuel consumption of the diesel generator increases with decrease in load as shown in Fig.3.2. Also the increase in specific fuel consumption with a decrease in load tends to be much larger below about 50% load than above 50% load. By optimally scheduling the generators at different loads the fuel consumption of the generators can be reduced.

In order to evaluate the effectiveness and performance of ITHS algorithm, its performance with Mincon method (Sequential Quadratic Programming), MinMax method, Harmony Search (HS), Improved Harmony Search (IHS), and Genetic Algorithm is compared. The parameters for the HS, IHS algorithm values are fixed as the same as those reported in [7, 112] and parameters of ITHS algorithm are then same as those reported in Chapter 2. For the HS algorithm, $HMS = 5$, $HMCR = 0.9$, $PAR = 0.33$ and $bw = 0.01$. For the IHS algorithm, $HMS = 5$, $HMCR = 0.9$, $PAR_{min} = 0.1$, $PAR_{max} = 0.99$, $bw_{min} = 0.0001$ and $bw_{max} = \left(\overline{x}_i - \underline{x}_i\right)/20$. For the ITHS algorithm, $HMS = 10$, $HMCR = 0.99$, $PAR_{min} = 0$, PAR_{max}

=1. According to [135] , the default values of GA parameters are: 20 individuals per generation, 10% of elite individuals, crossover probability is 0.5, rank fitness scaling, roulette selection, and scattered crossover operators. The detailed description of these algorithms can be found in the corresponding references. Since, evolutionary algorithms are heuristic in nature, so, 50 trials are performed to obtain the best solution for the evolutionary algorithms.

Two cases have been considered for the optimization of the scheduling of the diesel generators a) Diesel generators with equal rating. b) Diesel Generators with unequal ratings.

3.5.1   Case-I: Diesel generators with equal rating

Keppel's B280 semi-submersible oil rig is used as the case study oil rig. The oil rig is powered by 8 equal rating Wärtsilä 16V26 diesel generators. For equally rated units; the same SFC curve has been assumed. The Maximum load of each generator has been assumed as 4960 kW; the load of each generator has been converted to per unit. So, the maximum load of each generator is 1 pu. Since, the oil rig model considered has 8 generators and the installed generating capacity has been assumed equal to the total installed load of all consumers and losses in the system. The maximum total load demanded by the oil rig would be 8 pu.

Let's assume that the load demanded by oil rig is 3 pu. The convergence of the best fitness values for the objective function at a load of 3 pu using HS, IHS and ITHS algorithm are shown in Fig.3.3. In Fig.3.3, it can be seen that ITHS converges faster than HS and IHS algorithms. The self-adaptive pitch adjustment strategy adopted by the dynamic sub-populations based on the consciousness (Harmony Memory) helps the ITHS algorithm in maintaining the proper balance between diversification and intensification throughout the search process as compared to HS and IHS algorithm. The self-adaptive pitch adjustment

strategy not only alleviates the difficulties of parameter setting but also enhances the precision of the obtained solution. Similarly in IHS algorithm, variables *PAR* and *bw* explores the search space more widely and efficiently as compared to HS algorithm. The scheduling of the various generators at a load of 3 pu using both conventional methods and Evolutionary Algorithms are shown in Fig.3.4.

The MinMax method distributes the load equally among the 8 generators. Hence, each generator operates at 0.375 pu load. The MinCon method equally distributes the demanded load among 5 generators and switches off remaining 3 generators. Hence the loading of each generator is 0.6 pu, whereas GA optimally distributes the demanded load among the 4 generators in a range of 0.66 to 0.889, while keeping remaining 4 generators off.
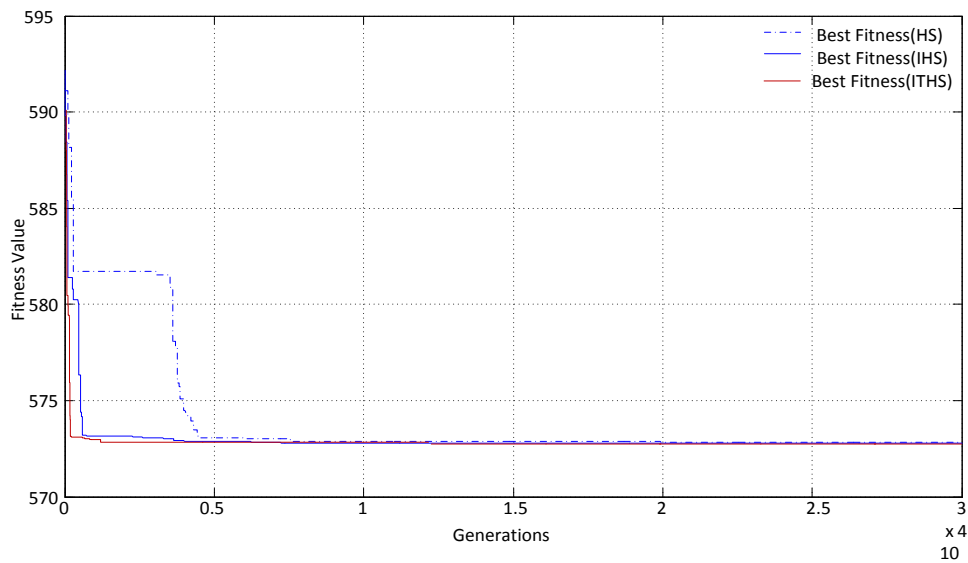
Fig. 3.3 Convergence of the HS, IHS and ITHS at 3 pu load

Generators	1	2	3	4	5	6	7	8
■ ITHS	0	0	0	0	0.6	0.9	0.9	0.6
□ IHS	0	0	0	0	0.59968	0.8998	0.8999998	0.60032
▣ HS	0	0	0	0	0.5989	0.8998	0.8999	0.6014
□ GA	0	0	0	0	0.66	0.75	0.889	0.701
□ MinCon	0	0	0	0.6	0.6	0.6	0.6	0.6
■ MinMax	0.375	0.375	0.375	0.375	0.375	0.375	0.375	0.375
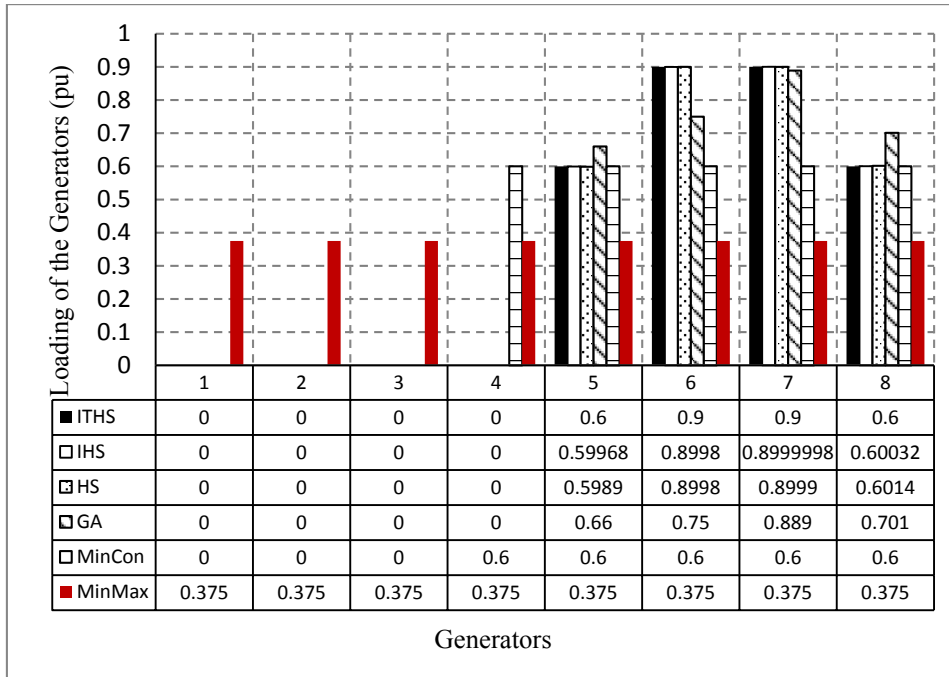
Fig. 3.4 Scheduling of the Diesel Generators at 3 pu load

In case of HS, IHS and ITHS algorithm also the demanded load is distributed among 4 generators and the Generators operate in the range of 0.6 to 0.9 pu load. Table 3.3 shows the initial selection of the harmony vectors that are stored in the Harmony Memory. The ITHS algorithm similar to HS algorithm generates a new vector, after considering all of the existing vectors, whereas GA only considers the two parent vectors. These features increase the flexibility of the ITHS algorithm and produce better solutions. The harmony vectors selected are random in nature. The randomization diversifies the search space and prevents premature convergence. However, self-adaptive pitch adjustment strategy adopted by the dynamic sub-populations based on the consciousness (Harmony Memory) is an important factor for the high efficiency of the ITHS method as compared to HS, IHS and other evolutionary algorithms.

TABLE.3.3. Initial Harmony Memory Matrix for the formulated problem for 3 pu load

P_1	P_2	P_3	P_4	P_5	P_6	P_7	P_8	Fittnes Value(F)
0.1057	0.6937	0.0446	0	0.2652	0.6524	0.6288	0.6096	601.3674
0.9307	0.4199	0.0053	0.2314	0.2639	0.6486	0.0874	0.4128	622.051
0.1268	0.2421	0.3867	0.5315	0.1443	0.9237	0.4981	0.1468	631.9757
0.3681	0	0.7018	0.289	0.1041	0.42	0.5643	0.5527	614.7837
0.4349	0.3582	0.3974	0.4054	0.4827	0.3971	0.2774	0.247	639.4664
0.8451	0.3581	0.59	0.5164	0.1761	0.5144	0	0	607.0608
0.6581	0.4303	0	0.4449	0.3533	0.54	0.082	0.4913	612.7599
0.2858	0.5293	0.2574	0.5565	0.3331	0.0141	0.3888	0.6351	622.2042
0.1206	0.3176	0.1407	0.7162	0.7949	0.4815	0	0.4284	616.3403
0.0648	0.2122	0.1565	0.1461	0.5672	0.2155	0.9053	0.7324	626.141

Table 3.4 shows the final Improved Harmony Memory Matrix and the variation in the elements of the harmony vectors is very less, this is the result of the pitch adjustment. Pitch adjustment helps HS intensify its search around the neighborhood of an optimal or nearly optimal solution. The fuel consumption rate (g/hr) for 3pu load for various optimization techniques adopted for scheduling of the generators can be seen in Table 3.4. It can be seen that fuel consumption rate of the oil rig at 3 pu load using MinMax method, MinCon method, GA, HS, IHS and ITHS are 642.22 g/kWh,584.62g/kWh, 576.049 g/kWh, 574.009 g/kWh,572.812 g/kWh, 572.7846 g/kWh and 572.6038 g/kWh respectively. It is evident from the numerical results that the fuel consumption rate for ITHS is less as compared to both MinCon method, MinMax Method and other evolutionary algorithms adopted for optimal scheduling of the diesel generators in the oil rig. Table 3.5 shows the total fuel consumed by the 8 generators at different loading conditions using MinMax method, MinCon Method, GA, HS, IHS and ITHS.

It can be observed that MinCon method, shedules the generator better than MinMax method till 3 pu load and consumes lower fuel than MinMax, but after 3 pu load MinMax method schedules the generator better than MinCon. Therefore, conventionally used optimization methods fail to optimally schedule the generators over the entire range of operation and

evolutionary algorithms optimally schedules the generators and reduces the total fuel consumption as compared to MinMax method and MinCon method over the entire range of operation for the diesel generators. But ITHS gives better convergence and results than IHS, HS, and GA because of better balance between diversification and intensification throughout the search.

TABLE.3.4. Final Harmony Memory Matrix for the formulated problem for 3 pu load

P_1	P_2	P_3	P_4	P_5	P_6	P_7	P_8	Fittnes Value(F)
0	0	0	0	0.6	0.9	0.9	0.6	572.6038
0	0	0	0	0.6	0.9	0.9	0.6	572.6038
0	0	0	0	0.6	0.9	0.9	0.6	572.6038
0	0	0	0	0.6	0.9	0.9	0.6	572.6038
0	0	0	0	0.6	0.9	0.9	0.6	572.6038
0	0	0	0	0.6	0.9	0.9	0.6	572.6038
0	0	0	0	0.6	0.9	0.9	0.6	572.6038
0	0	0	0	0.6	0.9	0.9	0.6	572.6038
0	0	0	0	0.6	0.9	0.9	0.6	572.6038

TABLE.3.5. Total fuel consumption rate of the generators at different loads

Total Load Demand (pu/hr)	MinMax Method	MinCon Method	GA	HS	IHS	ITHS
1	258.107	201	196	195.8	**195.8**	**195.7608**
2	466.24	393.1	391.376	385.8841	**385.8841**	**385.8841**
3	642.22	584.61	576.049	572.8122	**572.7846**	**572.6038**
4	765.7	804	764.2	759.7152	**759.6581**	**759.3780**
5	969.7	969.72	959.21	958.1713	**957.7065**	**947.1989**
6	1157.88	1159.7	1146.94	1145.5	**1145.3**	**1133.19**
7	1328.22	1342.33	1323.21	1321.5	**1321.2**	**1320.49**

3.5.2 Case-II: Diesel generators with Unequal rating

In this case, consider an oil rig that is powered by two 5000kW, two 3750kW, three 2500kW and a 1250kW diesel generators. Therefore, converting all the generator rating to the base of maximum rating generator that's 5000 kW. The oil rig is powered by two of 1 pu , two of 0.75 pu , three 0.5 pu and one 0.25 pu generator and the maximum load demand is 5.25 pu. The SFC curve has been assumed same for the all the diesel generators. ITHS algorithm has been applied for the optimal scheduling of the 8 diesel generators at different loading conditions of the thruster motors. The parameters of algorithms are assumed same as considered in previous case. In this case for unequal rating generators, the same conventional algorithms and evolutionary algorithms are employed to solve the formulated optimization problem. Each evolutionary algorithm is run for 50 trials under same conditions, to obtain the best solution.

TABLE.3.6. Comparision of the best solution for 0.5 pu load for Case (I)

Methods	P_1 (0.25 pu)	P_2 (0.5 pu)	P_3 (0.5 pu)	P_4 (0.5 pu)	P_5 (0.75 pu)	P_6 (0.75 pu)	P_7 (1 pu)	P_8 (1 pu)	Fittnes Value(F)
MinMax	0	0	0	0	0	0	0.5	0	101.092
MinCon	0	0.5	0.5	0	0	0	0	0	100.5
GA	0	0	0	0	0.667	0	0	0	96.47
HS	0	0	0	0	0.667	0	0	0	96.47
IHS	0	0	0	0	0.667	0	0	0	96.47
ITHS	0	0	0	0	0.667	0	0	0	96.47

TABLE.3.7. Comparision of the best solution for 2.5 pu load for Case (II)

Methods	P_1 (0.25 pu)	P_2 (0.5 pu)	P_3 (0.5 pu)	P_4 (0.5 pu)	P_5 (0.75 pu)	P_6 (0.75 pu)	P_7 (1 pu)	P_8 (1 pu)	Fittnes Value(F)
MinMax	-	-	-	-	-	-	-	-	NS
MinCon	0.476	0.476	0.476	0.476	0.476	0.476	0.476	0.476	507.56
GA	0	0.899	0.899	0	0.124	0	0.801	0.707	485.1
HS	0	0	0.609	0.702	0.8966	0.6776	0.6635	0	479.87
IHS	0	0	0	0.8999	0.6638	0	0.8999	0.6523	472.9757
ITHS	**0.1**	**0**	**0**	**0**	**0.9**	**0**	**0.9**	**0.9**	**472.3886**

TABLE.3.8. Total fuel consumption rate of the generators at different loads

Total Load Demand (pu/hr)	MinMax Method	MinCon Method	GA	HS Algorithm	IHS Algorithm	ITHS Algorithm
0.50	101.092	100.5	96.47	96.471	96.471	**96.471**
0.75	-	147.41	144.58	144.73	144.73	**143.1509**
1.00	-	196.23	194.89	192.94	189.9123	**189.8445**
2.00	393.10	385.88	383.8	380.76	379.827	**377.5860**
2.50	-	507.56	485.1	479.87	472.9757	**472.3886**
3.00	589.65	588.68	579.35	576.20	571.09	**566.5992**
3.75	-	722.36	719.05	715.88	712.9398	**706.7479**
4.00	799.34	763.79	761.61	759.86	757.14	**753.5722**
4.50	884.42	867.89	858.52	850.53	850.4192	**846.8966**
5.00	980.71	970.24	969.9	965.644	965.62	**965.4264**
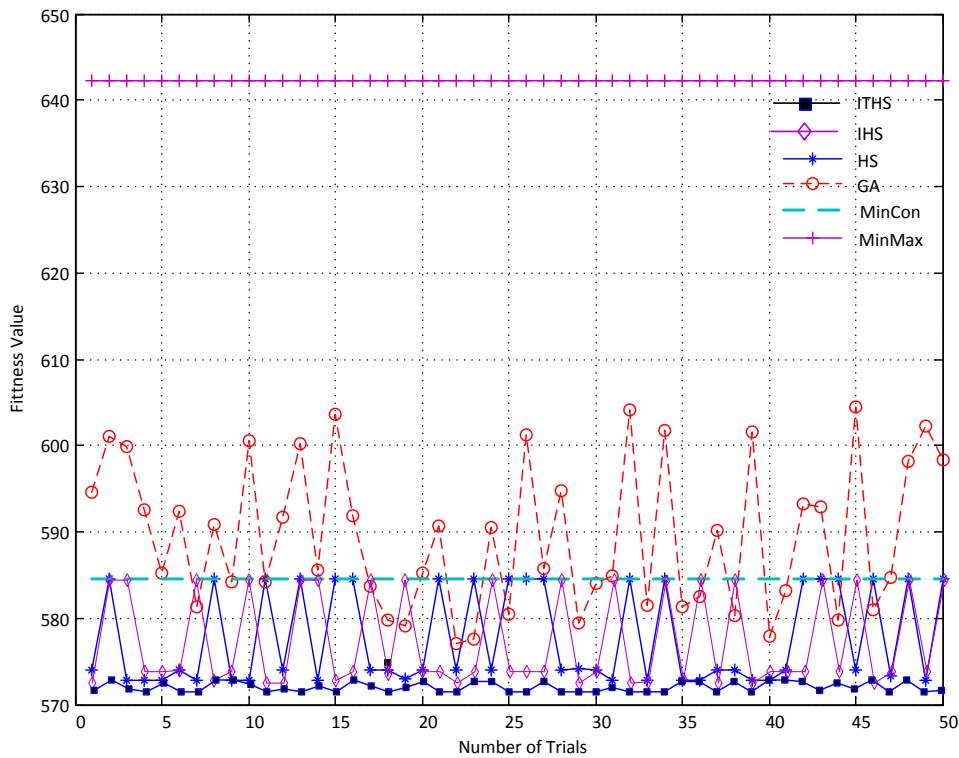
Fig. 3.5 Variation of solution for different methods at 3 pu load

Let's assume that the load demanded is 0.5 pu. The scheduling of the various generators at a load of 0.5 pu using conventional methods and evolutionary algorithms are shown in Table 3.6. The MinMax method loads the one of the 1 pu generator to 0.5 pu load. The MinCon method loads the 2 generators of 0.5 pu equally with 0.5 loads. Whereas, GA, HS,

IHS and ITHS algorithm loads the one of the 0.75 pu generators to 0.666 pu load. From Table 3.6, it can be seen that MinMax consumes 101.092 g/kWh, MinCon consumes 100.5 g/kWh and GA, HS, HIS and ITHS consume 96.47 g/kWh. So, evolutionary algorithms schedule the generators more optimally than conventional algorithms.

Table 3.7 shows the scheduling of the generators for a load of 2.5 pu. In conventional optimization techniques the initial starting points need to be specified. If the initial point is specified as 0, then MinMax method is unable to find the solution for a load demand of 2.5 pu. Whereas when, the initial points specified is 1, MinMax finds the solution for the optimization problem. Therefore, the conventional optimization methods are sensitive to starting points. Evolutionary algorithms don't need any initial starting condition to be specified.

From Table 3.8, it is evident that MinMax method is unable to find solution for some load conditions. MinCon schedules the generators under all loading conditions. It can be observed that MinCon method schedules the generators better than MinMax method and consumption of the fuel is lower when compared to MinMax method. Another observation from Table 3.8 is that at lower loads the difference in the optimal solution for evolutionary algorithms is not much. This is because at lower loads the feasible solution region or the search space is small and all the algorithms are able to explore the search space effectively and efficiently. But, as the load increases the feasible solution area (search space) also increases and both diversification and intensification play significant role in finding the optimal solution therefore there is significant variation in solution. Therefore, ITHS gives better results when compared to GA, HS, IHS and conventional methods for this case also. The subtlety is the fact that ITHS operates controlled diversification around good solutions, and intensification as well.

3.5.3 Diversity of the solution

Since evolutionary algorithms are heuristic in nature, the solution obtained is not unique. Experiments have been made to study the variation in the solution obtained by such algorithms. Each algorithm is tested for 50 trials. Fig.3.5 shows the variation in solutions obtained for 3 pu load by the different optimization techniques adopted for the formulated problem. The maximum fitness value, minimum fitness value, average fitness value and standard deviation of 50 test runs have been recorded for both case 1 and 2 and are summarized in Table 3.9 and 3.10. It can be seen that conventional optimization techniques give unique solution therefore standard deviation is zero for both MinMax and MinCon Method. It is observed from results that the average fitness value for ITHS is less as compared to other optimization methods, thus resulting in the higher quality solution and also ITHS method yields smaller standard deviation in fitness value when compared with GA, HS and IHS, thus resulting in more reliable solution.

TABLE.3.9. Comparision of different optimization techniques for 3 pu load (50 trials)

Fitness Value	MinMax Method	MinCon Method	Genetic Algorithm	HS Algorithm	IHS Algorithm	ITHS Algorithm
Maximum	642.2180	584.6120	604.4465	584.6125	584.6125	**574.0402**
Minimum	642.2180	584.6120	576.049	572.8122	572.7846	**572.6038**
Average	642.2180	584.6120	589.4690	577.6678	577.4582	**573.1819**
SD	0	0	8.5224	5.5116	5.3282	**0.5771**

TABLE.3.10. Comparision of different optimization techniques for 2.5 pu load (50 trials)

Fitness Value	MinMax Method	MinCon Method	Genetic Algorithm	HS Algorithm	IHS Algorithm	ITHS Algorithm
Maximum	-	507.56	503.307	484.86	484.86	**473.6456**
Minimum	-	507.56	485.1	479.87	472.9757	**472.3886**
Average	-	507.56	494.2203	482.12	478.7660	**472.7597**
SD	-	0	5.1796	2.5189	2.21	**0.3353**

3.6 Conclusion

In this chapter, we have successfully modeled the SFC curve for the diesel generator using cubic spline interpolation; the cubic spline is a powerful tool and can accurately interpolate the SFC at different loading conditions of the diesel generator as compared to other conventional methods. The accurate modeling of the SFC curve helps in optimal scheduling of the diesel generators. The design and dynamic scheduling of diesel-generators play a crucial role in oil rig for the power density and efficiency. The ability of the ITHS algorithm was demonstrated and its performance was compared with other optimization techniques. The optimal scheduling of the diesel generators using ITHS algorithm reduces the fuel consumption of the rig as compared to conventional MinMax, MinCon methods and also GA, HS and IHS under both the scenarios of equal and unequal ratings diesel generators. The ITHS algorithm also gives higher quality and more reliable solution. Therefore, it is clear from the results that the proposed ITHS can avoid the shortcoming of premature convergence of GA, HS and IHS. The self-adaptive pitch adjustment strategy adopted by ITHS algorithm improves the convergence and also solution quality as compared to classical HS and IHS algorithm.

CHAPTER 4. OPTIMAL THRUST ALLOCATION FOR SEMI-SUBMERSIBLE OIL RIG PLATFORMS

4.1 Introduction

In a semi-submersible oil rig platform the DP system automatically controls the position and heading of the oil rig subjected to environmental and external disturbances, using large rating azimuth thrusters fitted at its pontoon level [7, 8]. In this Chapter, a semi-submersible oil rig platform equipped with eight azimuth thrusters is considered as a case study for marine vessels. For vessels that are operating to DP class 2 or 3 standards, the vessel should be left with sufficient power and thrusters to maintain position after worst case failure. Therefore, the semi-submersible oil rig is equipped with redundant thruster configuration and is over-actuated as per the guidelines of IMO MSC Circ.645 and IMCA M 103 [10, 11]. In this Chapter, the over-actuated thrust allocation problem is formulated as an optimization problem with objective to reduce the fuel consumption of the oil rig platform. The solution of the formulated optimization problem is found using ITHS algorithm.

The rest of this chapter is arranged as follows: Section 4.2 provides an overview of the three degree of freedom (3-DOF) thrust allocation. The insight into these principles will help the reader in understanding the motivation for following an engineering approach for optimal thrust allocation in an over-actuated marine vessel. The details and drawbacks of the Lagrange multiplier method conventionally used for the thrust allocation in the case study of the marine vessel are discussed in Section 4.3. The thrust allocator tries to minimize the power consumption and takes forbidden/spoil zones into account. The details of the formulated optimization problem are presented in Section 4.4. The optimization problem formulated is subjected to both equality and inequality constraints. A novel constraint handling method based on Superiority of Feasible Solutions (SF) is presented in Section 4.5. Section 4.6 provides an overview of the practical oil rig platform. The results

obtained from the case study of the marine vessel with detailed discussions are presented in Section 4.7. Finally, the research findings are concluded in Section 4.8.

4.2   3-DOF Thrust Allocation

The scope of the paper is to present a solution of 3-DOF control allocation (horizontal plane motion). Movement along the z-axis (up/down) is ignored due the periodic behavior of the disturbances. In addition, the azimuth thrusters or other commonly used actuators do not have the ability to produce thrust along z-axis. However, the presented approach can also be extended for 6-DOF control allocation.

For horizontal plane motions (surge, sway and yaw) the thrust allocation problem is to select the control signals associated with the individual thrusters in order to produce the demanded surge force (F_X) , sway force (F_Y) and yaw moment (M_Z) (three generalized force components) [8]. In this work, origin is considered at center of the main drill well (O), positive F_X is towards the forward side of the oil rig platform, positive F_Y is towards the port side of the oil rig platform and positive M_Z is upwards as shown in Fig.4.1 [8].
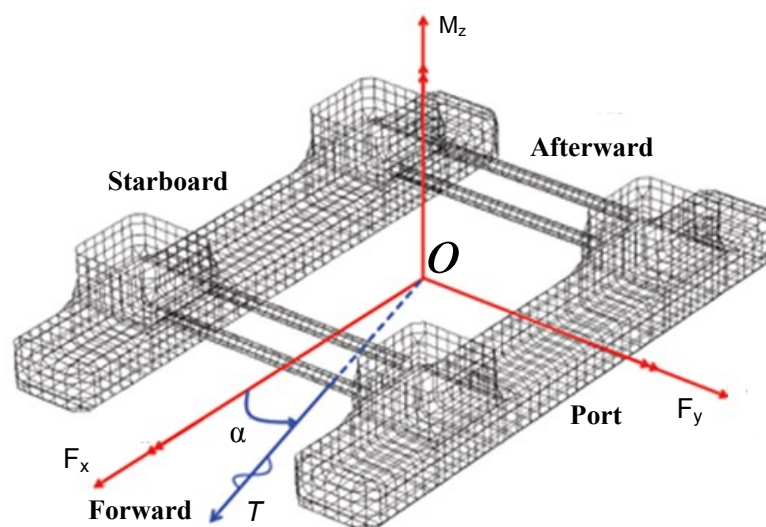
Fig. 4.1 Sign conventions used for thruster allocation

The forces and moment demanded by the DP system are represented by a force vector $\tau = \left(F_X,\ F_Y, M_Z\right)^T \in \mathbf{R}^3$. The forces and moment generated by the ith actuator with state $(T_i,\ \alpha_i)$ in cylindrical coordinates are given by (4.1- 4.3) [8, 13].

$$F_X^i = T_i \cos \alpha_i \tag{4.1}$$

$$F_Y^i = T_i \sin \alpha_i \tag{4.2}$$

$$M_Z^i = T_i \sin \alpha_i L_{Xi} - T_i \cos \alpha_i L_{Yi} \tag{4.3}$$

where, T_i is the magnitude of thrust produced by i^{th} actuator and α_i is the azimuth angle of the ith actuator. For each of the actuators, its position in horizontal plane with respect to the center of gravity of the ship (0, 0) is given by (L_{Xi}, L_{Yi}) as shown in Fig.4.2. Equations (4.1- 4.3) can be combined and rewritten in matrix notation as given by (4.4) [2, 6].

$$\tau_i = B(\alpha_i)T_i = \begin{bmatrix} F_X^i \\ F_Y^i \\ M_Z^i \end{bmatrix} = \begin{bmatrix} \cos \alpha_i \\ \sin \alpha_i \\ \sin \alpha_i L_{Xi} - \cos \alpha_i L_{Yi} \end{bmatrix} T_i \tag{4.4}$$
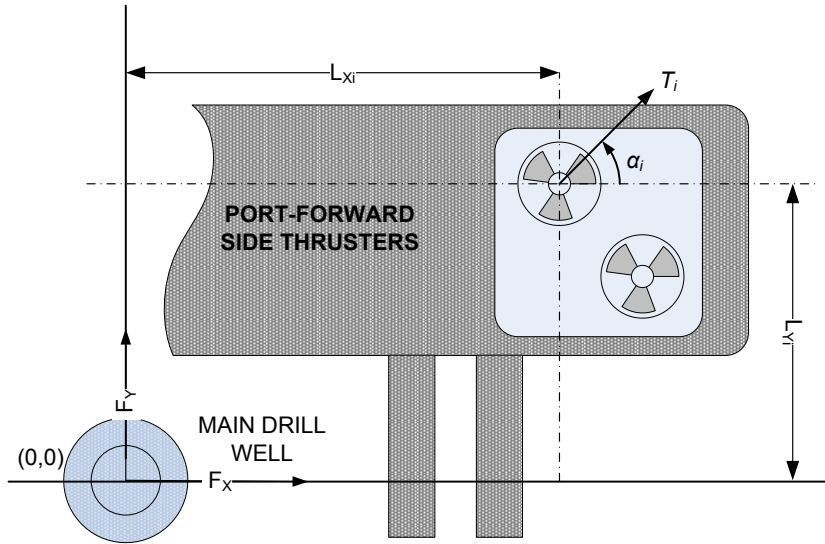
Fig. 4.2 Reference frame of ith actuator for calculation of forces and moment.

Assuming that the marine vessel is equipped with N actuators, then the force vector (τ) demanded is jointly produced by N actuators in order keep the vessel at the fixed position and is given by (4.5).

$$\tau = \sum_{i=1}^{N} \tau_i = \begin{bmatrix} \sum_{i=1}^{N} F_X^i \\ \sum_{i=1}^{N} F_Y^i \\ \sum_{i=1}^{N} M_Z^i \end{bmatrix} = \mathbf{B}(\boldsymbol{\alpha})\boldsymbol{T} \qquad (4.5)$$

Here, $T \in \mathbf{R^N}$ is a vector of the magnitude of the forces produced by each individual actuator. The thruster configuration matrix ($B \in \mathbf{R^{3 \times N}}$) is determined by the position of the individual thrusters. The ith column in configuration matrix corresponds to the generalized force produced by the ith thruster. However, each thruster has limited amount of thrust and limited directions in which it generates thrust. Therefore, for each thruster, the azimuth angle (α_i) and the thrust force (T_i) are constrained to the sets given by (4.6).

$$\mathcal{O}_i := \left\{ (\, \alpha_i, T_i) \mid \underline{\alpha}_i \leq \alpha_i \leq \overline{\alpha}_i, \underline{T}_i \leq T_i \leq \overline{T}_i \right\} \tag{4.6}$$

where, $\underline{\alpha}_i$ and $\underline{T}_i$, are the lower bounds on the azimuth angle and thrust force for the ith thruster, respectively and similarly, $\overline{\alpha}_i$ and $\overline{T}_i$ are the upper bounds on the azimuth angle and thrust force for the ith thruster, respectively. A set of all physically realizable surge and sway forces (F_X^i, F_Y^i) for the ith thruster is called the Attainable Thrust Region (ATR) of the ith thruster and is defined by (4.7) [59].

$$\mathcal{C}_i := \left\{ \left(F_X^i, F_Y^i \right)^T \left| \begin{array}{l} F_X^i = T_i \cos \alpha_i, \\ F_Y^i = T_i \sin \alpha_i, \\ (\, \alpha_i, T_i) \in \mathcal{O}_i \end{array} \right. \right\} \tag{4.7}$$

An azimuth thruster is physically capable of generating thrust in any direction as they can rotate 360 degrees. Typically azimuth thrusters are not used to produce thrust in the reverse mode, therefore, the minimum thrust force $(\underline{T}_i)$ is zero and maximum thrust force $(\overline{T}_i)$ is limited to rated thrust force (T_{iR}). Therefore, ATR of azimuth thruster is circular and hence convex. However, in practice the thrusters are not operated below the minimum thrust force of $(\underline{T}_i = 0.04 \times T_{iR})$ [137]. In addition, when two thrusters are positioned close enough the thruster-thruster interactions can cause thrust [26]. The thrust loss is very significant in case of an oil rig because the two thrusters are mounted in pairs and are located on the same leg of the oil rig. The thrust generated by the thruster is given by (4.8) [8].

$$T = \rho_W D^4 K_T |n| n \tag{4.8}$$

where, ρ_W is the density of the water, D is propeller diameter and n is the propeller speed. The non-dimensional thrust coefficient (K_T) in general is affected by the change in advance speed (V_a) and cross coupling drag caused by the other thrusters [12].

In order to overcome the thruster-thruster interaction loss, the forbidden zones or spoil zones are defined and excluded from the ATR of the neighbouring thrusters. The ATR for a set of I thrusters is given *Minkowski set addition* given by (4.9) [59].

$$\mathcal{C} := \mathcal{C}_1 \oplus \mathcal{C}_2 \oplus \dots \oplus \mathcal{C}_I \qquad (4.9)$$

The Minkowski set addition for two sets $X \subset \mathbf{R^N}$ and $Y \subset \mathbf{R^N}$ is defined by (4.10).

$$X \oplus Y := \{x + y \mid x \in X, y \in Y \} \qquad (4.10)$$

Each thruster is assumed to have a forbidden angle of $\pm\theta_f{}^\circ$ to the closest thruster in order to prevent thruster's direct interaction as shown in Fig.4.3. With the port-forward pair centre of angle of outboard thruster i is ϕ_i and for inboard thruster $(i+1)$ is ϕ_{i+1}. The positive angle is measured anticlockwise while negative angle is measured clockwise from the horizontal axis. Fig. 4.3 shows the ATRs for the two port-forward side thrusters i and $(i + 1)$.
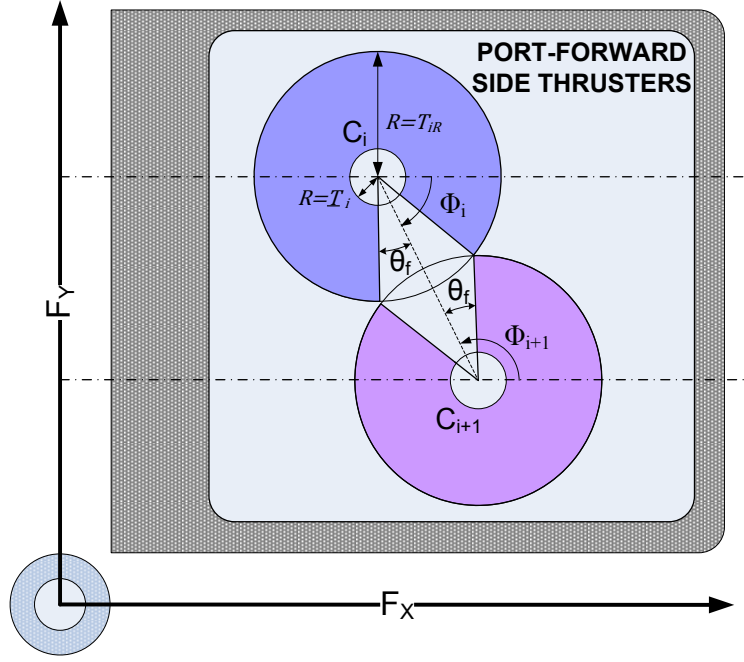
Fig. 4.3 Shaded region represents the ATR of ith and $(i+1)^{th}$ thruster

Based on Fig. 4.3, the azimuth angle (α_i) and thrust force (T_i) are constrained to the sets given by (4.11). The $\underline{\alpha}_i$ and $\overline{\alpha}_i$ for the ith thruster are given by (4.12 - 4.13). In (4.13), 360° is added to ensure $\overline{\alpha}_i > \underline{\alpha}_i$.

$$S_i := \left\{ (\alpha_i,\ T_i) \mid \underline{\alpha}_i \leq \alpha_i \leq \overline{\alpha}_i, \underline{T}_i \leq T_i \leq \overline{T}_i \right\} \tag{4.11}$$

$$\underline{\alpha}_i = \phi_i + |\theta_f| \tag{4.12}$$

$$\overline{\alpha}_i = \phi_i - |\theta_f| + 360° = \underline{\alpha}_i - 2|\theta_f| + 360° \tag{4.13}$$

Using (4.11- 4.13), the ATR for i^{th} thruster is given by (4.14) and the forbidden sector is $C_i/\bar{C}_i$.

$$\bar{C}_i := \left\{ \left(F_X^i, F_Y^i\right)^T \left| \begin{array}{l} F_X^i = T_i\cos \alpha_i, \\ F_Y^i = T_i\sin \alpha_i, \\ (\alpha_i, T_i) \in S_i \end{array} \right. \right\} \tag{4.14}$$

4.3   Lagrange Multiplier Optimization Method

The Lagrange multiplier method is used for the thrust allocation in the case study of marine vessels. The details of the method are analyzed in this section. In order to solve the thruster allocation problem by Lagrange multiplier method or quadratic programming (QP), the thrust vectors are converted to cartesian coordinates, also called extended thrust formulation [138], to form a convex linearly constrained quadratic programming problem. In cartesian coordinates, forces and moments generated by the ith actuator with state $(T_{X,i}, T_{Y,i})$ are given by reformulating (4.1-4.3)

$$F_X^i = T_{X,i} \tag{4.15}$$

$$F_Y^i = T_{Y,i} \tag{4.16}$$

$$M_Z^i = T_{X,i}L_{Yi} - T_{Y,i}L_{Xi} \tag{4.17}$$

where, $T_{X,i} \in R^N$ and $T_{Y,i} \in R^N$ are the thruster force in body x and y direction. Equations (4.15-4.17) can be combined and rewritten in matrix notation as given by (4.18).

$$\tau_i = \begin{bmatrix} F_X^i \\ F_Y^i \\ M_Z^i \end{bmatrix} = \begin{bmatrix} 1 & 0 \\ 0 & 1 \\ -L_{Yi} & L_{Xi} \end{bmatrix} \begin{bmatrix} T_{X,i} \\ T_{Y,i} \end{bmatrix} \tag{4.18}$$

The force vector (τ) demanded is jointly produced by N actuators in order keep the vessel

in the fixed position and is given by (4.19).

$$\tau = \sum_{i=1}^{N} \tau_i = \begin{bmatrix} \sum_{i=1}^{N} F_X^i \\ \sum_{i=1}^{N} F_Y^i \\ \sum_{i=1}^{N} M_Z^i \end{bmatrix} = \begin{bmatrix} 1_{1\times N} & 0_{1\times N} \\ 0_{1\times N} & 1_{1\times N} \\ -L_Y & L_X \end{bmatrix} \begin{bmatrix} T_X \\ T_Y \end{bmatrix} = B_c T_c \tag{4.19}$$

where, $1_{1\times N}$ and $0_{1\times N}$ are vectors of ones and zeros, respectively, and $L_X \in \mathbf{R^N}$ and $L_Y \in \mathbf{R^N}$ are vectors of the thruster positions in body x and y direction, respectively. The thruster configuration matrix $(B_c \in \mathbf{R^{3\times 2N}})$ is determined by the position of the individual thrusters and $T_c \in \mathbf{R^{2N}}$ is the state matrix of N thrusters. For each thruster, the azimuth angle (α_i) and thrust force (T_i) can be obtained using (4.20- 4.21).

$$\alpha_i = \tan^{-1} \frac{T_{Y,i}}{T_{X,i}} \tag{4.20}$$

$$T_i = \left\| (T_{X,i}, T_{Y,i})^T \right\|_2 = \sqrt{(T_{X,i})^2 + (T_{Y,i})^2} \tag{4.21}$$

The thrust allocation problem is formulated as a quadratic equality constrained minimization problem and solved using the Lagrange multiplier method.

$$\text{Minimize} \sum_{i=1}^{N} P_i(T_c) = \text{Minimize} \left(T_c{}^T W \, T_c \right) \tag{4.22}$$

subjected to

$$\tau = B_c T_c \tag{4.23}$$

Where, $W = \begin{bmatrix} W_1 & & \\ & \ddots & \\ & & W_N \end{bmatrix}$ is the weight matrix to compute power from thrust and $W \in$

$\mathbf{R^{2N \times 2N}}$. A sub-problem is formulated by combining the fitness function and equality constraint using the Lagrangian and the penalty parameters as shown in (4.23).

$$L(\lambda, T_c) = \left(T_c{}^T W \, T_c \right) + \lambda^T (\tau - B_c T_c) \tag{4.24}$$

Where, $\lambda \in \mathbf{R^3}$ are the Lagrangian multipliers. The solution of the sub-problem can be found using Karush–Kuhn–Tucker (KKT) condition. The KKT equations are necessary conditions for optimality for a constrained optimization problem [139]. If the problem is a so-called convex programming problem, then the KKT equations are both necessary and sufficient for a global solution point and solution is given by $T_c = W^{-1}B_c{}^T(B_c W^{-1}B_c{}^T)^{-1}\tau$. However, in the above solution thrust limits of the thrusters are not taken into account. The solutions will contain thrust values that the thrusters are not physically capable of producing. This problem can be overcome by adding saturation handling capability to the thrust allocator algorithm [60].

Apart from this, the formulation of power consumption of the thruster is not accurate. Traditionally, in the literature using QP solvers, the power consumption of a thruster is penalized by the term $T_c{}^T W \, T_c$ $(W \, T_c^2)$. However, since power is proportional to $|T_c|^{3/2}$ the formulated problem given by (4.22) can either over-predict or under-predict the power consumed by the thruster. The modeling of thruster power consumption will be discussed in more detail in Section 4.7.

4.4 Optimization Problem Formulation

For vessels that are operating to DP class 2 or 3 standards, the vessel should be left with sufficient power and number of thrusters to maintain its position after the worst case failure. Therefore, they are over actuated as per the guidelines of IMO MSC Circ.645 and IMCA M-103 azimuth thrusters can produce forces in different directions leading to an over-actuated control problem that can be formulated as an optimization problem. In this chapter, the thrust allocator tries to minimize the power consumption and takes forbidden/spoil zones into account. Therefore, the optimization problem can be formulated as given by (4.25-4.27).

$$\text{Minimize } J(\alpha, T) = \text{Minimize} \sum_{i=1}^{N} P_i(T_i) \tag{4.25}$$

subjected to

$$\tau - B(\alpha)T = 0 \tag{4.26}$$

$$\left(\underline{\alpha}_i \leq \alpha_i \leq \overline{\alpha}_i, \underline{T}_i \leq T_i \leq \overline{T}_i \right) \text{ or } (\alpha_i, T_i) \in S_i \tag{4.27}$$

Where, $P_i(T_i)$ is the power consumed by the ith thruster to produce a thrust force (T_i). Since the marine vessel is assumed to be equipped with N thrusters, the total power is represented by $\sum_{i=1}^{N} P_i(T_i)$. Eqn. (4.26) ensures that the error between the demanded generalized force (τ) and generalized force jointly produced by N actuators is close to zero to keep the vessel in the desired position. However, the thrust produced by each thruster is restricted to its ATR, this is ensured by (4.27).

4.5   Constraint Handling Using Superiority of Feasible Solutions

In the formulated constraint optimization problem the error between the demanded generalized force (τ) and generalized force jointly produced by N actuators must be close to zero to keep the vessel at the desired position. A general constraint optimization problem with N parameters to be optimized is usually written as a nonlinear programming problem as in (4.28 - 4.30) [140-142].

$$\text{Minimize } f(\vec{x}), \vec{x} = (x_1, x_2, x_3, \ldots \ldots x_N) \in \mathbf{R^N} \tag{4.28}$$

$$\text{subjected to: } g_i(\vec{x}) \leq 0, i = 1,2,3 \ldots \ldots p \tag{4.29}$$

$$h_j(\vec{x}) = 0, j = p+1, p+2, \ldots \ldots p+m \tag{4.30}$$

where, $f(\vec{x})$ is the objective function with $\vec{x}$ as the solution vector composed of decision variables (x_i) and $\vec{x} \in \mathcal{F} \subseteq \mathcal{X}$. The set $\mathcal{X}$ is a search space and is defined as an N-dimensional rectangle in $\mathbf{R^N}$ with all possible range of values for each decision variable (x_i) and is given by (4.31).

$$\mathcal{X}_i := \{x_i \mid \underline{x}_i \leq x_i \leq \overline{x}_i\} \tag{4.31}$$

Where, $\underline{x}_i$ and $\overline{x}_i$ are the lower and upper bounds for the ith decision variable respectively. $\mathcal{F}$ is the feasible search space such that $\mathcal{F} \subseteq \mathcal{X}$ and satisfies the additional constraints (4.29) and (4.30). The equality constraints can be transformed into inequality form using 4.32 and can be combined with other inequality constraints.

$$g_j(\vec{x}) = |h_j(\vec{x})| - \varepsilon \leq 0 \tag{4.32}$$

Most heuristic search methods use the penalty function approach of handling constraints. The penalty function approach involves a number of penalty coefficients, which must be set right in any problem to obtain feasible solutions. However, the performance of the search algorithm is greatly influenced by the penalty coefficients [142]. Several sophisticated penalty function approaches have been proposed, but all these approaches require extensive experimentation for setting up appropriate parameters needed to define the penalty function. In this chapter, the superiority of feasible solutions (SF) method is used for constraint handling. The superiority of feasible solutions method is based on the tournament selection operator, where two solutions are compared at a time, and the following criteria are always enforced [140]:

1. Any feasible solution is preferred to any infeasible solution.

2. Among two feasible solutions, the one having better objective function value is preferred.

3. Among two infeasible solutions, the one having smaller constraint violation is preferred.

Based on the above rules, the fitness function is evaluated using (4.33), where infeasible solutions are compared based on their constraint violation only.

$$F(\vec{x}) = \begin{cases} f(\vec{x}), \text{if } g_i(\vec{x}) \leq 0 \; \forall i = 1,2,3 \ldots \ldots p + m \\ f_{max} + \sum_{i=1}^{p+m} \langle g_i(\vec{x}) \rangle, \text{otherwise} \end{cases} \qquad (4.33)$$

The parameter f_{max} is the objective function value of the worst feasible solution in the population and $\langle g_i(\vec{x}) \rangle$ denotes the absolute value of the operand, if the operand is positive and returns a value zero, otherwise. Therefore, the fitness of an infeasible solution not only depends on the amount of constraint violation, but also on the population of solutions at hand. However, the fitness of a feasible solution is always fixed and is equal to its objective function value. If no feasible solution exists in a population, f_{max} is set to zero. However,

the method requires at least one feasible individual to be placed in the initial population which is similar to providing a starting feasible point for the optimization process. If the initial population has no feasible solution ($f_{max} = 0$) then there may be occasions when, $f_{max} + \sum_{i=1}^{p+m}\langle g_i(\vec{x})\rangle < f(\vec{x})$. Therefore, first rule of the tournament selection is violated. In order to overcome this a modified SF method is proposed. The fitness evaluation is modified in the proposed method and is given by (4.34).

$$F(\vec{x}) = \begin{cases} \dfrac{-1}{1 + f(\vec{x})}, \text{if } g_i(\vec{x}) \le 0 \ \forall i = 1,2,3 \dots\dots p + m \\ \displaystyle\sum_{i=1}^{p+m} \langle g_i(\vec{x})\rangle, \text{otherwise} \end{cases} \tag{4.34}$$

$F(\vec{x})$ is minimum for minimum value of $f(\vec{x})$ and the fitness function of the feasible solution is always lower than the infeasible solution. By doing this all the rules are satisfied and there is no need of an initial feasible individual.

4.6   The Practical Oil Rig Platform

This section provides an overview of the semi-submersible oil rig considered as a case study for marine vessels. The vessel is a four column stabilized semi-submersible oil rig. Four rectangular shaped stability columns, and two pontoons provide the buoyancy. The actuator layout of the Keppel's B280 semi-submersible oil rig is shown in Fig.4.4
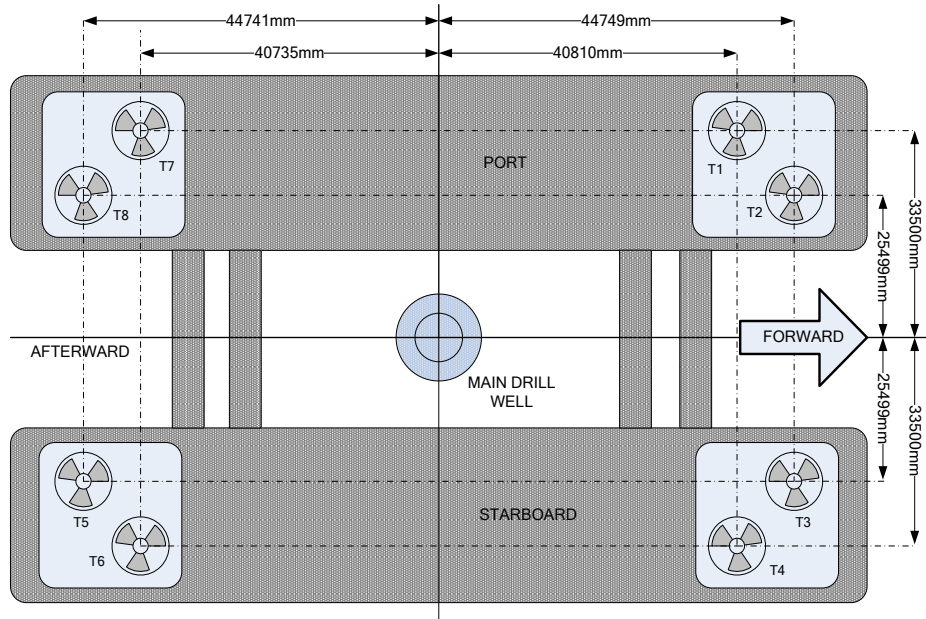
Fig. 4.4 Actuator layout of Keppel's B280 and corresponding dimensions with respect to origin at main drill well).

Eight azimuth thrusters located at the pontoon level of the oil rig are used by the DP system to control its position. The rated effective thrust (T_R) of each thruster is 780 kN at a motor power of 4000 kW at 600 rpm. The thrust (T) and the torue(Q) generated by a propeller are given by (4.35-4.36) [8, 9].

$$T = \rho_W D^4 K_T |n|n \tag{4.35}$$

$$Q = \rho_W D^5 K_Q |n|n \tag{4.36}$$

The power consumption (P) of a propeller is given by (4.37).

$$P = 2\pi n \, Q \tag{4.37}$$

Where, ρ_W is the density of the water, D is propeller diameter and n is the propeller speed. K_T and K_Q are the thrust and torque coefficients respectively. Using (4.43-4.45) power consumption of a propeller can be rewritten as in (4.38).

$$P = \frac{2\pi K_Q}{\sqrt{\rho_W}\, D K_T^{3/2}}\, T^{3/2} = \frac{2\pi}{\sqrt{\rho_W K_Q}\, D^{5/2}}\, Q^{3/2} \tag{4.38}$$

Therefore, power consumed by the propeller can be computed using $P1 = k_1|T|^{1.5} = 0.176|T|^{1.5}$. However, conventionally the relation between thrust (kN) and power consumed (kW) is given by $P2 = k_2 T^2 = 0.011 T^2$. This formulation is usually used in order to make the thrust allocation problem simpler. In order to validate both the power formulations, the output torque (Nm) and output Power (kW) are measured at different load levels for Keppel's B280 Semi-submersible oil rig. The error between the calculated power and the actual measured power for both the formulations is shown in Fig.4.5.
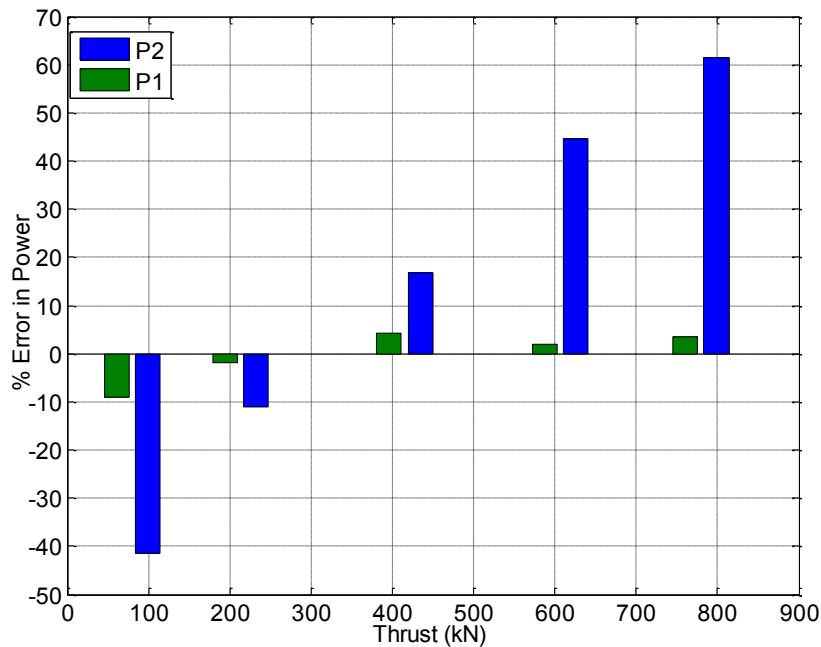
Fig. 4.5 % Error in Power calculated using $P1 = 0.176|T|^{1.5}$ and $P2 = 0.011 T^2$

It is evident from Fig. 4.5 that the power calculated using $P2 = k_2 T^2$ has an error between -40% to 60% whereas, the power calculated using $P1 = k_1|T|^{1.5}$ has an error between -

8% to 4%. Therefore, $P1$ is a better formulation as compared to $P2$.

Each thruster is assumed to have a forbidden angle of $(\pm\theta_f^\circ = \pm25^\circ)$ to the closest thruster with the port forward pair centre of angle of outboard thruster i as $(\phi_i = -63.44^\circ)$ and for inboard thruster $(i+1)$ as $(\phi_{i+1} = 116.56^\circ)$. Fig. 5.3 shows the ATRs for all the eight azimuth thrusters. Using (4.12-4.13), the corresponding $\underline{\alpha}_i$ and $\overline{\alpha}_i$ are computed as shown in (4.47) and (4.48).

$$\underline{\alpha}$$
$$= \{-38.44^\circ, 141.56^\circ, -91.56^\circ, 88.44^\circ, -38.44^\circ, 141.56^\circ, -91.56^\circ, 88.44^\circ\}$$

(4.7)

$$\overline{\alpha}$$
$$= \{271.56^\circ, 451.56^\circ, 218.44^\circ, 398.44^\circ, 271.56^\circ, 451.56^\circ, 218.44^\circ, 398.44^\circ\}$$

(4.8)
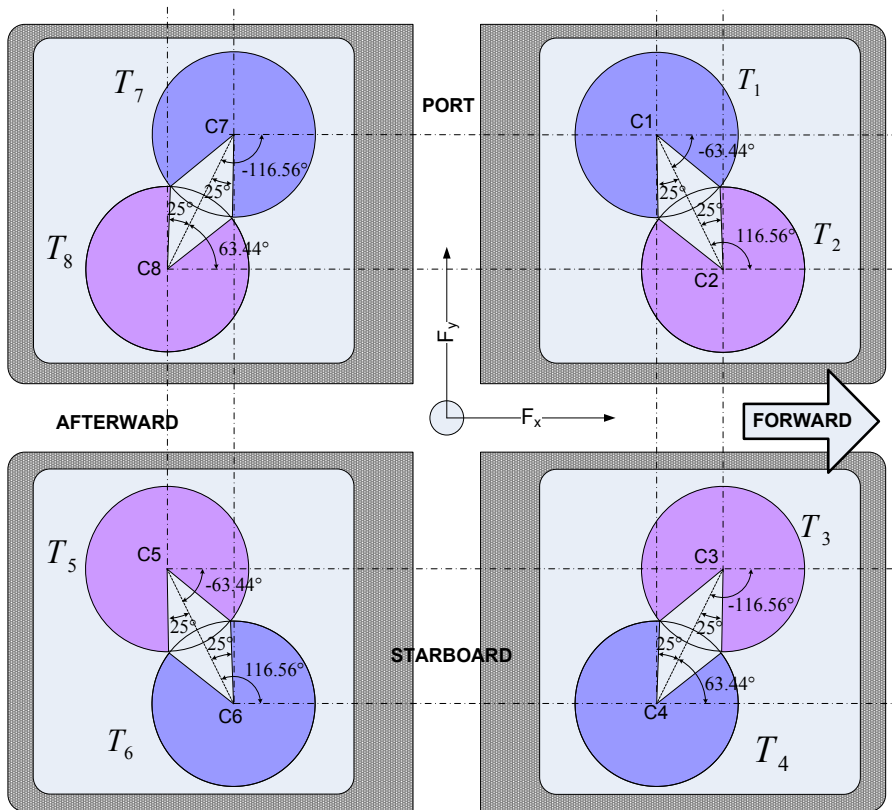
Fig. 4.6 Shaded region represents the ATR for the corresponding thruster.

106

4.7 Results and Discussion

In order to evaluate the effectiveness and efficiency of the ITHS algorithm, its performance with other conventional and evolutionary algorithms are compared. The algorithms for comparison are listed as follows:

- Mincon Method (Sequential Quadratic Programming)

- Harmony Search (HS)

- Improved Harmony Search (IHS)

- Genetic Algorithm

The parameters for the HS, IHS algorithms are fixed the same as those reported in [114] and parameters of ITHS algorithm is same as those reported in Chapter 2. For the HS algorithm, *HMS = 5, HMCR = 0.9, PAR = 0.33* and *bw = 0.01*. For the IHS algorithm, *HMS = 5, HMCR = 0.9, PAR_{min}* =0.1, PAR_{max} =0.99, *bw_{min} = 0.0001* and *bw_{max}* $=(\overline{x}_i - \underline{x}_i)/20$. According to [7,104] the default values of GA parameters are: 20 individuals per generation, 10% of elite individuals, crossover probability is 0.5, rank fitness scaling, roulette selection, and scattered crossover operators. The detailed description of these algorithms can be found in the corresponding references. In case of Mincon method the initial point plays a very crucial role in finding the optima. If the initial point is specified as lower bound ($\underline{\alpha}$, $\underline{T}$), the Mincon method is unable to find the solution for some of the demanded force vectors. Similar, is the case when initial point is specified as upper bound ($\overline{\alpha}$, $\overline{T}$). The initial point is chosen after trial and error as $(0.75\,\overline{\alpha}, 0.75\,\overline{T})$. Therefore, the conventional optimization methods are sensitive to starting points. Evolutionary algorithms do not need any initial starting point to be specified.

Keppel's B280 semi-submersible oil rig is used as the case study vessel, the oil rig was subjected to a sea load profile. The demanded longitudinal resultant thrust (F_X), lateral resultant thrust (F_Y), and moment (M_Z) at 50 time steps are shown in Fig. 4.7. For the first step time the demanded longitudinal resultant thrust $(F_X = 49.959\ \text{kN})$, lateral resultant thrust $(F_Y = -60.481\ \text{kN})$, and moment $(M_Z = -63787\ \text{kN})$. The performance of the algorithms is evaluated based on convergence speed and the final numerical result. Since, evolutionary algorithms are heuristic in nature, so, we performed 50 trials to obtain the best solution for the evolutionary algorithms. The convergence of the best fitness value for the objective function for the demanded force vector using ITHS, IHS, HS and GA is shown in Fig. 4.8. In Fig. 4.8, it can be seen that the ITHS algorithm converges faster than IHS, HS and GA.

(a)
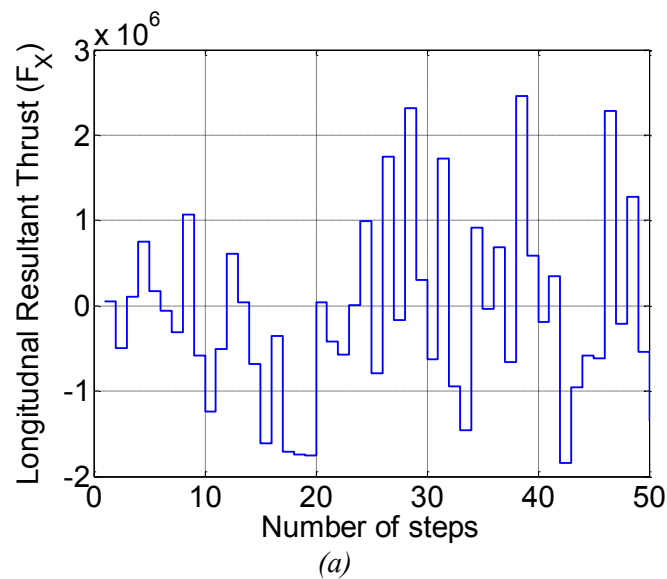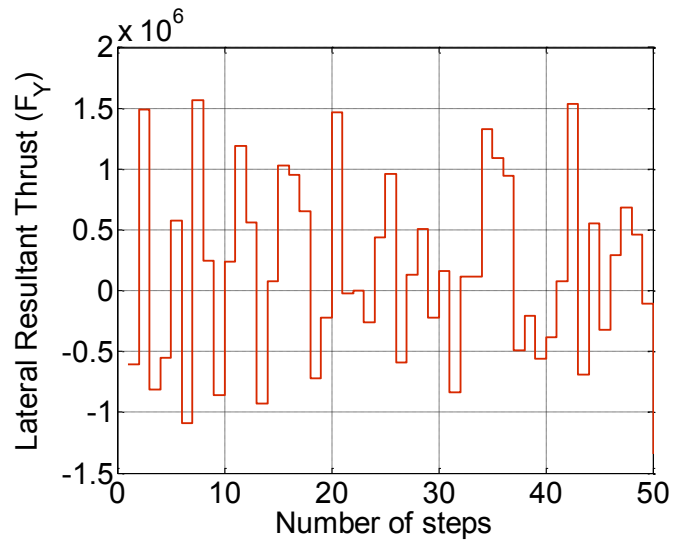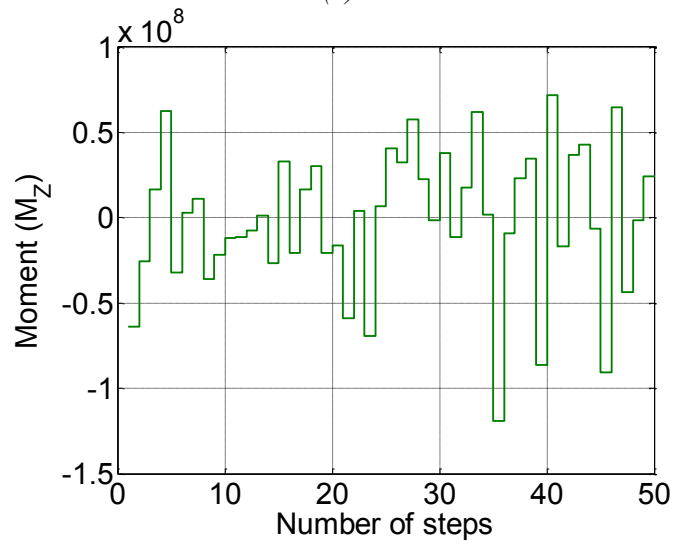
Fig. 4.7 The commanded (a)longitudinal resultant thrust (F_X), (b)lateral resultant thrust (F_Y), and (c) moment (M_Z) at 50 time steps
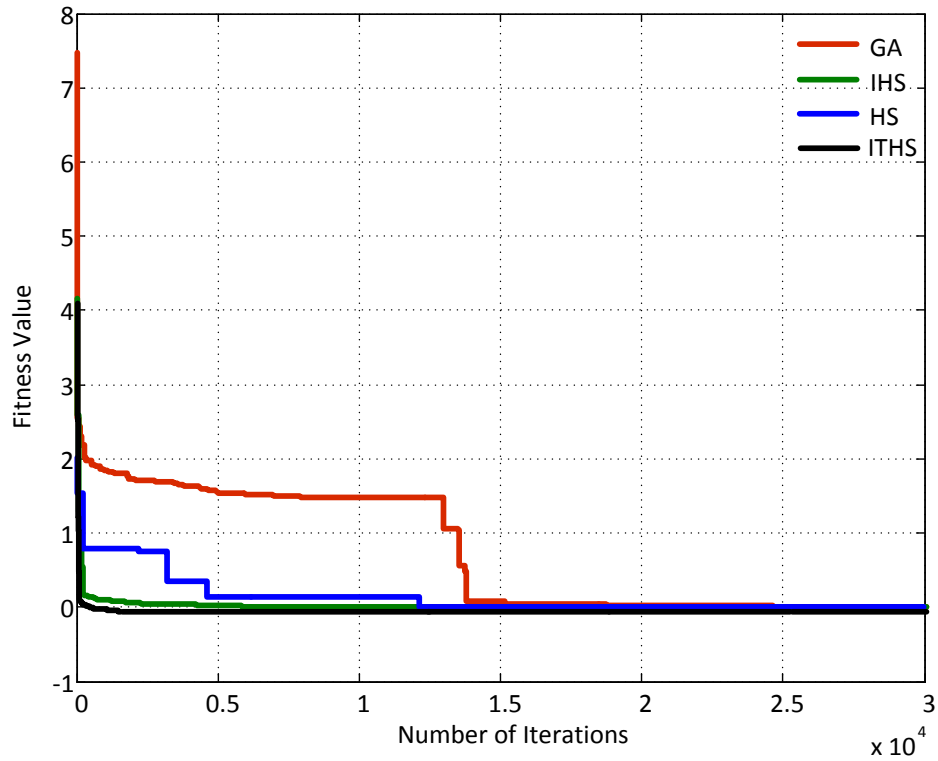
Fig. 4.8 Convergence of ITHS, IHS, HS and GA for demanded $F_X = 49.959\ kN$, $F_Y = -60.481\ kN$ and $M_Z = -63787\ kN$.

For the demanded force vectors shown in Fig. 4.7, the optimal solution is obtained using ITHS algorithm. From Fig. 4.6, it is observed that the ATRs of thruster pair (5, 6) and (7, 8) are similar to that of (1, 2) and (3, 4) respectively. Therefore, only the thrust forces and the corresponding azimuth angles for thruster 1 and 3 are shown in Fig. 4.9 - 4.10. The thrust forces and the azimuth angles for other thrusters are omitted to save space and considering that, they exhibit a similar trend.
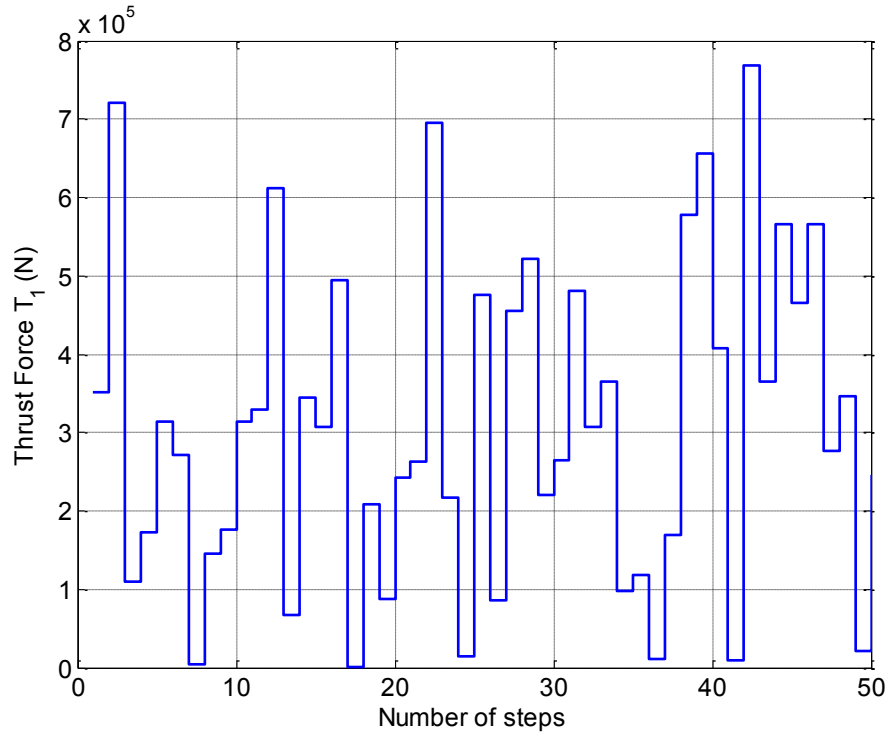
(a)
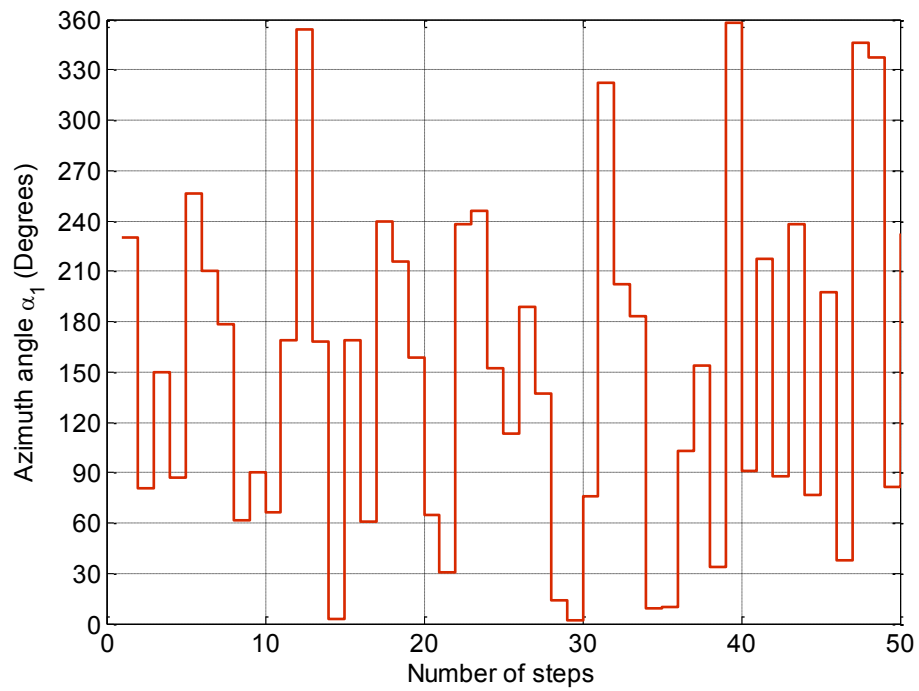
(b)

Fig. 4.9 (a) Delivered thrust forces and (b) corresponding azimuth angles for Thruster 1
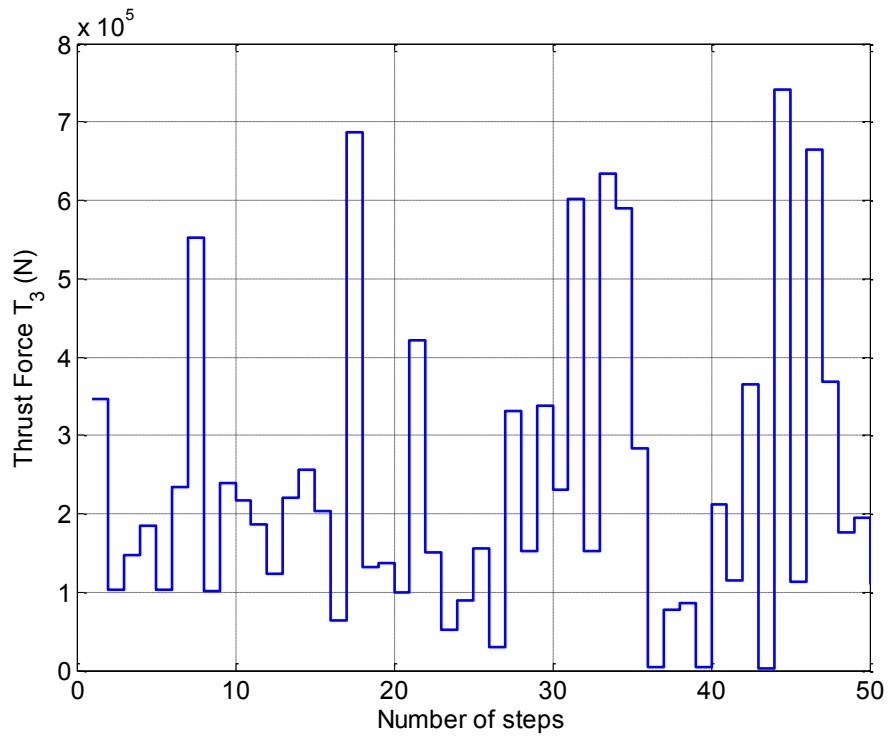
(a)
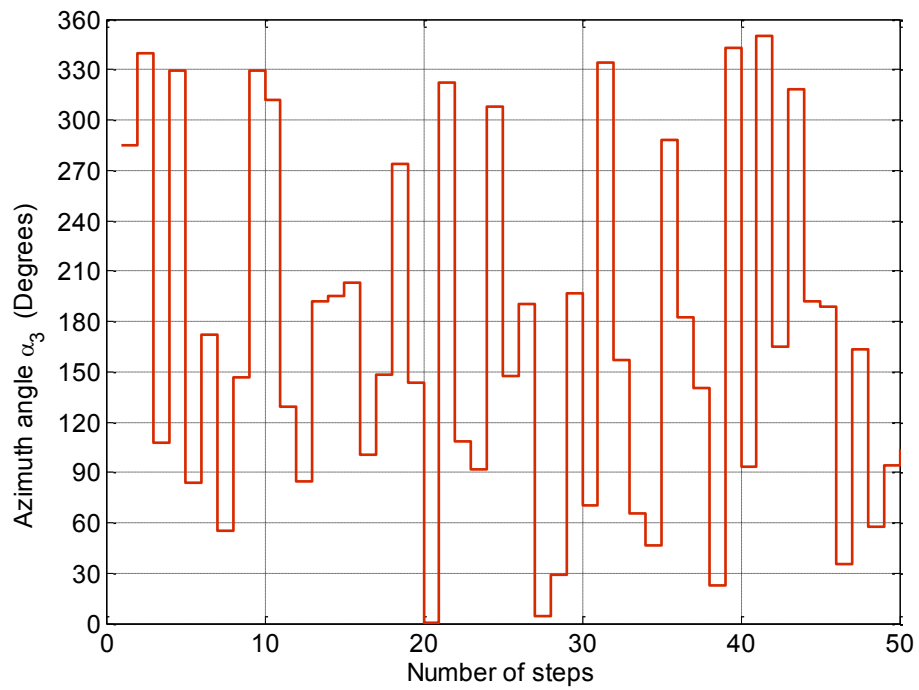
(b)

Fig. 4.10 (a) Delivered thrust forces and (b) corresponding azimuth angles for Thruster 3

The total power consumption of the eight thruster motors for 50 time steps for the ITHS, IHS, HS, GA and Mincon algorithm is shown in Fig. 4.11. It is evident from Fig. 4.11 that the power consumption for the ITHS algorithm is lower as compared to IHS, HS, GA and Mincon method. In case of Mincon method the total power consumption is almost constant because, it usually solves the formulated optimization problem by varying azimuth angles only and doesn't vary the thrust much. The evolutionary algorithms on the other hand find the solution for the formulated optimization problem by varying both thrust and azimuth angles of the thrusters. The ITHS algorithm similar to IHS and HS algorithm generates a new vector, after considering all of the existing vectors, whereas GA only considers the two parent vectors. These features increase the flexibility of the HS variants and produce better solutions as compared to GA. The harmony vectors selected are random in nature. The randomization diversifies the search space and prevents premature convergence. In addition, the self-adaptive pitch adjustment strategy adopted by ITHS algorithm further improves the convergence and also solution quality as compared to classical HS and IHS algorithm.
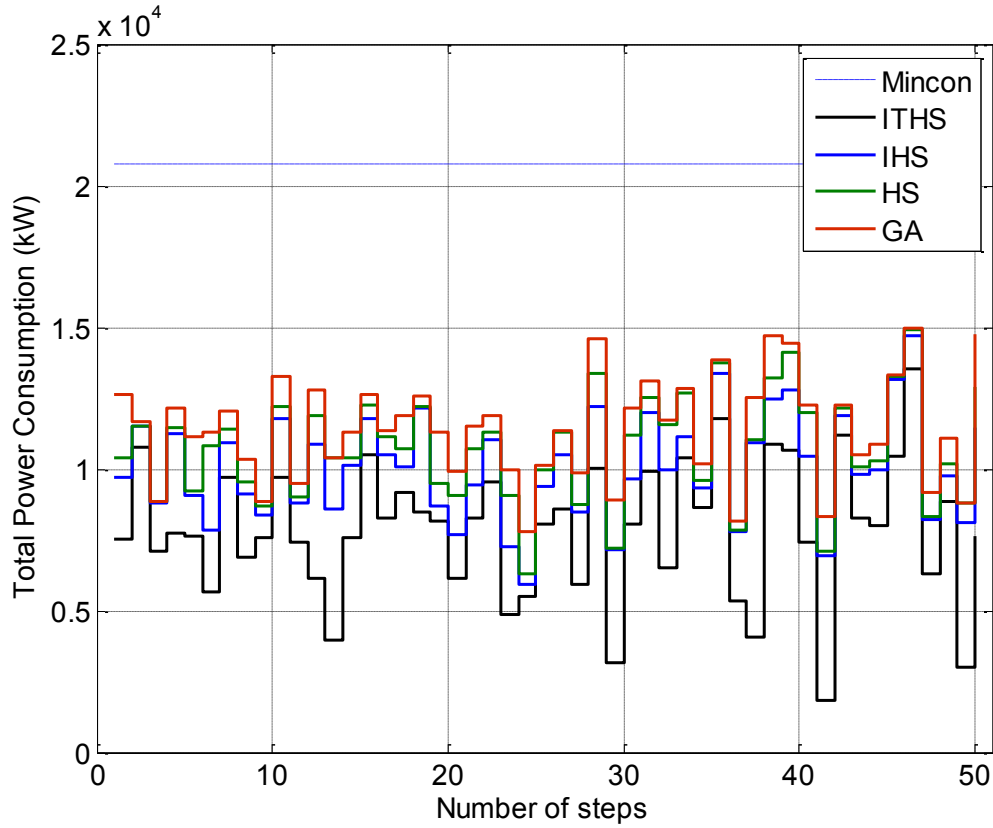
Fig. 4.11 *The Total power consumption during thruster allocation for 50 time steps for ITHS, IHS, HS, GA and Mincon algorithm.*

The total power consumed by the eight thruster motors during the entire load cycle is calculated by finding the area under the curve in Fig.4.11. For a step size (s) the total power is given by $\sum_{i=1}^{50} P_{Total}(i) \times s$, where, $P_{Total}(i)$ corresponds to total power consumed by the eight thruster motors for the ith step. Assuming that the step size (s) is 1, then the total power consumed eight thruster motors during the entire load cycle for Mincon, GA, HS, IHS and ITHS method is shown in Table 4.1. The percentage savings in total power consumption for thruster allocation as compared to Mincon method for GA, HS, IHS and ITHS method are 44.96%, 48.39%, 51.58% and 62.20% respectively.

Table 4.1. Total Power Consumption of the oil rig platform for the entire load cycle

Approach / Algorithm	Total Power Conventional Thrust Allocation (MW)	% Power Saving as compared to MinCon
Mincon	1039.2	-
GA	572.01	(44.96%)
HS	536.30	(48.39%)
IHS	503.22	(51.58%)
ITHS	392.84	(62.20 %)

4.8   Conclusion

In this chapter, the thruster allocation problem is formulated as a constrained optimization problem. The thrust allocator tries to minimize the power consumption by the thrusters and simultaneously ensures that the vessel is at the desired position. In addition, it also ensures that the thruster-thruster interaction is minimal. In this chapter, ITHS algorithm is used for solving the non-convex thrust allocation problem. The ability of the ITHS algorithm has been demonstrated and its performance is compared with other optimization techniques. The optimal thruster allocation using ITHS reduces the power consumption of the rig as compared to MinCon, GA, HS and IHS. The percentage savings in total power consumption by thrusters as compared to Mincon method for GA, HS, IHS and ITHS method are 44.96%, 48.39%, 51.58% and 62.20% respectively. It is clear from the results that the power consumption is minimal and the percentage savings in total power consumption for thruster allocation is maximum using the ITHS algorithm. In addition, the convergence for the ITHS algorithm is faster as compared to GA, HS and IHS method. Generally, it can be concluded that the ITHS algorithm's simplicity of implementation, high quality solution, along with the lower number of setting parameters makes it an ideal method when dealing with complex engineering optimization problems.

CHAPTER 5. ENERGY-EFFICIENT   THRUST ALLOCATION FOR SEMI-SUBMERSIBLE OIL RIG PLATFORMS

5.1   Introduction

In Chapter 4, the thrust allocator tries to minimize the power consumption of the oil rig platform. The power consumed by the oil rig platform depends on the thrust generated by the azimuth thrusters and the efficiency of the electrical propulsion system controlling the azimuth thruster. However, the formulated optimization based approach only focused on minimizing the power demanded by the thrusters and ignored the efficiency of the electrical propulsion system.

The thrust generated by an azimuth thruster is controlled by an electrical propulsion system and the efficiency of the lightly loaded electrical propulsion system is much less, than that of a more heavily loaded system. The load demanded during station keeping depends on the total environmental loads acting on the platform. During lower demand (calm weather conditions), if all the azimuth thrusters are operating then the electrical propulsion system of the azimuth thrusters are lightly loaded and operate in less efficient region. Therefore, one should distribute the maximum load for some of the azimuth thrusters and keep others idle. However, in conventional thrust allocation approach, since the efficiency of the electrical propulsion system is ignored, the thrusters may even operate in the inefficient region during lower load demand and increase the total power consumption of the oil rig platform. Since, efficiency greatly influences the power consumption of the system. Therefore, energy efficient systems have potential to reduce the power consumption of the system and have been widely used in different areas [36-43].

In this chapter, an energy-efficient thrust allocation approach is proposed and formulated as an optimization problem, with an objective to minimize the total power consumption by

ensuring that the electrical propulsion system operates in the efficient region and is subjected to force and moment constraints to ensure fixed position of the oil rig platform. In addition, the thrust direction constraints imposed on the azimuth thrusters due to forbidden/spoil zones is also considered. Forbidden/spoil zones are considered to avoid thruster-thruster interactions, which reduce the efficiency of the azimuth thrusters [26]. The formulated optimization problem is non-convex, due to the thrust direction constraints imposed on the azimuth thruster.

The rest of the chapter is arranged as follows. A detailed model to calculate the power consumption of the electrical propulsion system is explained in Section 5.2. The details of the energy-efficient thrust allocation optimization problem are presented in Section 5.3. The results obtained from the case study vessel with detailed discussions are presented in Section 5.4. Finally, the research findings are concluded in Section 5.5.

5.2   Modeling of Power Consumption of the Electrical Propulsion System

The electric propulsion system for a single thruster motor is shown in Fig. 5.1. The electric propulsion system of the semi-submersible oil rig platform is powered via an on-board power pool of eight generators, through a phase shifting transformer into a 12-Pulse rectifier. From this DC link voltage, a 3-Level Neutral Point Clamping (NPC) Voltage Source Inverter (VSI) creates varying frequency and amplitude AC voltage. High power induction motors are mounted vertically and used to propel the azimuth thrusters with the aid of an L-shaped gear transmission system. The thrust generated by the azimuth thrusters is controlled by VSI fed Induction motor drive. Eight azimuth thrusters located at the pontoon level of the oil rig platform are used by the DP system to control its position. The rated effective thrust (T_R) of each thruster is 780 kN at a rated motor power $\left(P_o(T_R)\right)$ of

4000 kW at 600rpm. The power consumed by the electric propulsion system depends on the thrust generated by the azimuth thrusters and the efficiency of the electric propulsion system controlling the azimuth thruster.
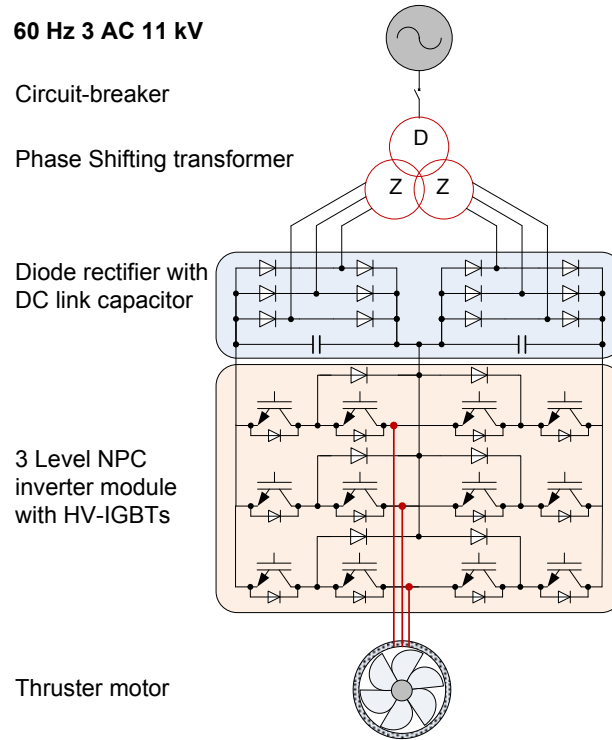
Fig. 5.1 Electrical Propulsion System for a single thruster motor

The total power consumption for station keeping of the semi-submersible oil rig platform equipped with N thrusters is given by Eqn.(5.1).

$$P_{Total} = \sum_{i=1}^{N} \frac{P_o(T_i)}{\eta_{System}(T_i)} = \sum_{i=1}^{N} \frac{P_o(T_R)T_i^{3/2}}{T_R^{3/2}\eta_{System}(T_i)} \tag{5.1}$$

where, $P_o(T_i) = P_o(T_R)(T_i/T_R)^{3/2}$ is the power consumed by the ith thruster to produce a thrust force (T_i)[13] and $\eta_{System}(T_i)$ is the efficiency of electric propulsion system for the

i^{th} thruster corresponding to thrust force (T_i). In order to calculate $\eta_{System}(T_i)$, losses in each sub-system of the electric propulsion system for the ith thruster are calculated.

5.2.1 Loss Model of Induction Motor

Three phase squirrel cage induction motors are used to propel the azimuth thrusters. The technical specifications of the induction motor are shown in Table.5.1. The motor parameters are derived using the Keppel FELS test reports and certificates of thruster motors [144].

Table.5.1. Parameters of the induction motor

Rated Power	4000 kW	Stator Resistance	0.0272 Ω
Rate Voltage	4160 V	Stator Inductance	0.3 Ω
Rated Current	690 A	Rotor Resistance	0.0204 Ω
Rated Speed	596 rpm	Rotor Inductance	0.7 Ω
Rated Frequency	50 Hz	Mutual Inductance	10.58 Ω

The fundamental frequency losses consist of copper losses, core losses (eddy current and hysteresis), stray losses, and mechanical losses (friction and windage). The total copper losses (P_{CU}) consist of stator copper loss and rotor copper loss are calculated using (5.2) [145].

$$P_{CU} = 3I_s^2 R_s + 3I_r^2 R_r \qquad (5.2)$$

where, R_s, I_s, R_r, I_r are the stator resistance, stator phase current, rotor resistance and rotor phase current respectively. The core losses (P_{Core}) are calculated using the Steinmetz

expressions of hysteresis and eddy current losses in case of sinusoidal flux distribution as shown in (5.3) [145].

$$P_{Core} = P_{Core\_s} + P_{Core\_r}$$
$$= (K_h \varphi^2 f + K_e \varphi^2 f^2) + (K_h \varphi^2 sf + K_e \varphi^2 (sf)^2) \tag{5.3}$$

where, K_h, K_e are hysteresis and eddy current loss constants respectively, f is the frequency of operation and φ is the flux and P_{Core_s}, P_{Core_r} are the stator and rotor core losses respectively. For ideal *v/f* operation, flux is assumed to be constant. Therefore, core loss depends on the frequency and slip of operation. The total core loss at any frequency (f) and slip (s) can be expressed in terms of its rated value as in (5.4) [146]. The slip (s) at a given load and is assumed to be proportional to load torque, s_R and f_R are the rated slip and frequency of the motor respectively.

$$P_{Core} = \frac{1}{2}\left[\left(\frac{1+s}{1+s_R}\right)\frac{f}{f_R} + \left(\frac{1+s^2}{1+s_R^2}\right)\left(\frac{f}{f_R}\right)^2\right]P_{Core_R} \tag{5.4}$$

The mechanical loss constitutes of bearing friction and windage loss. Mechanical loss at any speed w can be written in terms of its rated value as in (5.5) [147, 148].

$$P_{mech} = C_{mech}w^2 = P_{mech_R}(w/w_R)^2 \tag{5.5}$$

The rated mechanical losses $\left(P_{mech_R} = 5.4\ kW\right)$ and rated core loss $\left(P_{Core_R} = 34.3\ kW\right)$ are obtained from no load test results [149]. The additional losses also known as stray losses occur in an induction motor apart from copper, core and mechanical losses. The additional

losses are assumed to be proportional to the square of the rotor current and calculated using (5.6) [147, 149].

$$P_{Add} = P_{Add_R} \left(I_r / I_{r_R} \right)^2 \qquad (5.6)$$

Using IEC-60034-2-1 [149], the additional losses are determined by measuring the total losses, and subtracting from these losses the sum of the friction and windage loss, coreloss, stator loss, and rotor loss. The rated additional losses for the induction motor under consideration are 20.46 kW. Apart from fundamental frequency losses, harmonic losses occur in an induction motor when supplied by an inverter/non-sinusoidal source. The total harmonic motor loss for the induction motor is calculated for different load torques by measuring the difference between the total motor input power and the fundamental component of motor input power and shown in Fig. 5.2. A clear relation between harmonic motor loss and load could not be found. Therefore, a constant harmonic loss of $(P_h = 25.54\ kW)$ is assumed by taking the average value of the harmonic losses over the entire range of operation.

The total induction motor losses $\left(P_{IM_{T\_Loss}} \right)$ are calculated using (5.7) [149].

$$P_{IM_{T\_Loss}} = P_{CU} + P_{Core} + P_{mech} + P_{Add} + P_h \qquad (5.7)$$
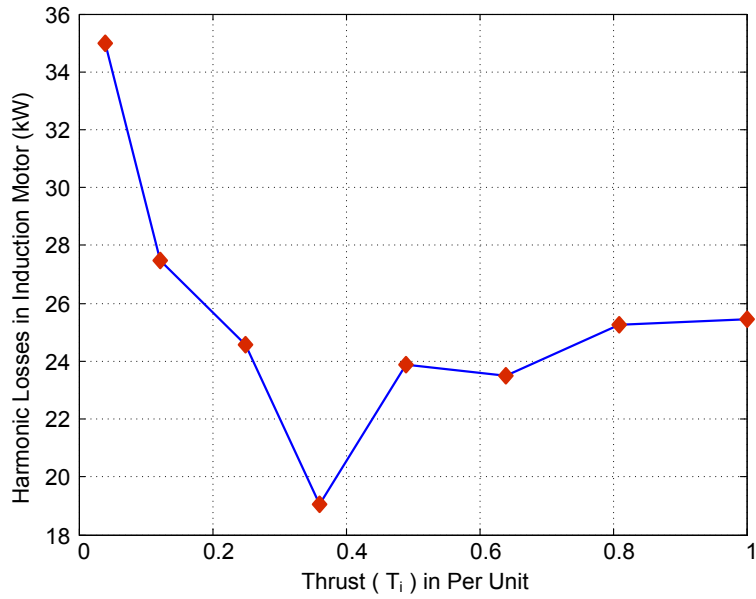
Fig. 5.2 Estimated Harmonic Losses (kW) at different loads

5.2.2 Loss Model of 3L-NPC Inverter

In Fig. 5.3 the design of single phase of Siemens Sinamics GM150 3L-NPC inverter is shown.
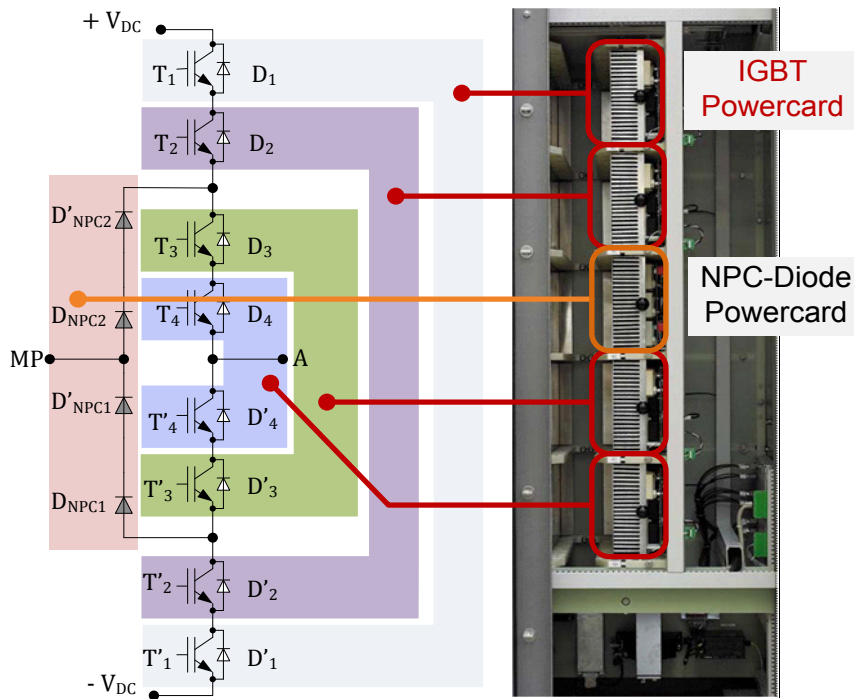
Fig. 5.3 Single phase of Siemens GM150 3L-NPC Inverter [150]

The modular phase design consists of four equal IGBT-Powercards and one NPC-Diode-Powercard. Each IGBT-Powercard comprises of two IGBT modules (including gate drivers). The two series connected IGBTs are located on neighbouring powercards. The NPC-Diode-Powercard consists of two double diode-modules and the corresponding RC snubbers for passive voltage balancing in the series connection [150]. For 4.16 kV drives, the series connection of two 3.3kV-IGBTs is used because it turns out to be more economical solution compared to the employment of a single 6.5kV-device [150]. Since the rated current of the induction motor is 690 A, the current rating of the IGBTs is 1200A [151]. Devices with voltage rating of 3.3kV and current rating of 1200A are available from several manufacturers.

In this paper, Eupec 3.3kV/1200A NPT-IGBT (FZ1200R33KF2) is used in the 3L-NPC inverter and inverter losses are calculated using the actual manufacturer's datasheet. The total losses $\left(P_{INV_{T\_Loss}}\right)$ in a 3L-NPC inverter consists of conduction losses $\left(P_{INV_{Con\_Loss}}\right)$ and switching losses $\left(P_{INV_{SW\_Loss}}\right)$. The semiconductor conduction $I - V$ characteristics and switching energy $E_{SW} - I$ characteristics at the maximum junction temperature $\left(T_j = 125\ °\text{C}\right)$ can be expressed as a function of the instantaneous inverter output current/stator input current (i_s) as shown in (4.12-4.13) [151-154].

$$u_{ON\_X} = u_{0X} + r_{0X}i_s \tag{5.8}$$

$$E_{SW} = (A_{0X} + B_{0X}i_s + C_{0X}i_s^2)\, U_C/U_{Base} \tag{5.9}$$

where, u_{0X}, r_{0X}, A_{0X}, B_{0X}, C_{0X} are the parameters of device X obtained from device datasheets [155] using curve fitting. The parameters obtained are shown in Table.5.2. In case of IGBT, A_{0X}, B_{0X}, C_{0X} have different values for turn-on and turn-off losses.

Table.5.2. Parameters of EUPEC 3.3 kV/1200 A NPT-IGBT (FZ1200R33KF2)

u_{0T}		1.7	V	u_{0D}	1.5	V
r_{0D}		2.6	mΩ	r_{0D}	1.5	Ω
B_{0T}	T_{ON}	1.1	mJ	A_{0D}	380	mV
	T_{Off}	0.82	mJ	B_{0D}	1.6	mΩ
C_{0T}	T_{ON}	0.0005	mJ	C_{0D}	0.0005	mΩ
	T_{Off}	0.00025	mJ	U_C	Vdc/2	V
U_{Base}		1800	V	f_C	1050	Hz

The conduction losses and the switching losses for each device is calculated using [153]. Using, Fig. 5.3 and [46] the total conduction $\left(P_{INV_{Con\_Loss}}\right)$ and switching losses $\left(P_{INV_{SW\_Loss}}\right)$ in a 3L-NPC inverter are given by (5.10-5.11) and the total losses $\left(P_{INV_{T\_Loss}}\right)$ in a 3L- NPC inverter is given by (5.12).

$$P_{INV_{Con\_Loss}} = 3\begin{pmatrix} 4P_{Con\_T1} + 4P_{Con\_T3} + 8P_{Con\_D1} \\ +4P_{Con\_DNPC1} \end{pmatrix} \qquad (5.10)$$

$$P_{INV_{SW\_Loss}} = 3\begin{pmatrix} 4P_{Sw\_T1} + 4P_{SW\_T3} + 4P_{Sw\_D1} \\ +4P_{SW\_DNPC1} \end{pmatrix} \qquad (5.11)$$

$$P_{INV_{T\_Loss}} = P_{INV_{Con\_Loss}} + P_{INV_{SW\_Loss}} \qquad (5.12)$$

where, $\boldsymbol{P_{Con\_x}}$ and $\boldsymbol{P_{Sw\_x}}$ are the conduction and switching losses for device x respectively.

5.2.3 Loss Model of 12 Pulse Rectifier

In a 12-pulse rectifier configuration, two B6 bridge rectifiers are connected in series. The 12 cell diodes that are built into the module are arranged in a stack. Each diode is provided with an RC protective circuit. The series connection avoids, issues associated with current sharing and eliminates the need for an inter-phase reactor. The switching losses have been ignored due to lower switching frequency in the rectifier. The total losses $\left(P_{REC_{T\_Loss}}\right)$ in a 12-pulse rectifier mainly constitute of conduction losses and are calculated using (5.13).

$$P_{REC_{T\_Loss}} = 4\left(P_o + P_{IM\ T\_Loss} + P_{INV_{T\_Loss}}\right)u_{ON\_D}/V_{DC} \tag{5.13}$$

Where, $\boldsymbol{P_o}$ is the output power of the motor. $\boldsymbol{P_{IM\ T\_Loss}}$ is the total loss across the induction motor. $\left(\boldsymbol{P_{INV_{T\_Loss}}}\right)$ is the total losses in a 3L- NPC inverter. $\boldsymbol{u_{ON\_D}}$ is the forward diode loss. $\boldsymbol{V_{DC}}$ id the dc link voltage.

5.2.4 Loss Model of Phase Shifting Transformer

Multi-pulse phase shifting zigzag transformers are used to mitigate current harmonics at the front end utility side. The three winding transformer has a delta-primary connection and two zigzag secondary winding connections. The relative phase shift of 30° in the two secondary windings is achieved either by the vector group Dd11.75d0.75 or Dd11.25d0.25 [55]. The thruster system unit 1, 3, 5, and 7 use phase shifting transformer of vector group Dd11.75d0.75 and thruster system unit 2, 4, 6, and 8 use phase shifting transformer of vector group Dd11.25d0.25. The transformer of vector group Dd11.75d0.75 and Dd11.25d0.25 provide a secondary phase shift of $-7.5°$, $22.5°$ and $7.5°, -22.5°$ respectively. The transformer secondary currents are rich in harmonics, with the harmonics of the order $6n \pm 1$, the primary of the transformer has harmonics of the order $12n \pm 1$ and at busbar the harmonics are of the order $24n \pm 1$. For, a given load the secondary

current drawn by both the secondary windings is the same. The fundamental component of the secondary current (I_{Sec1}) calculated using (5.14).

$$I_{Sec1} = \frac{0.5\big(P_o + P_{IM_{T\_Loss}} + P_{INV_{T\_Loss}} + P_{REC_{T\_Loss}}\big)}{\sqrt{3}V_{ll\_Sec}\cos\varphi_1} \tag{5.14}$$

where, V_{ll_Sec} is the line-line voltage of transformer secondary and $\cos\varphi_1$ is the displacement power factor. $\cos\varphi_1$ is modeled using the curve fitting technique based on the experimental test data obtained from the string test of Keppel's B280 and expressed as a function of thrust force (T_i) as shown in (5.15). In Fig. 5.4, the measured $\cos\varphi_1$ and modeled $\cos\varphi_1$ are compared.

$$\cos\varphi_1 = \frac{(0.9259\,T_i{}^2 - 0.07673T_i + 0.007371)}{(T_i{}^2 - 0.1135T_i + 0.02359)} \tag{5.15}$$
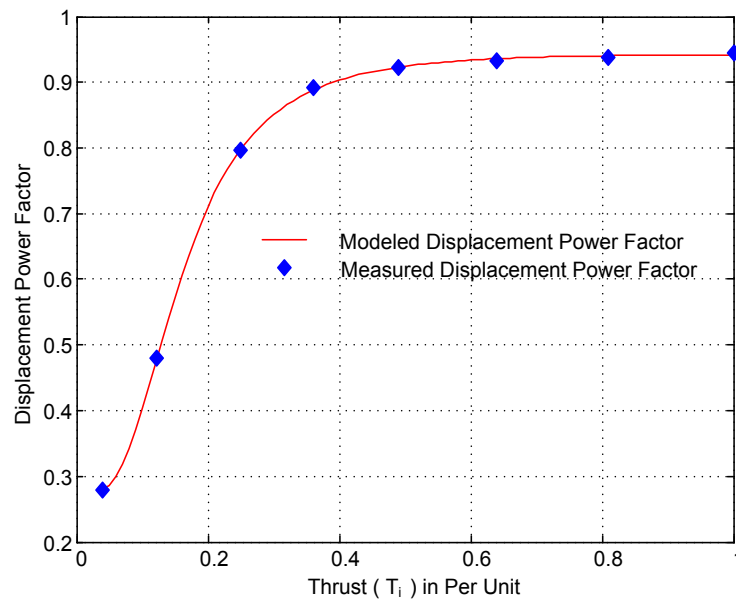
Fig. 5.4 Comparison of measured and modeled displacement power factor ($\cos\varphi_1$)

In the calculation of the copper losses of the transformer, both primary and secondary current harmonics have been ignored, because the magnitude of the current harmonics is

126

influenced by the equivalent synchronous reactance of the generators. Therefore, depends on the number of generators switched on, which cannot be known without knowing the input power of the electrical propulsion system. The fundamental frequency transformer secondary copper losses (P_{CU_Sec}) and primary copper losses (P_{CU_Prim}) are calculated using (5.16) and (5.17).

$$P_{CU\_Sec} = 3I_{Sec1}^2\left(R_{sec(\pm22.5°)} + R_{sec(\mp7.5°)}\right) \tag{5.16}$$

$$P_{CU\_Prim} = 3I_{Prim1}^2 R_{Prim} = 6\left(\frac{I_{Sec1}}{N_{tr}}\right)^2 R_{Prim} \tag{5.17}$$

where, $R_{sec(\pm22.5°)}$ and $R_{sec(\mp7.5°)}$ are the resistances of the secondary winding of the transformer with a phase shift of $(\pm22.5°)$ and $(\mp7.5°)$ respectively. R_{Prim} is the resistance of the transformer primary and N_{tr} is the transformer turns ratio.

The total transformer losses $(P_{TRANS_{T\_Loss}})$ for the phase shifting transformer are calculated using (5.18). In (5.18), $(P_{Core\_T} = 8.447\ kW)$ denotes core loss in the phase shifting transformer calculated using no-load test.

$$P_{TRANS_{T\_Loss}} = P_{CU\_Prim} + P_{CU\_Sec} + P_{Core\_T} \tag{5.18}$$

The efficiency of the electrical propulsion system of the single thruster motor can be calculated using (5.19).

$$\eta_{System}(T_i) =$$

$$\frac{P_o(T_i)}{P_{in}(T_i)} = \frac{P_o(T_i)}{\left(P_o(T_i) + P_{IM_{T\_Loss}} + P_{INV_{T\_Loss}} + P_{REC_{T\_Loss}} + P_{TRANS_{T\_Loss}}\right)} \tag{5.19}$$

The effectiveness of the efficiency computed using (5.19) is confirmed by comparison with

the efficiency of the electrical propulsion system measured at different loads as shown in Fig. 5.5.
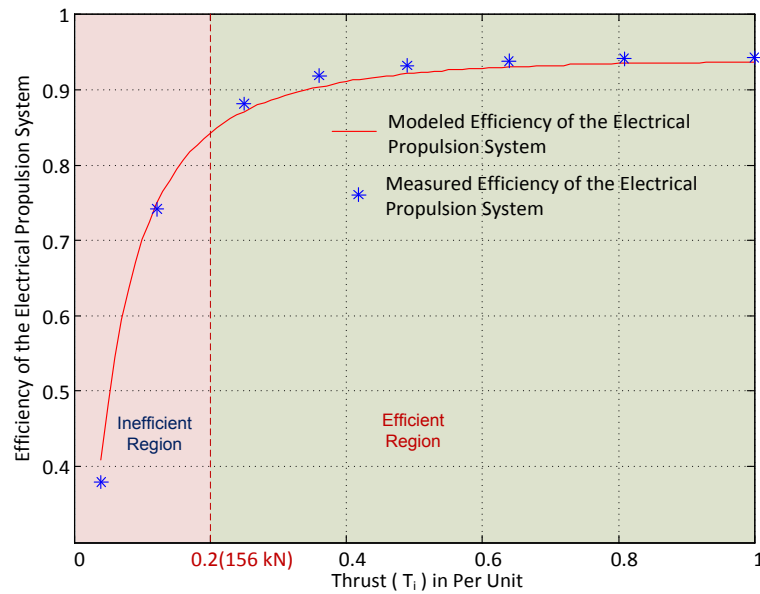
Fig. 5.5 Comparison of measured and modeled efficiency of the electrical propulsion system

5.3 Optimization Problem Formulation

The objective of the optimization problem is to minimize the total power consumption of the oil rig platform during station keeping. The power consumed by the electric propulsion system depends on the thrust generated by the azimuth thrusters and the efficiency of the electric propulsion system controlling the azimuth thruster. The efficiency curve as shown in Fig. 5.5 highlights that the efficiency of a lightly loaded electrical propulsion system is much less, than that of a more heavily loaded system. Therefore, during lower load demand, one should distribute the maximum load to some of the azimuth thrusters and keep remaining thrusters switched OFF. Since, the minimum thrust force of the azimuth thruster $\left(\underline{T}_i = 0.04 \times T_{iR} \right)$ is not equal to zero. Therefore, a switching sequence $(k = [k_1, k_2, k_3, \dots k_N]')$ is introduced to control the switching ON and OFF of the thruster units. The switching variable (k_i) is defined by (5.20).

$$k_i = \begin{cases} 1, if\ i^{th}\ thruster\ unit\ is\ ON \\ 0, if\ i^{th}\ thruster\ unit\ is\ OFF \end{cases} \tag{5.20}$$

The total power consumption for station keeping of the semi-submersible oil rig platform equipped with N thrusters given by (5.1) is modified and rewritten as given by (5.21).

$$P_{Total} = \sum_{i=1}^{N} \left(\frac{P_o(T_i)k_i}{\eta_{System}(T_i)} \right) \tag{5.21}$$

Therefore, for $k_i = 0$, the power demanded by the ith thruster is zero and for $k_i = 1$, the power demanded by the ith thruster is $(P_o(T_i)/\eta_{System}(T_i))$. Similarly, the forces and moment generated by the ith thruster as explained in (4.4) are modified and rewritten as in (5.22).

$$\tau_i = \begin{bmatrix} F_X^i \\ F_Y^i \\ M_Z^i \end{bmatrix} = \begin{bmatrix} \cos \alpha_i \\ \sin \alpha_i \\ \sin \alpha_i L_{Xi} - \cos \alpha_i L_{Yi} \end{bmatrix} k_i T_i = B(\alpha_i)k_i T_i \tag{5.22}$$

The force vector (τ) demanded is jointly produced by N thrusters in order to keep the oil rig platform at the fixed position. However, for $k_i = 0$, the forces and moments generated by the ith thruster is zero. Therefore, τ is expressed by (5.23).

$$\tau = \sum_{i=1}^{N} \tau_i = \begin{bmatrix} \sum_{i=1}^{N} F_X^i \\ \sum_{i=1}^{N} F_Y^i \\ \sum_{i=1}^{N} M_Z^i \end{bmatrix} = B(\alpha)T_k \tag{5.23}$$

where, $T_k = k.*T = [k_1 T_1, k_2 T_2, k_3 T_3 \ldots k_N T_N]'$ and $k.*T$ is the element-by-element

multiplication of k and T. The switching sequence introduced has no effect on the ATRs of the azimuth thrusters.

Now, using (5.21-5.23), the optimization problem can be formulated with an objective to minimize the total power consumption by ensuring that the thruster system operates in efficient zone and is subjected to force and moment constraints to ensure fixed position of the oil rig platform. In addition, the thrust direction constraints imposed on the azimuth thrusters due to forbidden/spoil zones is also considered. The formulated optimization problem is given by (5.24-5.27).

$$\text{Min } P_{Total}(\alpha, T, k) = \text{Min}\left(\sum_{i=1}^{N} \frac{P_o(T_i) \times k_i}{\eta_{System}(T_i)}\right) \tag{5.24}$$

subjected to

$$\tau - \text{B}(\alpha)T_k = 0 \tag{5.25}$$

$$\left(\underline{\alpha}_i \leq \alpha_i \leq \overline{\alpha}_i, \ \underline{T}_i \leq T_i \leq \overline{T}_i\right) \text{ or } (\alpha_i, T_i) \in S_i \tag{5.26}$$

$$T_{ki} = k_i T_i, \ k_i \in \{0,1\} \tag{5.27}$$

where, $P_o(T_i)$ is the power consumed by the ith thruster to produce a thrust force (T_i). Eqn. (5.25) ensures that the error between the demanded generalized force (τ) and generalized force jointly produced by N thrusters is close to zero to keep the oil rig platform at the fixed position. Eqn. (5.26) ensures that the thrust produced by each thruster is restricted to its ATR. The switching variable k_i is used, because, the key idea of the optimization is to distribute the maximum load for some of the azimuth thrusters and keep others idle.

The variables of the formulated optimization problem are (α, T, k). The original thrust allocation problem is non-convex, due to the thrust direction constraints imposed on the azimuth thruster [13, 60]. In the formulated optimization problem, in addition to the optimum azimuth angles (α) and thrust forces (T), the proposed algorithm also finds the

optimum thruster switching sequence (k). Since, the element of the switching sequence ($k_i \in \{0,1\}$) can be either zero or one. Therefore, the formulated optimization problem is a mixed integer non-convex optimization problem. The formulated mixed integer non-convex constrained optimization problems are hard to solve using iterative optimization methods such as Newton's method, Sequential Quadratic Programming (SQP), Gradient descent etc. The iterative numerical optimization methods are very fast and need less computational time, however, these methods are highly sensitive to starting points and frequently converge to a local optimum solution or diverge altogether. Therefore, conventional methods fail to find the optimum solution for the non-convex thrust allocation problem and often be trapped in local minima. Metaheuristic algorithms eradicate some of the afore-mentioned difficulties and can be used in solving non-convex optimization problems.

5.4   Results and Discussions

In order to evaluate the effectiveness and performance of ITHS algorithm, its performance is compared with Mincon Method (Sequential Quadratic Programming), Improved Harmony Search (IHS), Harmony Search (HS) and Genetic Algorithm. The parameters for the HS, IHS algorithms are fixed as the same as those reported in [7, 112] and parameters of ITHS algorithm is same as those reported in Chapter 2. For the HS algorithm, *HMS = 5, HMCR = 0.9, PAR = 0.33* and *bw = 0.01*. For the IHS algorithm, *HMS = 5, HMCR = 0.9, PAR$_{min}$* =0.1, PAR$_{max}$ =0.99, *bw$_{min}$* = 0.0001 and *bw$_{max}$* $= \left(\overline{x}_i - \underline{x}_i \right)/20$. According to [7], the default values of GA parameters are: 20 individuals per generation, 10% of elite individuals, crossover probability is 0.5, rank fitness scaling, roulette selection, and scattered crossover operators. The detailed description of these algorithms can be found in the corresponding references.

Keppel's B280 semi-submersible oil rig platform is used as the case study of the marine vessel, the oil rig platform was subjected to a sea load profile. The demanded longitudinal resultant thrust (F_X), lateral resultant thrust(F_Y), and moment (M_Z) for 50 time steps are shown in Fig. 5.6 (a), (b), (c) respectively. In case of Mincon method, the initial point plays a very crucial role in finding the optima. The DP operator or the user has to use capability plots and logically select the switching sequence of the thrusters for each of the loading conditions. Therefore, the DP operator must provide initial guess of switching sequence. In order to show the effect of different switching sequence of thrusters on the performance of the Mincon method, the first step time with the demanded longitudinal resultant thrust $(F_X = 49.959$ kN), lateral resultant thrust $(F_Y = -60.481$ kN), and moment$(M_Z = -63787$ kN $-$ m) are chosen. The initial points for thrusters are chosen after trial and error as $(0.75\,\overline{\alpha}, 0.75\,\overline{T})$. If the initial point is specified as lower bound ($\underline{\alpha}, \underline{T}$), the Mincon method is unable to find the solution for some of the demanded force vectors. Similar, is the case when initial point is specified as upper bound ($\overline{\alpha},\ \overline{T}$). Initially the switching sequence $(k1 = \{1, 0, 1, 0, 1, 0, 0, 0\})$ is chosen. Therefore, $x_o = \left[0.75\,\overline{\alpha}, 0.75\,\overline{T},\ k1\right]$ is the initial starting point for the Mincon method. Now, for the same load condition the switching sequence $(k2 = \{1, 1, 0, 0, 0, 0, 0, 1\})$ is chosen. Therefore, $x_o = \left[0.75\,\overline{\alpha}, 0.75\,\overline{T},\ k2\right]$ is the initial starting point for the Mincon method. The loading of different thrusters for both the switching sequences is shown in Table.5.3. It is observed from Table.5.3, that for different switching sequences the power consumption of the electrical propulsion system is different. Therefore, performance of the conventional optimization techniques is sensitive to the choice of the initial point. Evolutionary algorithms do not need any initial starting point to be specified.

Table.5.3. Loading of different thrusters for both the switching sequences

Thrust No. Switching Sequence		1	2	3	4	5	6	7	8	Power (kW)
(k1)	T (in PU)	0.974	0.750	0.500	0	0.643	0	0	0	10640.2
	$\alpha°$	271.3	308.4	73.61	171.27	151.53	331.64	-90.44	110.06	
(k2)	T (in PU)	0.746	0.783	0	0	0	0	0	0.923	9526.11
	$\alpha°$	232.71	254.66	215.40	397.78	-37.79	449.31	195.73	398.43	

For the demanded force vectors shown in Fig. 5.6, the optimal solution is obtained using ITHS algorithm. From Fig. 5.6, it is observed that the ATRs of thruster pair (5, 6) and (7, 8) are similar to that of (1, 2) and (3, 4) respectively. Therefore, only the thrust forces and the corresponding azimuth angles for thruster 1 and 3 are shown in Fig. 5.7-5.8. The thrust forces and the azimuth angles for other thrusters are omitted to save space and considering that, they exhibit a similar trend.

The total power consumption of the oil rig platform during thruster allocation for 50 time steps with energy-efficient thrust allocation approach and conventional thrust allocation approach for IHS, HS, GA and Mincon is shown in Fig. 5.9. In case of Mincon method, the total power consumption of the oil rig platform for conventional thrust allocation approach is almost constant because, it usually solves the formulated optimization problem by varying azimuth angles only and does not vary the thrust much. In case of energy-efficient thrust allocation approach the switching sequence helps Mincon method to perform better and provides additional control for varying the thrust.
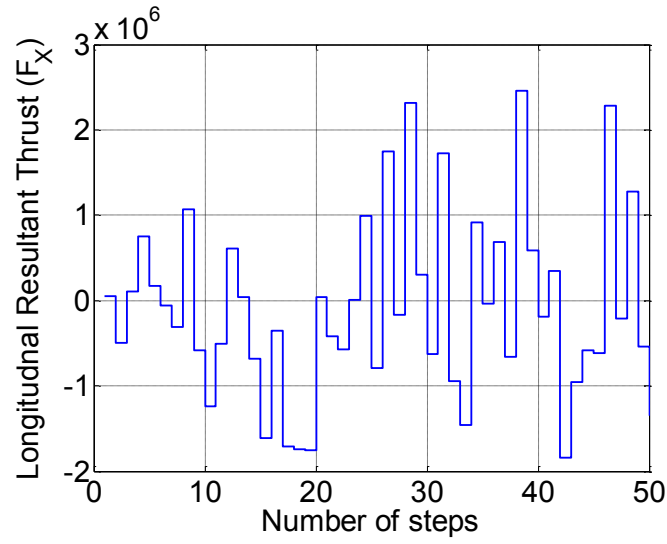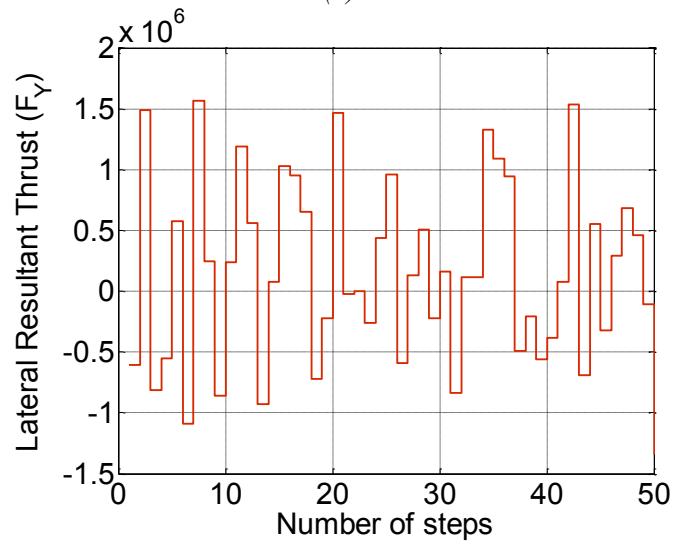
Fig. 5.6 The commanded (a)longitudinal resultant thrust (F_X), (b)lateral resultant thrust (F_Y), and (c) moment (M_Z) at 50 time steps
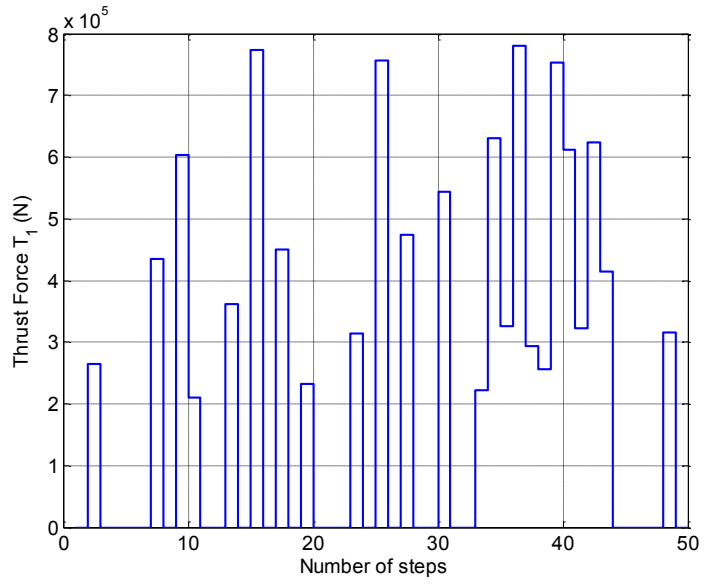
(a)
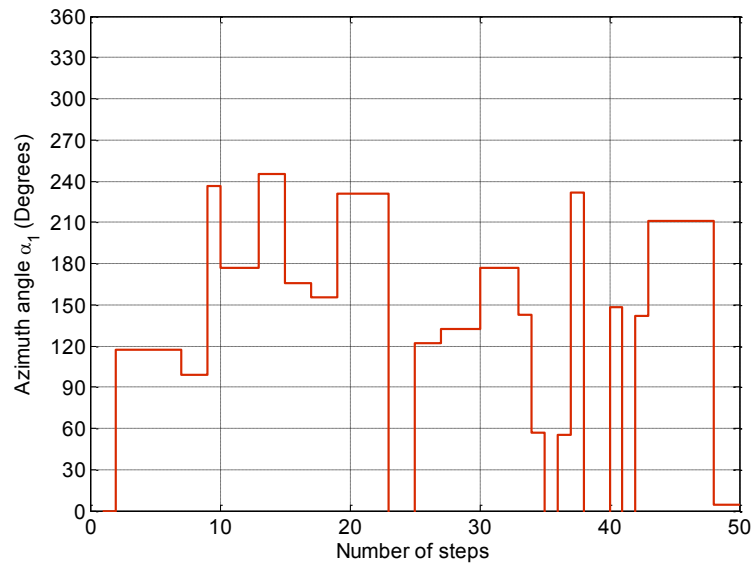
(b)

Fig. 5.7 (a) Thrust forces and (b) corresponding azimuth angles for Thruster 1
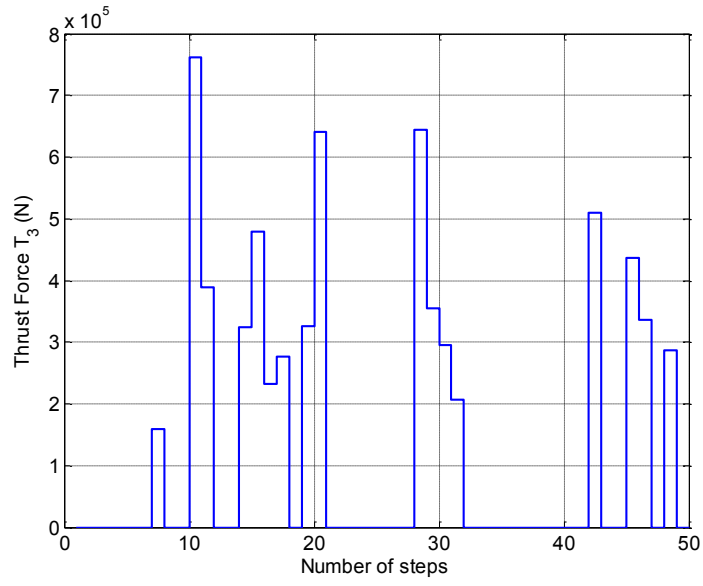
(a)
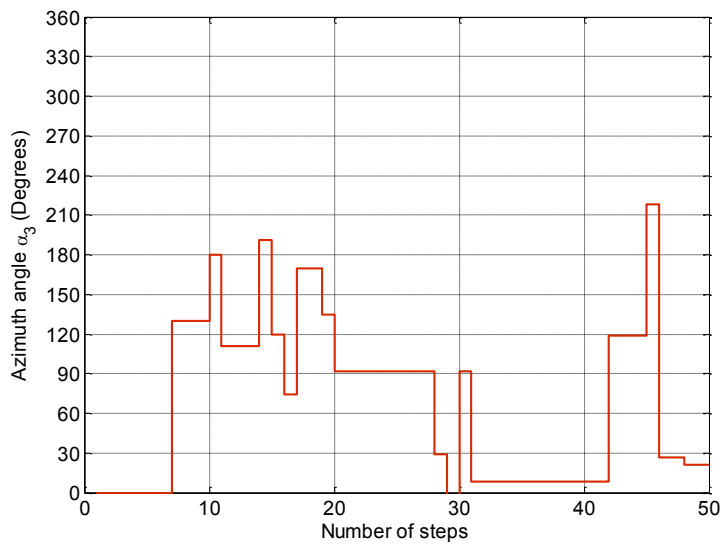
(b)

Fig. 5.8 (a) Thrust forces and (b) corresponding azimuth angles for Thruster 3.
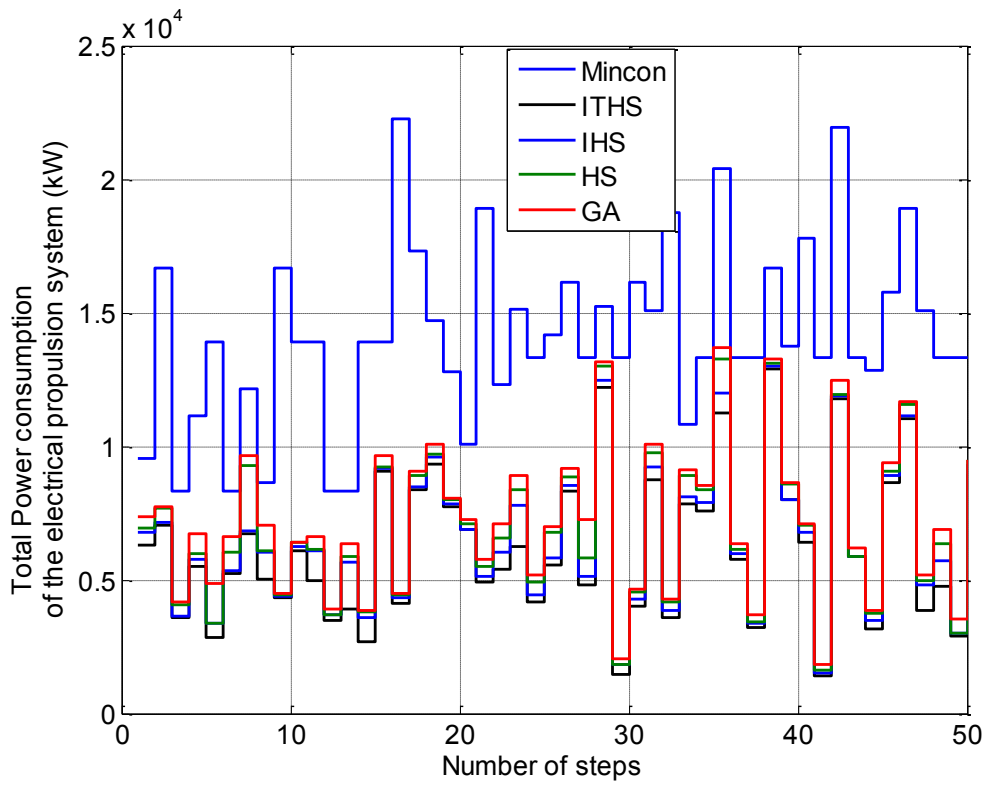
(a)
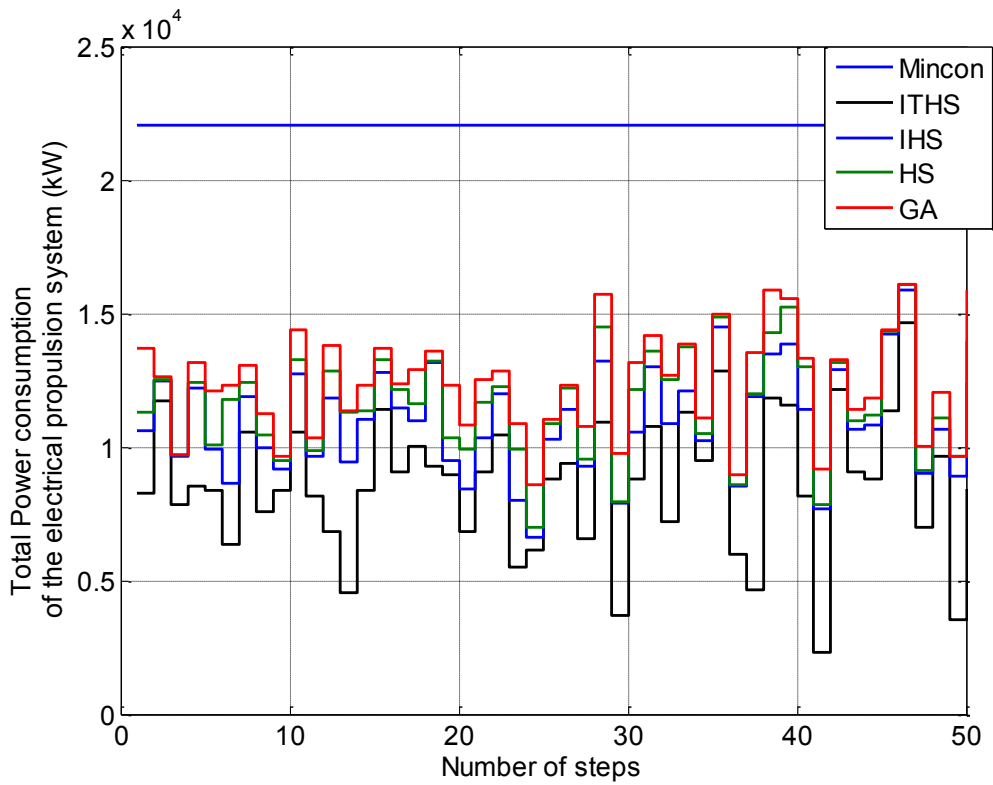
(b)

Fig. 5.9 Total power consumption of the oil rig platform during thruster allocation for 50 time steps with (a) energy-efficient thrust allocation and (b) conventional thrust allocation

137

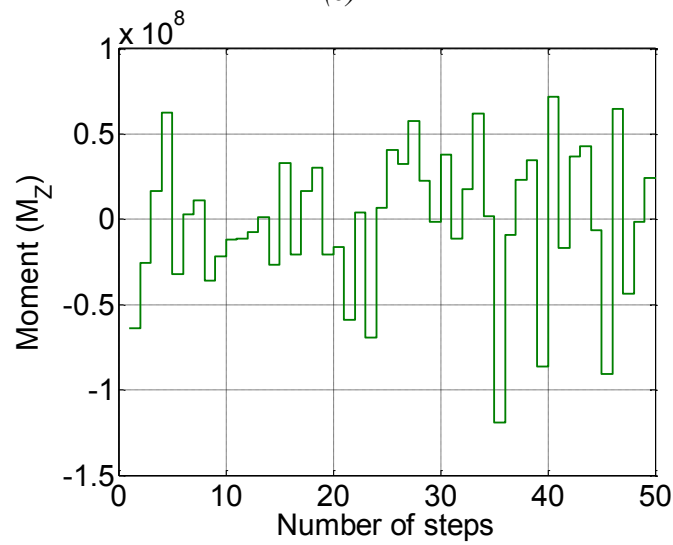Evolutionary algorithms on the other hand find the solution for the formulated optimization problem by varying both thrust and azimuth angles of the thrusters in both the cases. As observed from Fig.5.9 that the power consumption for ITHS is less as compared to HIS, HS, GA and Mincon method in both the cases. In case of energy-efficient thrust allocation approach and conventional thrust allocation approach, the total power consumed by the oil rig platform during the entire load cycle is calculated by finding the area under the curve in Fig. 5.9 (a) and Fig. 5.9 (b) respectively. For a step size (s) the total power is given by $\sum_{i=1}^{50} P_{Total}(i) \times s$, where, $P_{Total}(i)$ corresponds to total power consumed by for the ith step. Assuming the step size (s) as 1, then the total power consumed by oil rig platform during the entire load cycle for Mincon, GA, HS, IHS and ITHS method is shown in Table.5.4. The percentage savings in total power consumption for energy-efficient thruster allocation as compared to Mincon method for GA, HS, IHS and ITHS method are 48.76 %, 51.13 %, 53.90 % and 56.43% respectively. The percentage savings in total power consumption for energy-efficient thruster allocation as compared to GA for HS, IHS and ITHS method is 4.62 %, 10.02 % and 14.98 % respectively.

Table.5.4. Total Power Consumption of the oil rig platform for the entire load cycle

Approach / Algorithm	Total Power for Conventional Thrust Allocation (MW)	Total Power for Energy-Efficient Thrust Allocation (MW)
Mincon	1103	707.67
GA	620.84	362.61
HS	583.19	345.86
IHS	548.32	326.26
ITHS	**431.98**	**308.29**

It can also be observed from Table.5.4 that the total power consumption of the oil rig platform for energy-efficient thrust allocation approach is lower as compared to conventional thrust allocation approach for all the considered algorithms. In energy-

efficient thrust allocation approach, the thruster allocator automatically decides the switching sequence and efficiently turns off some of the thrusters as shown in Fig. 5.7(a)-5.8(a). Since some of the thrusters are turned off, the remaining thrusters operate in the efficient region (at higher load). It can be seen from Fig. 5.7(a)-5.8(a) that loading of the thruster motors is above 20 % (>156 kN) of the rated load. Therefore, each thruster operates in the efficient region as shown in Fig. 5.5. In the conventional thrust allocation approach, since the efficiency of the propulsion system is ignored, the thrusters may even operate in the inefficient region (at lower load). It is observed from Fig. 5.10(a) that loading of the thruster in certain cases is even below 20 % (< 156 kN) of the rated load and operate in the inefficient region as shown in Fig. 5.5. Therefore, the total power consumption of the oil rig platform for energy-efficient thrust allocation approach is lower as compared to conventional thrust allocation approach.

In addition, the proposed approach causes lower wear and tear to the thrusters, because the turned off thrusters retain their previous loads azimuth angle as shown in Fig. 5.7(b)-5.8(b), whereas in conventional thrust allocation approach, all the thrusters are turned on and the change in the azimuth angle is very rapid as shown in Fig. 5.10(b). Therefore, the change in azimuth angle for energy-efficient thrust allocation approach is lower as compared to conventional thrust allocation approach. In order to reduce the wear and tear of the thrusters, the rate of change of azimuth angle $(\Delta\alpha)$ can be constrained and minimized. However, this approach reduces the ATR of the thrusters and therefore, may increase the power consumption.
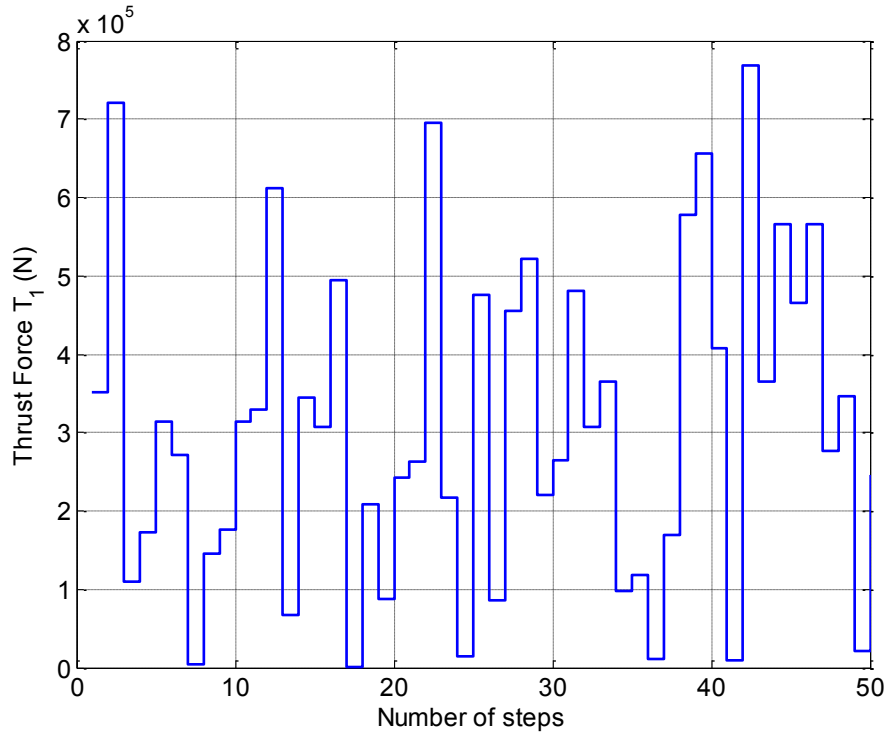
(a)
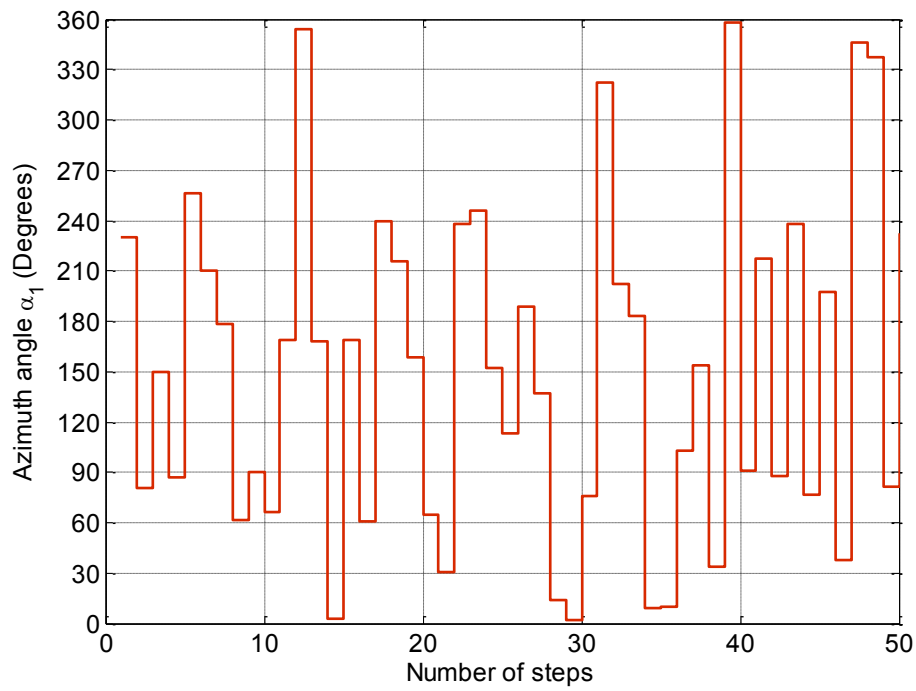
(b)

Fig. 5.10 (a) Delivered thrust forces and (b) corresponding azimuth angles for Thruster 1

Furthermore, the proposed approach enhances the dynamic performance of the drive, because, the thrusters operate in the efficient region (at higher load) and it is well known that the performance of the induction motor drive is better at higher loads as compared to when operating at lower loading. Since, the electrical drive system tends to operate at higher loading, the conventional and much simpler v/f control can be used to control the induction motor. The drawbacks of the v/f control at lower speeds are automatically eliminated using the proposed approach. The major advantage of the proposed approach is that, there is no need of additional hardware integration and the proposed approach can be integrated in the existing system by changing the DP software.

The future research should focus on other objectives such as minimization of Voltage Total Harmonic Distortion (VTHD) or maximization of the reliability of the propulsion system using optimal thrust allocation approach. Furthermore, the proposed problem can be formulated as multi-objective optimization problem with focus on power, power quality or reliability. In this paper, the rate of change of thruster azimuth angle ($\Delta\alpha$) and thrust (ΔT) are not considered because of the high inertia of the oil rig. In addition, the oil rig is also supported by mooring lines to further restrict the movement. However, in vessels with only azimuth thrusters, the constraint due to $\Delta\alpha$ and ΔT can be considered and further studied. The proposed approach is used to find a solution for 3-DOF can also be extended for 6-DOF control allocation problem.

5.5 Conclusions

In this chapter, an energy-efficient thrust allocation problem for semi-submersible oil rig platform is formulated as a mixed integer constrained optimization problem. ITHS algorithm is used to find the solution of the formulated optimization problem. The optimal thrust allocation using ITHS reduces the total power consumption of the oil rig platform as compared to Mincon, GA HS and IHS. The percentage savings in total power consumption for energy-efficient thrust allocation as compared to Mincon method for GA and HS, IHS and ITHS method are 48.76 %, 51.13 %, 53.90 % and 56.43% respectively. The proposed ITHS method can avoid the shortcoming of premature convergence of GA, HS and IHS method. Therefore, the power consumption is minimal in case of the ITHS method. The total power consumption of oil rig platform for energy-efficient thrust allocation approach is lower as compared to conventional thrust allocation approach for all the algorithms. It proves that the proposed approach is effective in reducing the power consumption of the semi-submersible oil rig platform. Generally, it can be concluded that simplicity of implementation, higher energy saving potential, along with enhanced dynamic performance and need of simpler controller makes it an ideal approach for marine applications.

CHAPTER 6. VOLTAGE HARMONIC DISTORTION COMPLIANT ENERGY-EFFICIENT THRUST ALLOCATION FOR SEMI-SUBMERSIBLE OIL RIG PLATFORMS USING AN INTELLIGENTLY TUNED HARMONY SEARCH ALGORITHM

6.1 Introduction

In Chapter 5, the thrust allocator tries to minimize the power consumption of the oil rig platform by ensuring that each thruster operates in the efficient region. The conventional thrust allocation approaches only focus on minimizing the power demanded by the thrusters. Therefore, the load demanded by the azimuth thrusters of vector group Dd11.75d0.75 and vector group Dd11.75d0.75 may not be the same and hence leads to higher voltage Total Harmonic Distortion (V_{THD}^{Bus}) and Individual Harmonic Distortion (V_h^{Bus}) at 11 kV busbar.

The V_{THD}^{Bus} and V_h^{Bus} at 11 kV busbar can be limited by (a) switching more generators (reduces source reactance), (b) reducing the loading of the thruster motors and (c) equaling the load demanded by the azimuth thrusters of vector group Dd11.75d0.75 and vector group Dd11.75d0.75. However, switching extra generator and reducing the loading of the thruster motors would be energy inefficient. Similarly, reducing the loading of the thruster motors would also lead to higher power consumption. The option (c) doesn't ensure the V_{THD}^{Bus} and V_h^{Bus} at 11 kV busbar are within the limits. Therefore, there is a tradeoff between the requirements of low power consumption of the oil rig platform and low THD. The best solution to this tradeoff is the optimization of power consumption of the oil rig platform with THD constraints

In this chapter, the Voltage Harmonic Distortion compliant Energy-Efficient Thrust allocation approach is proposed, with an objective to minimize the total power consumption by ensuring that the electrical propulsion system operates in efficient zone and is subjected to force and moment constraints to ensure fixed position of the oil rig platform. The thrust direction constraints imposed on the azimuth thrusters due to forbidden/spoil zones is also considered. In addition, the constraints imposed on V_{THD}^{Bus} and V_{IHD}^{Bus} have also been incorporated in the optimization problem. The formulated mixed integer non-convex optimization problem is solved using ITHS algorithm.

The rest of the Chapter is arranged as follows. A detailed model to calculate V_{THD}^{Bus} and V_h^{Bus} at 11 kV busbar is explained in Section 6.2. The analysis of Harmonic Cancellation in a Quasi-24 Pulse Rectifier system is explained in Section 6.3. The details of the formulated Voltage Harmonic Distortion compliant Energy-Efficient Thrust allocation optimization problem are presented in Section 6.4. The results obtained from the case study vessel with detailed discussions are presented in Section 6.5. Finally, the conclusions of the test results are presented in Section 6.6.

6.2   Modeling of the Voltage Harmonic Distortion in the Electrical Propulsion System

In the semi-submersible oil rig platforms the thrust generated by the azimuth thrusters is controlled by VSI fed induction motor drive. The rectifiers (AC/DC converters) draw non-sinusoidal current from the transformer secondary and introduce excessive levels of current and voltage harmonics. Harmonic distortions in the electrical power system is an important factor for safe and reliable operation of the marine vessels, as it adversely affect the electric and electronic subsystems [45-47]. Therefore, marine regulating bodies have imposed

stringent limits on voltage total harmonic distortion and individual harmonic distortion at the point of common coupling. In this section a detailed mathematical model of the electrical propulsion system of the oil rig is developed to analyze V_{THD}^{Bus} and V_{IHD}^{Bus} at 11 kV busbar.

The electric propulsion system for a single thruster motor is shown in Fig. 6.1.
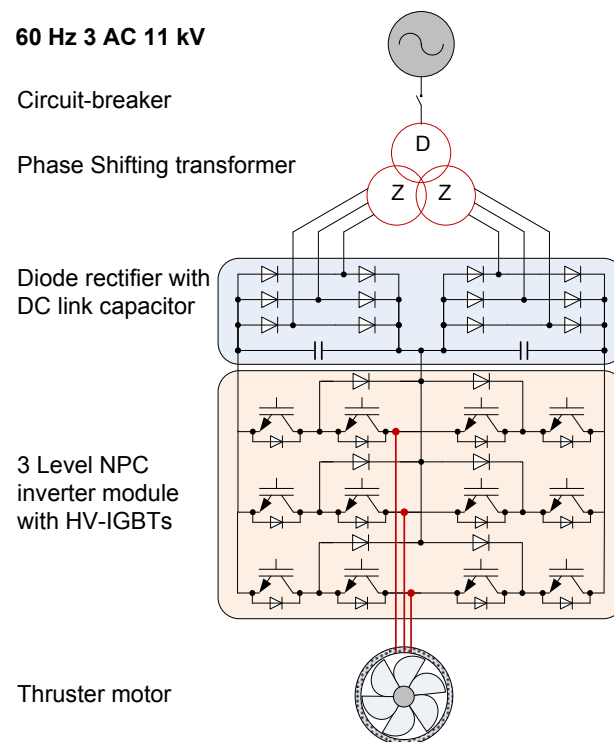
Fig. 6.1 Electrical Propulsion System for a single thruster motor

The electric propulsion system of the semi-submersible oil rig platform is powered via an on-board power pool of eight generators, through a phase shifting transformer into a 12-Pulse rectifier. From this DC link voltage, a 3-Level Neutral Point Clamping (NPC) Voltage Source Inverter (VSI) creates varying frequency and amplitude AC voltage. Three phase squirrel cage induction motors are used to propel the azimuth thrusters. The detailed

model of the electrical propulsion system of the oil rig platform is developed in MATLAB Simulink.

The generators are simulated using conventional voltage source in series with the equivalent sub-transient reactance of the generator ($X_d'' = 0.16$ pu). Each thruster system uses a 12-pulse rectifier system, powered by a phase shifting transformer with two secondary windings. In the 12-pulse rectifier system, the relative phase shift of 30° in the two secondary windings with respect to primary winding is achieved either by the vector group Dd11.75d0.75 or Dd11.25d0.25 [55]. The vector group Dd11.75d0.75 produces a phase shift of $-7.5°, +22.5°$ and Dd11.25d0.25 produces a phase shift of $-22.5° + 7.5°$. Depending on winding connections, the line-to-line voltage of the transformer secondary winding may lead or lag its primary voltage by a phase angle. The winding connections for a $Dd11.\delta d0.\delta$ with a phase shift of $-\delta$ and δ are shown in are shown in Fig. 6.2.
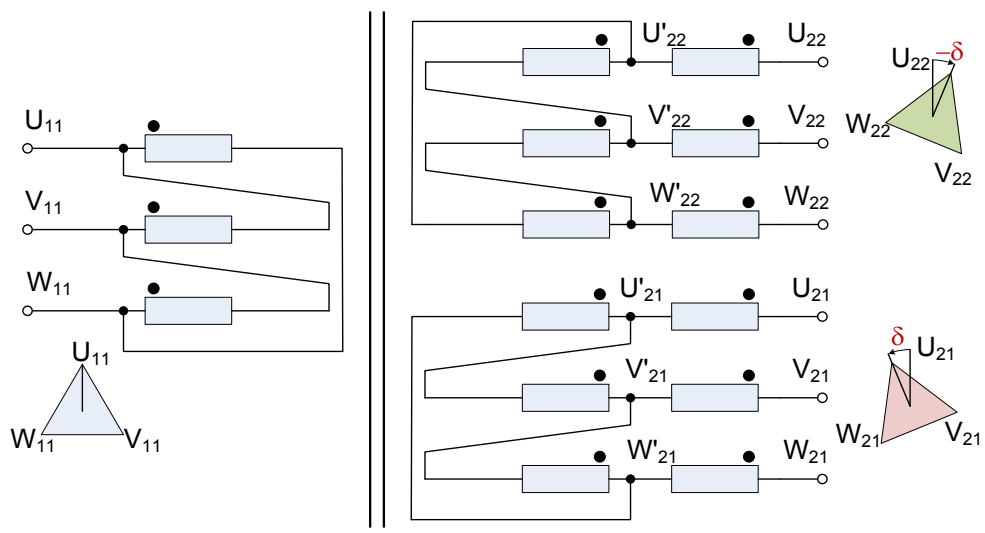
Fig. 6.2 Winding connections for a $Dd11.\delta d0.\delta$ vector group.

The specifications for the phase shifting transformers are shown in Table. 6.1 that corresponds to the name plate of the transformer.

146

Table.6.1. Specifications of the phase shifting transformer

Rated Power	4860 kVA
Primary Voltage	11 kV
Secondary Voltage	2x2200 V
Primary Current	255 A
Secondary Current	2x638 A
Frequency	60 Hz

Both Dd11.75d0.75 and Dd11.25d0.25 transformers are modeled using MATLAB Simulink. The parameters for the zigzag transformer are calculated from the no-load and short-circuit tests results provided by Keppel FELS [144] . The DZZ transformer is modeled using 3-windings transformer as shown in Fig. 6.3 and the parameters calculated are shown in Table 6.2.
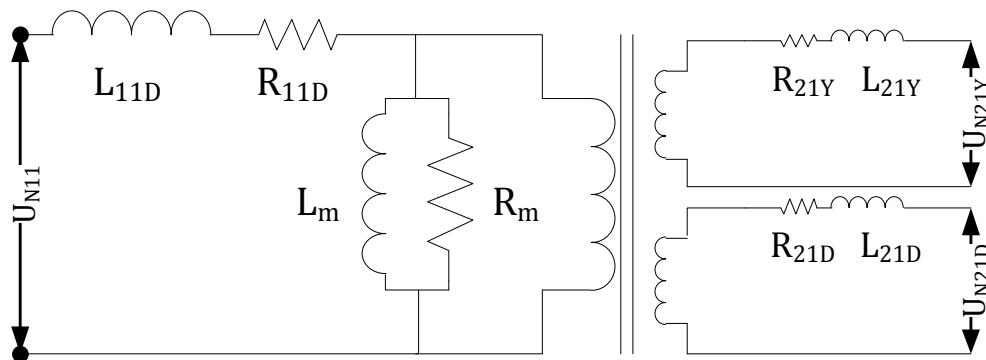
Fig. 6.3 Equivalent electrical circuit of DZZ transformer

Table.6.2. Parameters for the DZZ transformer

Parameters	$\delta = \pm 7.5°$	$\delta = \pm 22.5°$
$R11D$	91.92 $m\Omega$	89.46 $m\Omega$
$L11D$	6.0956 mH	5.9325 mH
$R21D$	2.15 $m\Omega$	0.243 $m\Omega$
$L21D$	1.42692 mH	0.016165 mH
$R21Y$	83.83 $\mu\Omega$	699 $\mu\Omega$
$L21Y$	0.00559 mH	0.046 mH
Rm	42973.83 Ω	
Lm	31.7 H	

In medium voltage drives, a diode rectifier is often used as a front-end converter due to its simple structure and low manufacturing cost. The 12-Pulse rectifier is achieved by cascading two 6-Pulse rectifiers in series as shown in Fig. 6.   1.

The 3L-NPC inverter converts the DC output of the rectifiers to variable frequency and variable voltage and powers the three phase squirrel cage induction motors to propel the azimuth thrusters. The technical specifications of the induction motor are shown in Table.6.3. The motor parameters are derived using the Keppel FELS test reports and certificates of thruster motors [144].

Table.6.3. Parameters of the induction motor

Rated Power	4000 kW	Stator Resistance	0.0272 Ω
Rate Voltage	4160 V	Stator Inductance	0.3 Ω
Rated Current	690 A	Rotor Resistance	0.0204 Ω
Rated Speed	596 rpm	Rotor Inductance	0.7 Ω
Rated Frequency	50 Hz	Mutual Inductance	10.58 Ω

Based on the modeled single thruster unit the rest of the units are also modeled and connected as shown in Fig.6.1.

6.3   Analysis of Harmonic Cancellation in a Quasi-24 Pulse Rectifier System

The main purpose of this section is to analysis of harmonic cancellation in a quasi-24 pulse rectifier system. The thruster units T1, T3, T5, and T7 use phase-shifting transformer of vector group Dd11.75d0.75 and thruster units T2, T4, T6, and T8 use phase-shifting transformer of vector group Dd11.25d0.25. The secondary side line currents (i_{S21}^x, i_{S22}^x) of vector group Dd11.75d0.75 $(x \in \{1,3,5,7\})$ are expressed as in (6.1) and (6.2).

$$i_{S21}^x = \sum_{h=1,5,7,11\ldots}^{\infty} \hat{I}_h^x \sin h(\omega t + 22.5°), x \in \{1,3,5,7\} \tag{6.1}$$

$$i_{S22}^x = \sum_{h=1,5,7,11\ldots}^{\infty} \hat{I}_h^x \sin h(\omega t - 7.5°), x \in \{1,3,5,7\} \tag{6.2}$$

where, $\hat{I}_h^x$ is the peak value of the hth order harmonic current. The secondary side line currents of vector group Dd11.75d0.75 when referred to primary of the transformer are denoted as $(i_{S21}^t)'$ and $(i_{S22}^t)'$ respectively and expressed as in (6.3) and (6.4) [51, 156].

$$(i_{S21}^x)' = \frac{1}{n_{tr}} \left(\sum_{h=1,7,13}^{\infty} \hat{I}_h^x \sin(h(\omega t + 22.5°) - 22.5° \right.$$

$$\left. + \sum_{h=5,11,17}^{\infty} \hat{I}_h^x \sin(h(\omega t + 22.5°) + 22.5°) \right) \tag{6.3}$$

$$
(i_{S22}^x)' = \frac{1}{n_{tr}} \left(\sum_{h=1,7,13}^{\infty} \hat{I}_h^x \sin(h(\omega t - 7.5°) + 7.5°) \right.
$$

$$
\left. + \sum_{h=5,11,17}^{\infty} \hat{I}_h^x \sin(h(\omega t - 7.5°) - 7.5°) \right)
\tag{6.4}
$$

The first term on the right-hand side of (6.3-6.4) includes all the harmonic currents of **positive sequence** ($h = 1, 7, 13 \dots$), while the second term represents all the **negative sequence** harmonics ($h = 5, 11, 17 \dots$). Using (6.4), the primary side line current $\left(i_{p21}^x \right)$ of vector group Dd11.75d0.75 ($x \in \{1,3,5,7\}$) is given by (6.5).

$$
i_{p11}^x = (i_{S21}^x)' + (i_{S22}^x)' = \frac{2}{n_{tr}} \left(\begin{array}{c} \hat{I}_1^x \sin \omega t + \hat{I}_{11}^x \sin(11\omega t + 90°) \\ + \hat{I}_{13}^x \sin(13\omega t + 90°) + \hat{I}_{23}^x \sin 23\omega t \\ + \hat{I}_{25}^x \sin 25\omega t + \cdots \end{array} \right)
\tag{6.5}
$$

Using (6.5), the line side current at the 11 kV busbar demanded by thruster units of vector group Dd11.75d0.75 ($x \in \{1,3,5,7\}$) is given by (6.6).

$$
i_{Bus}' = \left(\begin{array}{c} A_1 \sin \omega t + A_{11} \sin(11\omega t + 90°) \\ + A_{13} \sin(13\omega t + 90°) + A_{23} \sin 23\omega t \\ + A_{25} \sin 25\omega t + \cdots \end{array} \right)
\tag{6.6}
$$

where,

$$
A_h = \frac{2}{n_{tr}} \sum_{x=1,3,5,7} \hat{I}_h^x \; , h = 12k \pm 1(k = 0,1,2,3 \dots, h > 0)
$$

Similarly, the line side current at the 11 kV busbar demanded by thruster units of vector group Dd11.25d0.25 ($x \in \{2,4,6,8\}$) is given by (6.7).

$$i''_{Bus} = \begin{pmatrix} B_1 \sin \omega t + B_{11} \sin(11\omega t + 90°) \\ +B_{13} \sin(13\omega t + 90°) + B_{23} \sin 23\omega t \\ +B_{25} \sin 25\omega t + \cdots \end{pmatrix} \qquad (6.7)$$

where,

$$B_h = \frac{2(-1)^k}{n_{tr}} \sum_{x=2,4,6,8} \hat{I}_h^x \ , h = 12k \pm 1(k = 0,1,2,3 \ldots , h > 0)$$

Therefore, the total line side current at the 11 kV busbar is $i_{Bus} = i'_{Bus} + i''_{Bus}$ and the total current harmonic distortion at 11kV busbar (I_{THD}^{Bus}) is given by (6.8).

$$I_{THD}^{Bus} = \frac{\sqrt{\sum_{h=2}^{hmax}(A_h + B_h)^2}}{(A_1 + B_1)} \times 100\ \% \qquad (6.8)$$

The hth order individual voltage harmonic distortion (V_h^{Bus}) and V_{THD}^{Bus} at the 11 kV busbar is given by (6.9-6.10) respectively.

$$V_h^{Bus} = \frac{X_1 h(A_h + B_h)}{V_1} \times 100\ \% \qquad (6.9)$$

$$V_{THD}^{Bus} = \frac{\sqrt{\sum_{h=2}^{hmax}(V_h^{Bus})^2}}{V_1} \times 100\ \% \qquad (6.10)$$

where, V_1 is the fundamental component of voltage and X_1 is the equivalent source reactance. The value of X_1 depends on the total number of generators switched ON (n_{Gen}) and sub-transient reactance of the generator (X''_d) and is calculated using (6.11).

$$X_1 = X''_d / n_{Gen} \qquad (6.11)$$

The total number of generators switched ON (n_{Gen}) is given by (6.12).

$$n_{Gen} = P_{Total}/P_R^{Gen} \tag{6.12}$$

where, P_{Total} is the total power consumption for station keeping of the semi-submersible oil rig platform and ($P_R^{Gen} = 4960$ kW) is the rated power of the generator. It is evident from (13), that V_{THD}^{Bus} can be decreased by decreasing the value of X_1. Therefore, V_{THD}^{Bus} can be controlled by increasing the n_{Gen}. However, increasing n_{Gen} would result in inefficient operation of diesel generators and increase in the power consumption of the oil rig platform. The other parameter that can decrease V_{THD}^{Bus} is ($A_h + B_h$). The value of $A_h + B_h$ can be reduced to zero for specific harmonics by ensuring (6.13) is fulfilled.

$$A_h + B_h = \sum_{x=1,3,5,7} \hat{I}_h^x - \sum_{x=2,4,6,8} \hat{I}_h^x = 0, \tag{6.13}$$

$h = 12k \pm 1, k = (1,3,5 \dots)$

Therefore, by intelligently controlling the loading of the thruster units, the harmonics of order 11, 13, 35 and 37 can be eliminated and hence, V_{THD}^{Bus} can be further reduced.

In order to illustrate variation of V_{THD}^{Bus} with change in the loading of the thrusters, a simplified case with only two thrusters units T1 and T2 is considered and loading of each thruster unit is varied from 0 to 1 p.u. The thruster unit T1 uses phase-shifting transformer of vector group Dd11.75d0.75 and thruster unit T2 uses phase-shifting transformer of vector group Dd11.25d0.25. The variation of V_{THD}^{Bus} with change in the loading of T1 and

T2 is shown in Fig. 6.4. It is evident that V_{THD}^{Bus} increases with increase in loading and then suddenly decreases because of the reduction in source reactance due to switching ON of the extra generator. The extra generator is switched ON when the power demanded is greater or equal to $2P_R^{Gen}$. In addition it is observed from Fig. 5.6 that V_{THD}^{Bus} decreases as the difference between T1 and T2 decreases. Therefore, a valley like shape can be observed and is in accordance with (6.13).
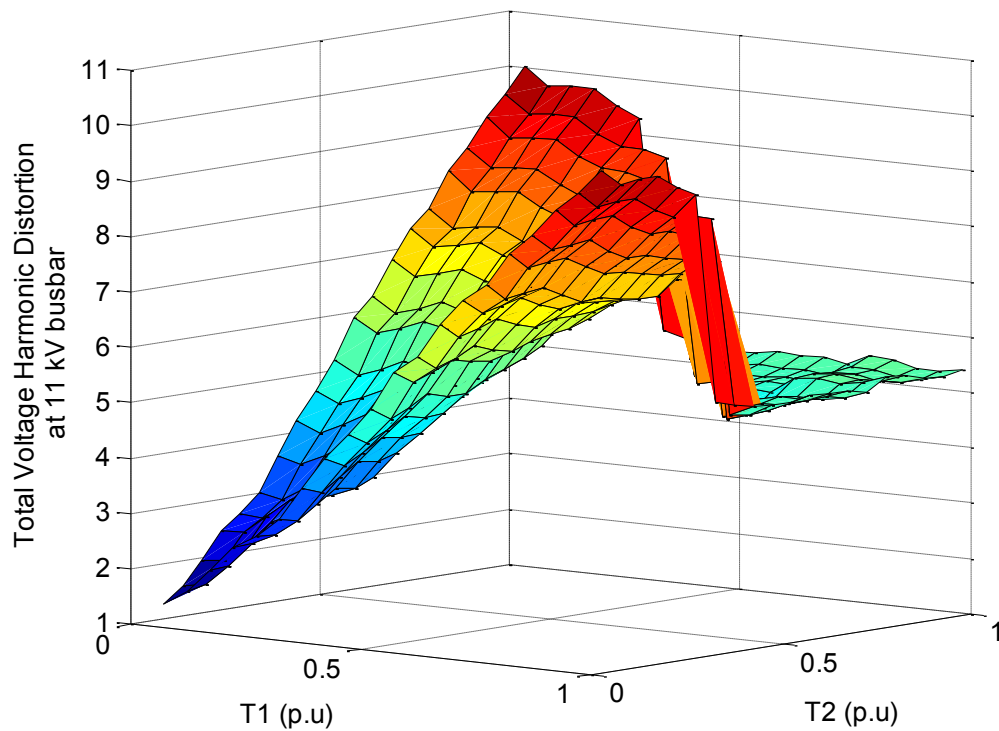
Fig. 6.4 Variation of V_{THD}^{Bus} with change in the loading of T1 and T2.

6.4 Voltage Harmonic Distortion Compliant Energy-Efficient Thrust Allocation Approach

During drilling operation the oil rig platform needs to maintain the fixed position. In order to maintain the fixed position, the thrust allocator needs to determine the magnitude and

direction of the thrust required for each azimuth thruster to create a force and moment equilibrium. However, there exist multiple solutions for the thrust-allocation problem because, the oil rig platform is over-actuated and the azimuth thrusters fitted at oil rig platform's pontoon level can produce forces in different directions. Therefore, the solution to the thrust allocation problem can be found by formulating it as an optimization problem. Harmonic distortion in the electrical power system is an important factor for safe and reliable operation of the marine vessels, as it adversely affects the electric and electronic subsystems. In this thesis work, a Harmonic compliant Energy-Efficient Thrust allocation approach is proposed, with an objective to minimize the total power consumption by ensuring that the electrical propulsion system operates in efficient zone and is subjected to force and moment constraints to ensure fixed position of the oil rig platform. The thrust direction constraints imposed on the azimuth thrusters due to forbidden/spoil zones is also considered. In addition, the constraints imposed on V_{THD}^{Bus} and V_{IHD}^{Bus} are also been incorporated in the optimization problem. The details of the proposed Voltage Harmonic Distortion compliant Energy-Efficient Thrust allocation approach are explained in this section.

6.4.1   Objective Function

The objective of the proposed thrust allocation approach is to minimize the total power consumption of the oil rig platform during station keeping. The power consumed by the electric propulsion system depends on the thrust generated by the azimuth thrusters and the efficiency of the electric propulsion system controlling the azimuth thruster. The total power consumption for station keeping of the semi-submersible oil rig platform equipped with N thrusters is given by (6.14)[54].

$$P_{Total} = \sum_{i=1}^{N} \frac{P_o(T_i)}{\eta_{System}(T_i)} = \sum_{i=1}^{N} \frac{P_o(T_R){T_i}^{3/2}}{{T_R}^{3/2}\eta_{System}(T_i)} \tag{6.14}$$

where, $P_o(T_i) = P_o(T_R)(T_i/T_R)^{3/2}$ is the power consumed by the ith thruster to produce a thrust force (T_i). $\eta_{System}(T_i)$ is the efficiency of electric propulsion system for the ith thruster corresponding to thrust force (T_i) and T_R is the rated effective thrust of each azimuth thruster. T_R is 780 kN at a rated motor power $\big(P_o(T_R)\big)$ of 4000 kW at 600rpm. The efficiency of electric propulsion system for the ith thruster corresponding to thrust force (T_i) can be calculated using (6.15).

$$
\begin{aligned}
\eta_{System}(T_i) &= \frac{P_o(T_i)}{P_{in}(T_i)} \\[2mm]
&= \frac{P_o(T_i)}{\big(P_o(T_i) + P_{IM_{T\_Loss}} + P_{INV_{T\_Loss}} + P_{Rec} + P_{TRANS_{T\_Loss}}\big)}
\end{aligned} \tag{6.15}
$$

The details of the calculation are explained in Chapter 5 [54]. The efficiency curve shown in Fig.6.5 highlights that the efficiency of a lightly loaded electrical propulsion system is much less, than that of a more heavily loaded system. Therefore, during lower load demand, one should distribute the maximum load to some of the azimuth thrusters and keep remaining thrusters switched OFF.
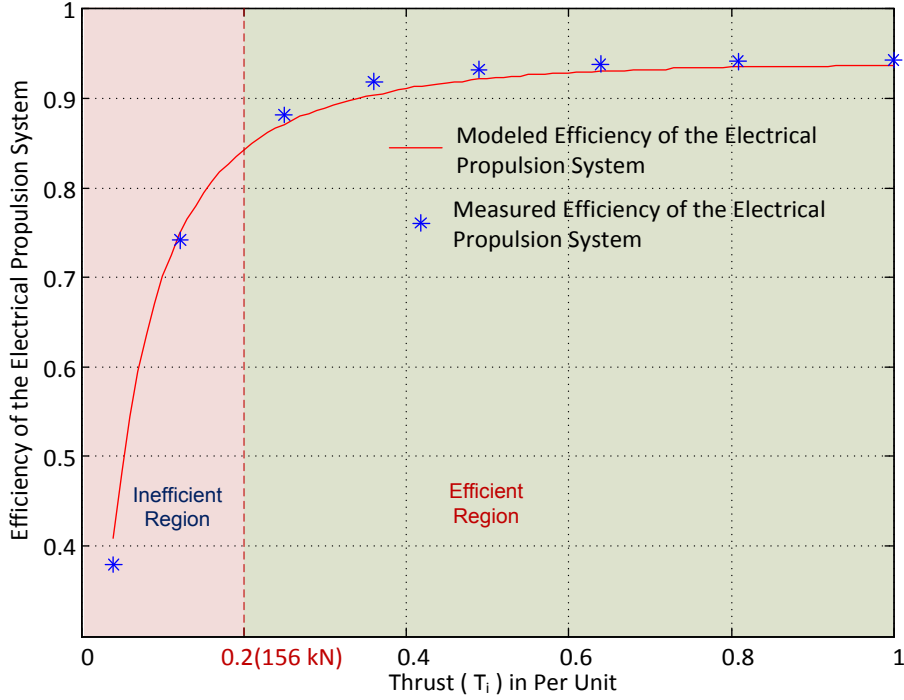
Fig. 6.5 Comparison of measured and modeled efficiency of the electrical propulsion system

Typically azimuth thrusters are not used to produce thrust in the reverse mode, therefore, the minimum thrust force $(\underline{T}_i)$ is zero and maximum thrust force $(\overline{T}_i)$ is limited to rated thrust force (T_{iR}). However, in practice the thrusters are not operated below the minimum thrust force of $(\underline{T}_i = 0.04 \times T_{iR})$ [41]. Since, the minimum thrust force of the azimuth thruster $(\underline{T}_i = 0.04 \times T_{iR})$ is not equal to zero. Therefore, a switching sequence $(k = [k_1, k_2, k_3, \ldots k_N]')$ is introduced to control the switching ON and OFF of the thruster units. The switching variable (k_i) is defined by (6.16).

$$k_i = \begin{cases} 1, if\ i^{th}\ thruster\ unit\ is\ ON \\ 0, if\ i^{th}\ thruster\ unit\ is\ OFF \end{cases} \tag{6.16}$$

The total power consumption for station keeping of the semi-submersible oil rig platform equipped with N thrusters given by (6.11) is modified and rewritten as given by (6.17).

$$P_{Total} = \sum_{i=1}^{N} \left(\frac{P_o(T_i)k_i}{\eta_{System}(T_i)} \right) \tag{6.17}$$

Therefore, for $k_i = 0$, the power demanded by the ith thruster is zero and for $k_i = 1$, the power demanded by the ith thruster is $\left(P_o(T_i)/\eta_{System}(T_i) \right)$.

6.4.2 Equality Constraints

The most important task of the DP system is to maintain the fixed position of the oil rig platform during drilling operation. Therefore, thrust allocator needs to determine the magnitude and direction of the thrust required for each azimuth thruster to create a force and moment equilibrium. The proposed thrust allocation approach takes in account the horizontal plane motions (surge, sway and yaw). The forces and moment demanded by the DP system are represented by a force vector $\tau = \left(F_X, \ F_Y, M_Z \right)' \in \mathbf{R}^3$. The thrust allocation problem is to select the control signals associated with the individual thrusters in order to produce the demanded surge force (F_X) , sway force (F_Y) and yaw moment (M_Z) (three generalized force components). The forces and moments generated by the ith thruster with state $(T_i, \ \alpha_i)$ in cylindrical coordinates are given by (6.18) [18, 42].

$$\tau_i = \begin{bmatrix} F_X^i \\ F_Y^i \\ M_Z^i \end{bmatrix} = \begin{bmatrix} \cos \alpha_i \\ \sin \alpha_i \\ \sin \alpha_i L_{Xi} - \cos \alpha_i L_{Yi} \end{bmatrix} k_i T_i = B(\alpha_i) k_i T_i \tag{6.18}$$

The contribution of the forces and moment generated by the ith thruster depends on the corresponding switching variable (k_i). For the switching variable $k_i = 0$, the forces and moments generated by the ith thruster is zero. Assuming, that the marine vessel is equipped

with N thrusters, then the force vector (τ) demanded is jointly produced by N thrusters in order keep the vessel at the fixed position and is given by (6.19).

$$\tau = \sum_{i=1}^{N} \tau_i = \begin{bmatrix} \sum_{i=1}^{N} F_X^i \\ \sum_{i=1}^{N} F_Y^i \\ \sum_{i=1}^{N} M_Z^i \end{bmatrix} = \mathrm{B}(\alpha)T_k \qquad (6.19)$$

where, $T_k = k.* T = [k_1 T_1, k_2 T_2, k_3 T_3 \ldots k_N T_N]'$ and $k.* T$ is the element-by-element multiplication of k and T. $T = [T_1, T_2, T_3 \ldots T_N]' \in \mathbf{R^N}$ is a vector of the magnitude of the force produced by each individual thruster. The thruster configuration matrix $(\mathrm{B}(\alpha) \in \mathbf{R^{3 \times N}})$ is determined by the position of the individual thrusters. The ith column in configuration matrix corresponds to the generalized force produced by the ith thruster. Eqn.(6.19) ensures that the error between the demanded generalized force (τ) and generalized force jointly produced by N thrusters is close to zero to keep the oil rig platform at the fixed position.

6.4.3 Variable Bounds

Each thruster has limited amount of thrust and limited directions in which it generates thrust. Therefore, for each thruster, the azimuth angle (α_i) and the thrust force (T_i) are constrained to the sets given by (6.20).

$$O_i := \left\{ (\alpha_i, T_i) \mid \underline{\alpha}_i \leq \alpha_i \leq \overline{\alpha}_i, \underline{T}_i \leq T_i \leq \overline{T}_i \right\} \qquad (6.20)$$

where, $\underline{\alpha}_i$ and $\underline{T}_i$, are the lower bounds on the azimuth angle and thrust force for the ith thruster, respectively and similarly, $\overline{\alpha}_i$ and $\overline{T}_i$ are the upper bounds on the azimuth angle and thrust force for the ith thruster, respectively. A set of all physically realizable surge and sway forces (F_X^i, F_Y^i) for the ith thruster is called the *Attainable Thrust Region* (ATR) of the ith thruster and is defined by (6.21) [25].

$$
C_i := \left\{ \left(F_X^i, F_Y^i \right)^T \middle| \begin{array}{l} F_X^i = T_i \cos \alpha_i, \\ F_Y^i = T_i \sin \alpha_i, \\ (\alpha_i, T_i) \in \mathcal{O}_i \end{array} \right\}
\tag{6.21}
$$

The minimum thrust force is $\left(\underline{T}_i = 0.04 \times T_R \right)$ and maximum thrust force $\left(\overline{T}_i \right)$ is limited to rated thrust force (T_{iR}). In addition, when two thrusters are positioned close enough the thruster-thruster interactions cause the thrust loss [26]. The thruster loss is very significant in case of an oil rig platform because the two thrusters are mounted in pairs and are located on the same leg of the oil rig platform. In order to overcome the thruster-thruster interaction loss, the forbidden zones or spoil zones are defined and excluded from the ATR of the neighboring thrusters. Each thruster is assumed to have a forbidden angle of $(\pm\theta_f^\circ = \pm 25°)$ to the closest thruster with the port forward pair centre of angle of outboard thruster i as $(\phi_i = -63.44°)$ and for inboard thruster $(i+1)$ as $(\phi_{i+1} = 116.56°)$ as shown in Fig 5.8.
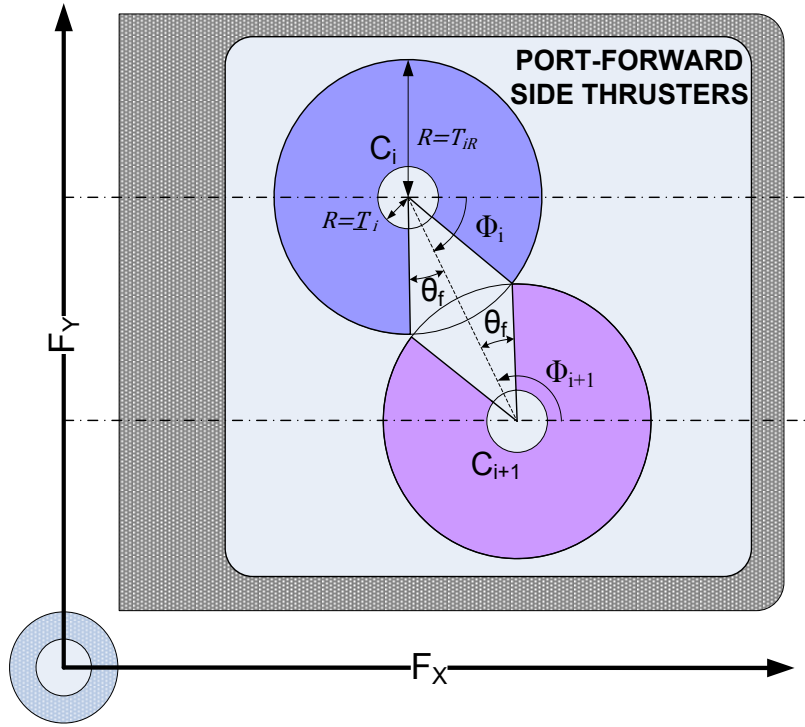
Fig. 6.6 Shaded region of the circle represents the ATR of ith and $(i+1)^{th}$ thruster

Using Fig.6.6, $\underline{\alpha}_i$ and $\overline{\alpha}_i$ for the ith thruster are given by (6.22-6.23). In (6.23), 360° is added to ensure $\overline{\alpha}_i > \underline{\alpha}_i$.

$$\underline{\alpha}_i = \phi_i + |\theta_f| \tag{6.22}$$

$$\overline{\alpha}_i = \phi_i - |\theta_f| + 360° = \underline{\alpha}_i - 2|\theta_f| + 360° \tag{6.23}$$

Using (6.22 - 6.23), the corresponding $\underline{\alpha}_i$ and $\overline{\alpha}_i$ are computed as shown in (6.24 - 6.25).

$$\underline{\alpha} = \begin{Bmatrix} -38.44°, 141.56°, -91.56°, 88.44°, \\ -38.44°, 141.56°, -91.56°, 88.44° \end{Bmatrix} \tag{6.24}$$

160

$$\bar{\alpha} = \begin{Bmatrix} 271.56°, 451.56°, 218.44°, 398.44°, \\ 271.56°, 451.56°, 218.44°, 398.44° \end{Bmatrix}$$

<div align="right">(6.25)</div>

In addition to the azimuth angles (α) and thrust forces (T), the proposed algorithm also finds the optimum thruster switching sequence (k). The switching variable $k_i \in \{0,1\}$.

6.4.4 Inequality Constraints

There are two inequality constraints to be met. V_{THD}^{us} and V_{IHD}^{Bus} at 11 kV busbar should be within the specified limits as shown in (6.26).

$$V_{THD}^{Bus} \le V_{THD}^{Limit}, V_h^{Bus} \le V_h^{Limit}$$

<div align="right">(6.26)</div>

According to IEC-60092-101[44] and IEEE-519 [45], the total voltage harmonic distortion the point of common coupling should be less than 5% and individual harmonic distortion should be less than 3%. Measurements are to be taken at least up to the 50th harmonic. Similar limits are imposed by marine certifying bodies such as DNV (Det Norske Veritas – Norwegian classification society) and ABS (American Bureau of Shipping) [2, 5]. Therefore, V_{THD}^{Limit} and V_h^{Limit} is chosen as 5% and 3% respectively.

6.4.5 Formulated Optimization Problem

Using (6.17), (6.19-6.20), the optimization problem can be formulated as given by (6.27-6.31).

$$\text{Min } P_{Total}(\alpha, T, k) = \text{Min}\left(\sum_{i=1}^{N} \frac{P_o(T_i) \times k_i}{\eta_{System}(T_i)} \right)$$

<div align="right">(6.27)</div>

subjected to

$$\tau - B(\alpha)T_k = 0 \tag{6.28}$$

$$\left(\underline{\alpha}_i \leq \alpha_i \leq \overline{\alpha}_i, \underline{T}_i \leq T_i \leq \overline{T}_i \right) \tag{6.29}$$

$$T_{ki} = k_i T_i, \ k_i \in \{0,1\} \tag{6.30}$$

$$V_{THD}^{Bus} \leq V_{THD}^{Limit}, V_h^{Bus} \leq V_h^{Limit} \tag{6.31}$$

where, $P_o(T_i)$ is the power consumed by the ith thruster to produce a thrust force (T_i). Eqn.(6.28) ensures that the error between the demanded generalized force (τ) and generalized force jointly produced by N actuators is close to zero to keep the vessel in the desired position. Eqn. (6.29) ensures that the thrust produced by each thruster is restricted to its ATR. The switching variable k_i is used, because, the key idea of the optimization is to distribute the maximum load for some of the azimuth thrusters and keep others idle. Eqn. (5.31) ensures that for the corresponding thruster loads the $V_{THD}^{Bus} \leq V_{THD}^{Limit}$ and $V_h^{Bus} \leq V_h^{Limit}$. In the formulated optimization problem, in addition to the optimum azimuth angles (α) and thrust forces (T), the proposed algorithm also finds the optimum thruster switching sequence (k). Since, the element of the switching sequence $(k_i \in \{0,1\})$ can be either zero or one. Therefore, the formulated optimization problem is a mixed integer non-convex optimization problem, therefore, classical optimization techniques fail to find the optimum solution and often get trapped in local minima. Metaheuristic algorithms eradicate some of

the afore-mentioned difficulties and can be used in mixed integer non-convex optimization problem.

6.5 Results and Discussions

The proposed Voltage Harmonic Distortion compliant Energy-Efficient Thrust allocation is applied to a case study of semi-submersible oil rig platform. Keppel's B280 semi-submersible oil rig platform is used as the case study of the marine vessel, the oil rig platform was subjected to a sea load profile. The demanded longitudinal resultant thrust (F_X), lateral resultant thrust(F_Y), and moment (M_Z) for 50 time steps are shown in Fig. 6.9 (a), (b), (c) respectively.
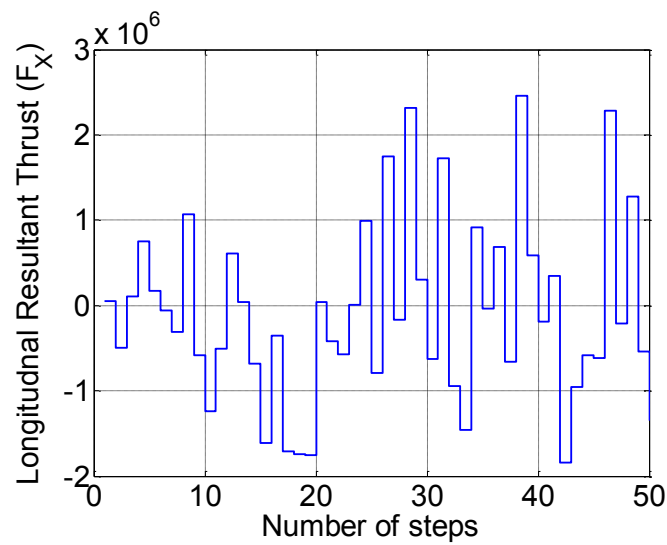
(a)
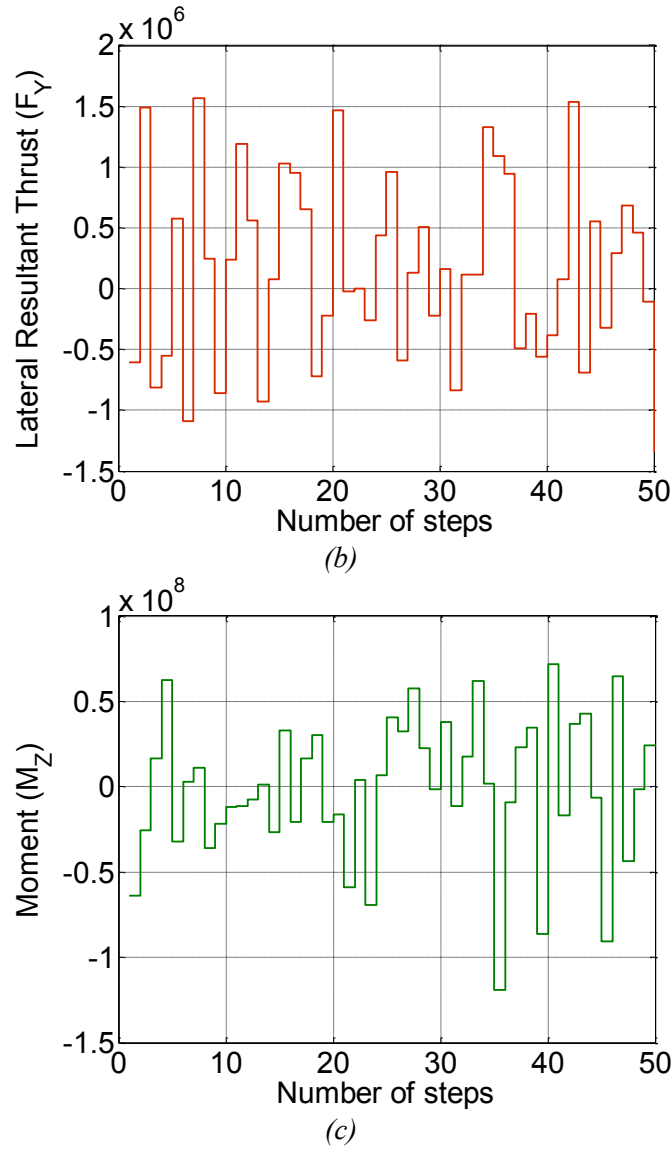
Fig. 6.7 The commanded longitudinal resultant thrust (F_X), lateral resultant thrust (F_Y), and

moment (M_Z) for 50 time steps

In order to evaluate the effectiveness and performance of ITHS algorithm, we compare its performance with Mincon Method (Sequential Quadratic Programming), Genetic Algorithm, Harmony Search (HS) and Improved Harmony Search (HS). The parameters for the HS, IHS algorithms are fixed as the same as those reported in [7, 112]. For the HS algorithm, *HMS = 5, HMCR = 0.9, PAR = 0.33* and *bw = 0.01*. For the IHS algorithm, *HMS = 5, HMCR = 0.9, PAR_{min} =0.1*, PAR_{max} =0.99, bw_{min} = 0.0001 and bw_{max}

$= \left(\overline{x}_i - \underline{x}_i \right)/20$. According to [7], the default values of GA parameters are: 20 individuals per generation, 10% of elite individuals, crossover probability is 0.5, rank fitness scaling, roulette selection, and scattered crossover operators. The detailed description of these algorithms can be found in the corresponding references.

In case of Mincon method, the initial point plays a very crucial role in finding the optima. However, for none of the initial point, Mincon method is able to find the solution for the formulated optimization problem for all the 50 time steps. The Mincon method needs good starting point for each instance of the optimization problem to find feasible solution for the formulated optimization problem. This problem can be eliminated by using meta-heuristic algorithms. Therefore, GA, HS, IHS and ITHS algorithms are able to find the feasible solution for the formulated optimization problem.

The V_{THD}^{Bus} at 11 kV busbar for Energy Efficient thrust allocation approach and Voltage Harmonic Distortion Compliant Energy Efficient thrust allocation for ITHS, IHS, HS and GA is shown in Fig. 6.8. It is evident from Fig. 6.8 that for Energy Efficient thrust allocation approach the $V_{THD}^{Bus} \geq V_{THD}^{Limit}$ at most of the instances for all the optimization algorithms. However, Voltage Harmonic Distortion Compliant Energy Efficient thrust allocation ensures that $V_{THD}^{Bus} \leq V_{THD}^{Limit}$ for all the optimization algorithms. Similarly Voltage Harmonic Distortion Compliant Energy Efficient thrust allocation also ensures $V_h^{Bus} \leq V_h^{Limit}$ for all the optimizations. The results for V_h^{Bus} are are omitted to save space and considering that, they exhibit a similar trend.

(a)

(b)

166
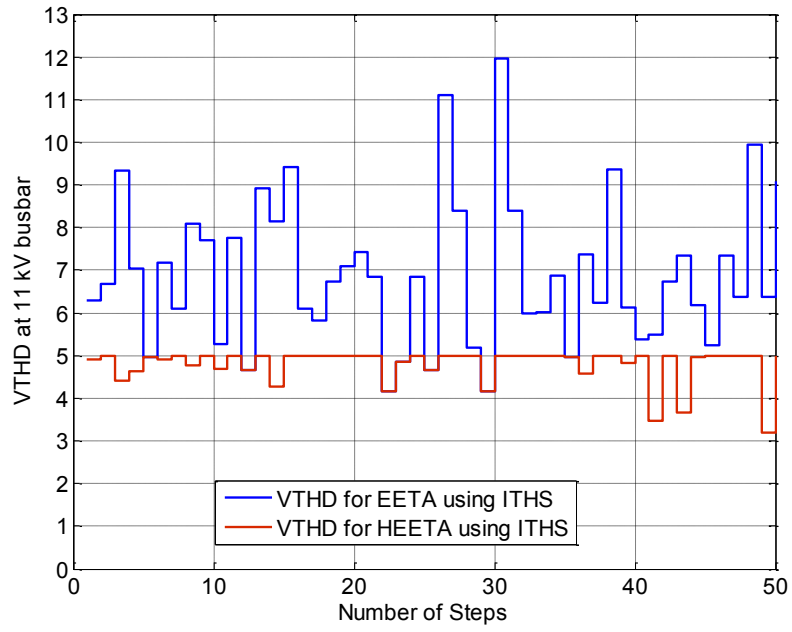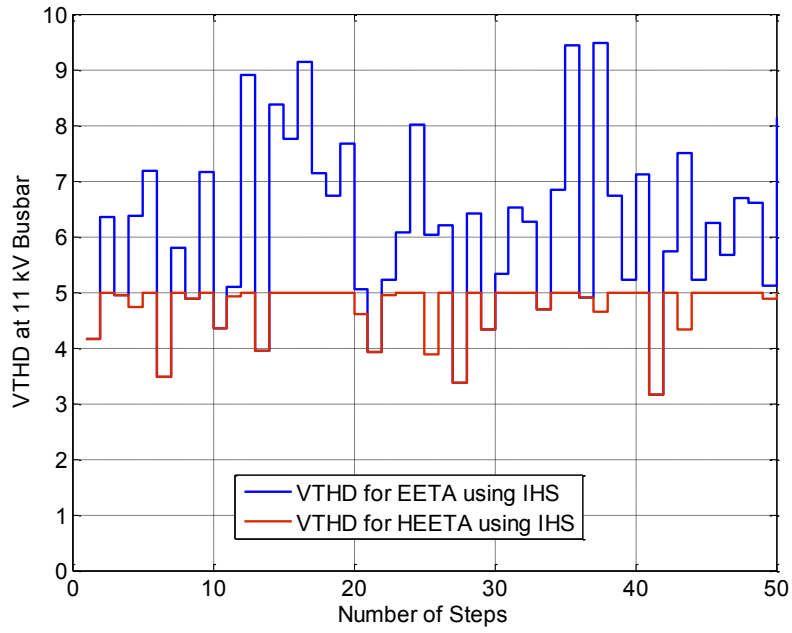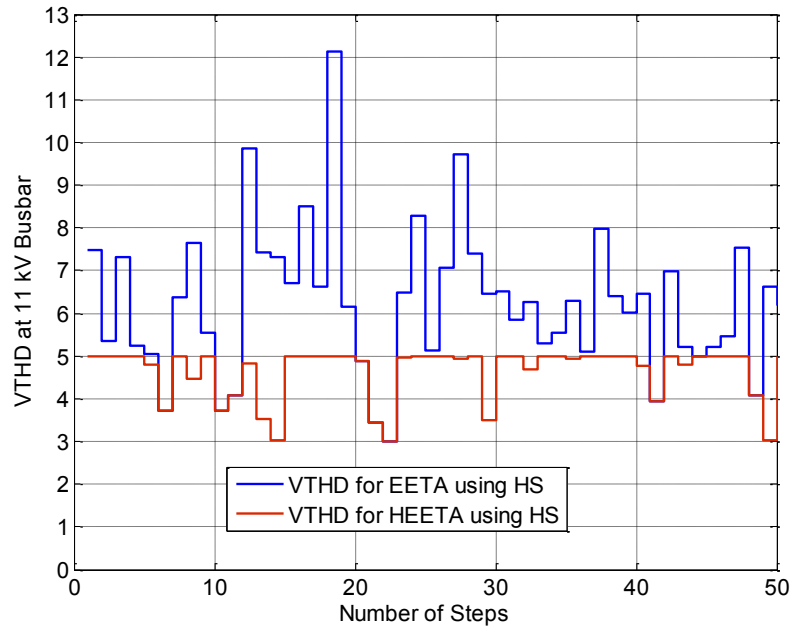
(c)
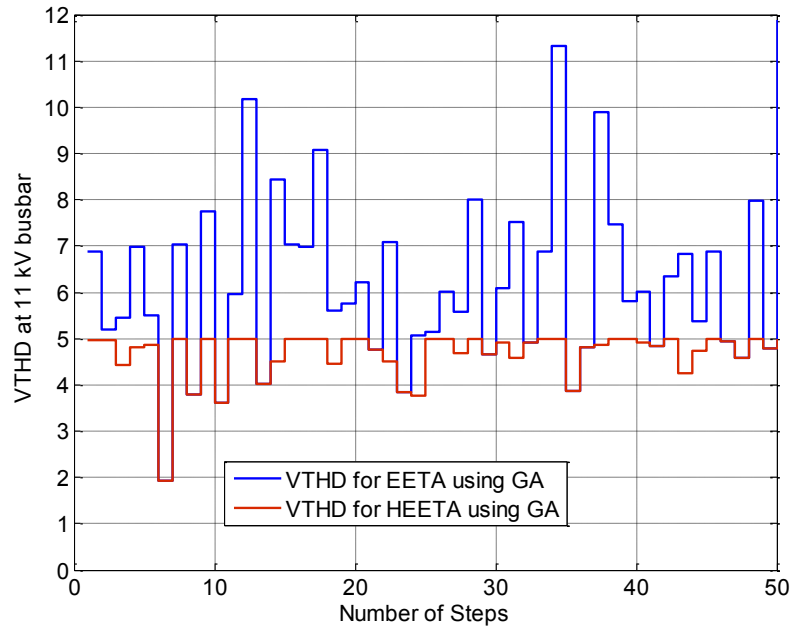
(d)

Fig. 6.8 V_{THD}^{Bus} for Energy Efficient Thrust Allocation (EETA) and Harmonic compliant Energy-Efficient Thrust allocation (HEETA) using (a) ITHS, (b) IHS, (c) HS, and (d) GA

However, in order to ensure that $V_{THD}^{Bus} \leq V_{THD}^{Limit}$ and $V_h^{Bus} \leq V_h^{Limit}$, the Voltage Harmonic Distortion Compliant Energy Efficient thrust allocation sacrifices the efficiency of the thruster drive. Therefore, the total power consumption of the oil rig platform during thruster allocation for 50 time steps with the proposed Voltage Harmonic Distortion Compliant Energy Efficient thrust allocation approach is higher than that of and conventional Energy Efficient thrust allocation approach for ITHS, IHS, HS and GA.

The total power consumption of the oil rig platform during thruster allocation for 50 time steps with the proposed conventional Energy Efficient thrust allocation and Voltage Harmonic Distortion Compliant Energy Efficient thrust approach for ITHS, IHS, HS and GA is shown in Fig. 6.9 (a) and 6.9(b) respectively.
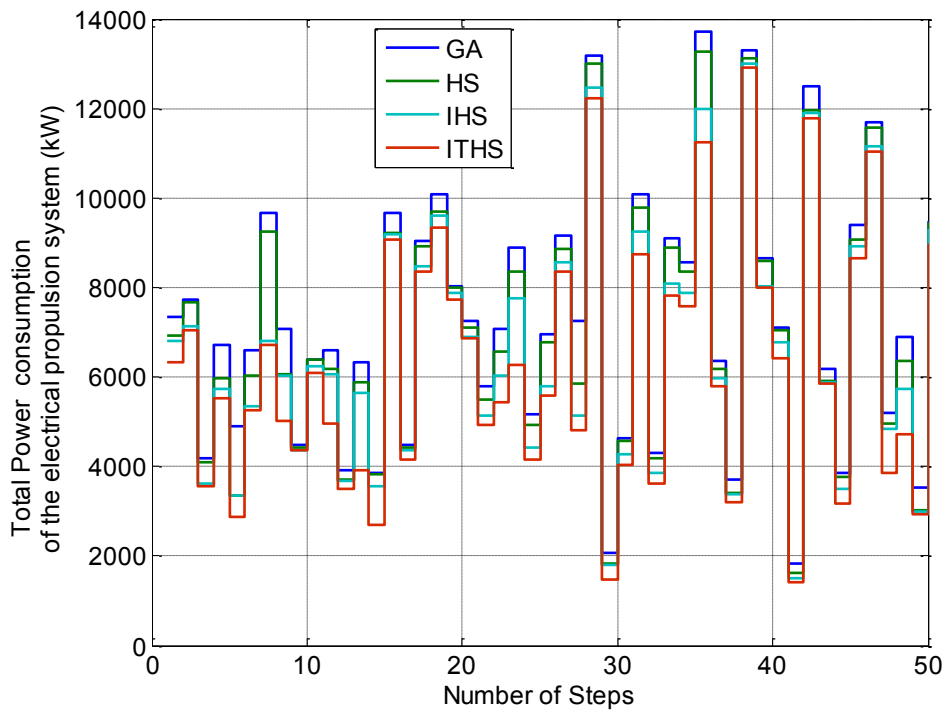
(a)
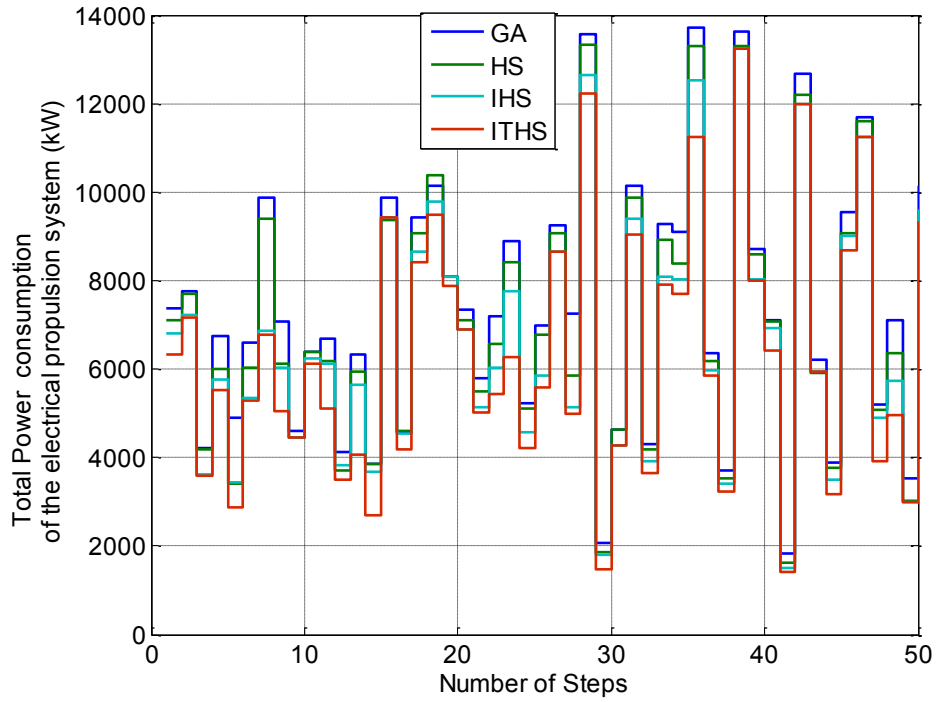
(b)

Fig. 6.9 Total power consumption of the oil rig platform during thruster allocation for 50 time steps with (a) Energy Efficient Thrust Allocation (b) Harmonic compliant Energy-Efficient Thrust allocation

It is evident from Fig. 6.9 that the power consumption for ITHS is less as compared to IHS, HS and GA method in both the cases. The self-adaptive pitch adjustment strategy adopted by the dynamic sub-populations based on the consciousness (Harmony Memory) helps the ITHS algorithm in maintaining the proper balance between diversification and intensification throughout the search process as compared to GA, HS and IHS algorithm. The self-adaptive pitch adjustment strategy not only alleviates the difficulties of parameter setting but also enhances the precision of the obtained solution.

In case of Energy Efficient thrust allocation and Voltage Harmonic Distortion Compliant Energy Efficient thrust allocation approach, the total power consumed by the oil rig platform during the entire load cycle is calculated by finding the area under the curve in Fig.6.9(a) and Fig.6.9(b) respectively. For a step size (s) the total power is given by $\sum_{i=1}^{50} P_{Total}(i) \times s$, where, $P_{Total}(i)$ corresponds to total power consumed by for the ith step. Assuming the step size (s) as 1, then the total power consumed by oil rig platform during the entire load cycle for GA, HS, IHS and ITHS method is shown in Table.6.4. The percentage savings in total power consumption for Voltage Harmonic Distortion Compliant Energy Efficient thrust allocation approach as compared to GA for HS, IHS and ITHS method is 4.64 %, 9.40 % and 14.18% respectively.

The major advantage of the proposed approach is that, there is no need of additional hardware integration for limiting the voltage harmonics and the proposed approach can be integrated in the existing system by changing the DP software.

Table.6.4. Total Power Consumption of the oil rig platform for the entire load cycle

Approach / Algorithm	Total Power for Energy Efficient Thrust Allocation (MW)	Total Power for Harmonic compliant Energy Efficient Thrust Allocation (MW)
Mincon	707.67	NS*
GA	362.61	364.70
HS	345.86	347.78
IHS	326.26	330.39
ITHS	**308.29**	**312.98**

6.6   Conclusions

In this paper, a Voltage Harmonic compliant Energy-Efficient thrust allocation problem for semi-submersible oil rig platform is formulated to enhance the efficiency and also ensure that the electric propulsion system meets the harmonic limits as per marine standards. Harmonic distortion in the electrical power system is an important factor for safe and reliable operation of the marine vessels, as it adversely affects the electric and electronic subsystems.

The Voltage Harmonic compliant Energy-Efficient thrust allocation is formulated as a mixed integer non-convex optimization problem, which is difficult to solve using state of art iterative methods. In this paper, the ITHS algorithm is used to find the solution of the formulated optimization problem. The proposed Voltage Harmonic compliant Energy-Efficient thrust allocation ensures that $V_{THD}^{Bus} \leq V_{THD}^{Limit}$ and $V_h^{Bus} \leq V_h^{Limit}$ but sacrifices a bit of efficiency of the thruster drive. Therefore, the total power consumption of the oil rig platform during thruster allocation for 50 time steps with the proposed Voltage Harmonic Distortion Compliant Energy Efficient thrust allocation approach is higher than that of and conventional Energy Efficient thrust allocation approach for ITHS, IHS, HS and GA. The ITHS algorithm reduces the total power consumption of the oil rig platform as compared to GA, HS and IHS. The percentage savings in total power consumption for Voltage Harmonic Distortion Compliant Energy Efficient thrust allocation approach as compared to GA for HS, IHS and ITHS method is 4.64 %, 9.40 % and 14.18% respectively. It proves that the proposed approach is effective in meeting the harmonic limits for the semi-submersible oil rig platform for all the optimization algorithms without any additional hardware setup.

CHAPTER 7.   CONCLUSIONS AND FUTURE WORK

7.1   Conclusions

The objective of this thesis is to design intelligent thrust allocation algorithms and intelligent power management system to reduce the emissions, enhance the efficiency and safety of marine vessels. This chapter briefly restates the motivation of the thesis work, the identified problem areas and various findings in each problem area. Finally, the direction of the future work is also provided.

In Chapter 2, an ITHS algorithm is proposed to enhance the performance and efficiency of the HS algorithm. The proposed ITHS algorithm maintains a proper balance between diversification and intensification throughout the search process by automatically selecting the proper pitch adjustment strategy based on its Harmony Memory. The self-adaptive pitch adjustment strategy not only alleviates the difficulties of parameter setting but also enhances the precision of the obtained solution. The proposed ITHS algorithm is evaluated for the 17 benchmark problems and with eight state-of-the-art HS variants. The numerical results obtained indicate that the proposed ITHS algorithm offers better performance compared with the eight state-of-the-art HS variants. Furthermore, to evaluate the performance and efficiency of the proposed algorithm on larger dimension problems, a scalability study is also conducted, and the results are compared with other variants of HS. Finally, the numerical results reflect the superiority of the proposed ITHS algorithm in terms of accuracy, convergence speed, and robustness when compared with other state-of-the-art HS variants. The lower number of setting parameters and fast convergence makes it an ideal method when dealing with complex engineering optimization problems.

In Chapter 3, successfully modeled the SFC curve for the diesel generator using cubic spline interpolation; the cubic spline is a powerful tool and can accurately interpolate the SFC at different loading conditions of the diesel generator as compared to other conventional methods. The accurate modeling of the SFC curve helps in optimal scheduling of the diesel generators. The design and dynamic scheduling of diesel-generators play a crucial role in oil rig for the power density and efficiency. The ability of the ITHS algorithm was demonstrated and its performance was compared with other optimization techniques. The optimal scheduling of the diesel generators using ITHS reduces the fuel consumption of the rig as compared to conventional MinMax, MinCon methods and also GA, HS and IHS under both the scenarios of equal and unequal ratings diesel generators. Generally, it can be concluded that the ITHS algorithm's simplicity of implementation, high quality solution, along with the lower number of setting parameters makes it an ideal method when dealing with complex engineering optimization problems.

In Chapter 4, the thruster allocation problem is formulated as a constrained optimization problem. The thrust allocator tries to minimize the power consumption by the thrusters and simultaneously ensures that the vessel is at the desired position. In addition, it also ensures that the thruster-thruster interaction is minimal. In this chapter ITHS algorithm is used for solving the non-convex thrust allocation problem. The ability of the ITHS algorithm has been demonstrated and its performance is compared with other optimization techniques. The optimal thruster allocation using ITHS reduces the power consumption of the rig as compared to MinCon, GA, HS and IHS. The percentage savings in total power consumption by thrusters as compared to Mincon method for GA, HS, IHS and ITHS method are 44.96%, 48.39%, 51.58% and 62.20% respectively.

In Chapter 5, an energy-efficient thrust allocation problem for semi-submersible oil rig platform is formulated as a mixed integer constrained optimization problem. ITHS algorithm is used to find the solution of the formulated optimization problem. The optimal thrust allocation using ITHS reduces the total power consumption of the oil rig platform as compared to Mincon, GA, HS and IHS. The percentage savings in total power consumption for energy-efficient thrust allocation as compared to Mincon method for GA and HS, IHS and ITHS method are 48.76 %, 51.13 %, 53.90 % and 56.43% respectively. It proves that the proposed approach is effective in reducing the power consumption of the semi-submersible oil rig platform. Generally, it can be concluded that simplicity of implementation, higher energy saving potential, along with enhanced dynamic performance and need of simpler controller makes it an ideal approach for marine applications.

In Chapter 6, a Voltage Harmonic compliant Energy-Efficient thrust allocation problem for semi-submersible oil rig platform is formulated to enhance the efficiency and also meet the harmonic limits as per marine standards. The Voltage Harmonic compliant Energy-Efficient thrust allocation is formulated as a mixed integer non-convex optimization problem, which is difficult to solve using state of art iterative methods. In this paper, the ITHS algorithm is used to find the solution of the formulated optimization problem. The proposed Voltage Harmonic compliant Energy-Efficient thrust allocation ensures that $V_{THD}^{Bus} \leq V_{THD}^{Limit}$ and $V_h^{Bus} \leq V_h^{Limit}$ but sacrifices a bit of efficiency of the thruster drive. Therefore, the total power consumption of the oil rig platform during thruster allocation for 50 time steps with the proposed Voltage Harmonic Distortion Compliant Energy Efficient thrust allocation approach is higher than that of and conventional Energy Efficient thrust allocation approach for ITHS, IHS, HS and GA. The ITHS algorithm reduces the total

power consumption of the oil rig platform as compared to GA, HS and IHS. The percentage savings in total power consumption for Voltage Harmonic Distortion Compliant Energy Efficient thrust allocation approach as compared to GA for HS, IHS and ITHS method is 4.64 %, 9.40 % and 14.18% respectively. It proves that the proposed approach is effective in meeting the harmonic limits for the semi-submersible oil rig platform for all the optimization algorithms without any additional hardware setup.

In all, the main objectives as laid out in Chapter 1 of this thesis have been achieved. The findings of this work have been published in international technical conferences and journals for benefit of the future researchers and users to study about intelligent thrust allocation approaches and intelligent power management system for marine vessels. A list of the publications from this thesis work is provided.

7.2   Future work

In this thesis, intelligent thrust allocation algorithms are developed for minimizing the power consumption of the vessel and intelligent power management system is for optimal scheduling of the diesel generator. However, there are other issues related to marine power system which are worth considering and are explained below.

➢ **Formulation of Optimization Problem for Preventing Blackout**

Blackout is short-term or long term loss of electrical power in an electrical power system. The electrical faults or overloading of generators are the normal causes for blackout in an electrical power system. In semi-submersible oil rig platform,

blackout can lead to loss of position keeping and may hamper the overall safety of the oil rig.

In this thesis, the prime focus of the scheduling of the diesel generators was to minimize the fuel consumption. The reliability (prevention of blackout) of the power system was not considered. In order to prevent a blackout, the system must always have a sufficient power reserve or available power to its full online capacity. Therefore during optimal scheduling of the diesel generators to obtain minimum fuel consumption, blackout must be considered as a constraint. The generator must always operate within the maximum continuous safe loading limit to minimize the probability of blackout. If the load per generator becomes higher than that of maximum continuous safe loading limit, the next generator must be started. The inclusion of additional constraint due to blackout prevention would ensure both efficient and safe operation.

➢ **Intelligent Thrust Allocation to enhance reliability of the electrical propulsion system**

In energy efficient thrust allocation and Voltage Harmonic Distortion compliant Energy-Efficient thrust allocation approach, the switching variable k_i is used to control the switching ON and OFF the ith thruster unit. In addition, both the approaches focus on minimization of the power of the electric propulsion system and reliability of the electrical propulsion system is not considered. In order to ensure that the overall reliability of the electrical propulsion system shown in Fig. 7.1 is maintained, the thrust allocation approaches proposed in this thesis can be modified. The reliability indexes of each thruster drive can be calculated either

using mathematical models or real-time condition monitoring hardware units. The obtained reliability indexes of each thruster unit must govern its corresponding switching variable switching variable k_i. The thruster units with lower reliability index will have lower probability of being switched ON ($k_i = 1$) and thruster units with higher reliability index will have higher probability of being switched ON. Therefore, modified thrust allocation approach would ensure both energy-efficient and reliable operation of the electrical propulsion system.
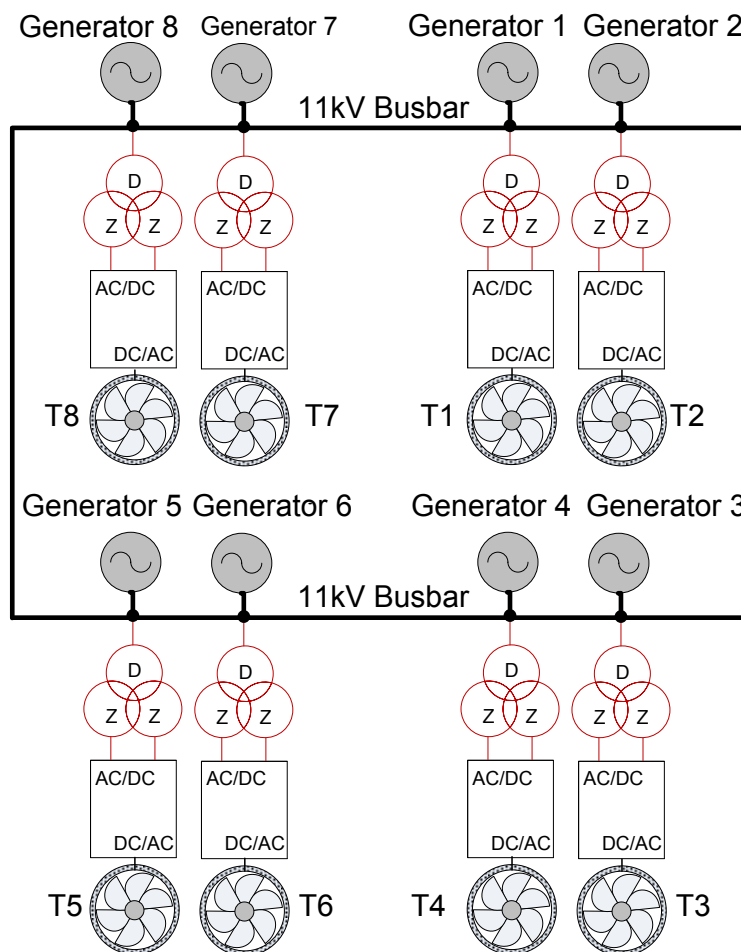
Fig. 7.1. SLD of the electrical propulsion system of the Keppel's B280

LIST OF PUBLICATIONS

Journal Publications

Published

1. **P. Yadav**, R. Kumar, S. K. Panda, and C. S. Chang, "An Intelligent Tuned Harmony Search algorithm for optimisation," *Information Sciences,* vol. 196, pp. 47-72, 2012.

2. **P. Yadav**, R. Kumar, S. K. Panda, and C. S. Chang, "An Improved Harmony Search algorithm for optimal scheduling of the diesel generators in oil rig platforms," *Energy Conversion and Management,* vol. 52, pp. 893-902, Feb 2011.

3. **P. Yadav**, R. Kumar, S. K. Panda, and C. S. Chang, "Energy-Efficient Thrust allocation for Semi-submersible Oil Rig Platforms using Improved Harmony Search Algorithm," *IEEE Transactions on Industrial Informatics,* vol. 8 (4), pp. 913 – 924, 2012.

Accepted

1. **P. Yadav**, R. Kumar, S. K. Panda, and C. S. Chang, "Optimal Thrust allocation for Semi-submersible Oil Rig Platforms using Improved Harmony Search Algorithm," accepted in *IEEE Transactions on Ocean Engineering.*

Submitted

1. **P. Yadav,** R. Kumar, S. K. Panda, and C. S. Chang, "Voltage Harmonic Distortion Compliant Energy-Efficient Thrust Allocation for Semi-Submersible Oil Rig Platforms using an Intelligent Tuned Harmony Search Algorithm" submitted to *IEEE Transactions on Power Delivery.*

Conference Publications

Accepted

1. **P. Yadav**, R. Kumar, S. K. Panda, and C. S. Chang, "Improved harmony search algorithm based optimal design of the brushless DC wheel motor," in *2010 IEEE International Conference on Sustainable Energy Technologies, ICSET 2010*, Kandy, Srilanka, 2010, pp. 1-5.

2. **P. Yadav**, R. Kumar, S. K. Panda, and C. S. Chang, "Optimization of the power generation scheduling in oil-rig platforms using genetic algorithm," Bari, 2010, pp. 2292-2297.

3. **P. Yadav**, C. W. Cheah, A. S. Allana, T. Lye, C. S. Chang, S. K. Panda, and S. K. Sahoo, "Investigation of current harmonics in thruster AC drives in oil-rig platforms," in *Eighth International Conference on Power Electronics and Drive Systems, PEDS 2009*, Taipei, Taiwan, R.O.C, 2009, pp. 920-925.

4. D. C. Hoang, **P. Yadav**, R. Kumar, and S. K. Panda, "A robust harmony search algorithm based clustering protocol for wireless sensor networks," in *2010 IEEE International Conference on Communications Workshops, ICC 2010* Cape Town, South Africa, 2010, pp. 1-5.

BIBLIOGRAPHY

[1] IMO, "Second IMO GHG Study 2009," 2009.

[2] P. CRIST, "Greenhouse Gas Emissions Reduction Potential from International Shipping," *Joint Transport Research Centre of the OECD and the International Transport Forum,* 2009.

[3] J. J. Corbett and a. J. Winebrake, "The Impacts of Globalisation on International Maritime Transport Activity," presented at the Global Forum on Transport and Environment in a Globalising World, Guadalajara, Mexico, 2008.

[4] K.-P. W. Lindegaard, "Acceleration Feedback in Dynamic Positioning," PhD Thesis, Department of Engineering Cybernetics, Norwegian University of Science and Technology (NTNU), 2003.

[5] J. F. Hansen, "Modelling and Control of Marine Power System," PhD Thesis, Department of Engineering Cybernetics, Norwegian University of Science and Technology (NTNU), 2000.

[6] A. K. Ådnanes, "Maritime electrical installations and diesel electric propulsion," ABB AS Marine 2003.

[7] P. Yadav, R. Kumar, S. K. Panda, and C. S. Chang, "An Improved Harmony Search algorithm for optimal scheduling of the diesel generators in oil rig platforms," *Energy Conversion and Management,* vol. 52, pp. 893-902, Feb 2011.

[8] T. Fossen, *Guidance and control of ocean vehicles*. England: John Willey & Sons Ltd, 1994.

[9] E. Ruth, Ø. N. Smogeli, T. Perez, and A. J. Sørensen, "Antispin thrust allocation for marine vessels," *IEEE Transactions on Control Systems Technology,* vol. 17, pp. 1257-1269, 2009.

[10] IMCA, "Guidelines for the design and operation of dynamically positioned vessels," The International Marine Contractors Association (IMCA) IMCA M 103, 1994.

[11] IMO, "Guidelines for vessels with dynamic positoning systems," International Maritime Organization, London, Technical Report MSC/Circ.645, 1994.

[12] E. Ruth, "Propulsion Control and Thrust Allocation on Marine Vessels," PhD thesis, Norwegian University of Science and Technology, Trondheim, Norway, 2008.

[13] T. Fossen and T. A. Johansen, " A survey of control allocation methods for ships and underwater vehicles," in *14th IEEE Mediterranean Conference on Control and Automation*, Ancona, Italy, 2006, pp. 1-6.

[14]   Keppel-FELS, "DP Analysis," 10632-4372/D018, 2007.

[15]   Keppel-FELS, "One-Line Diagram 11 kV Switchboard, Ultra Deepwater Development Semi-Submersible DSS21-DPS2," DEV.07.0003.003.890 ed, 2005.

[16]   Tri-Zen, "The Genesis of LNG Bunkers," Jan, 2012.

[17]   I. Sørfonn, "Power Management Control of Electrical Propulsion Systems," presented at the Dynamic Positioning Conference, Houston, 2007.

[18]   D. Radan, " Integrated Control of Marine Electrical Power Systems," PhD thesis, Dept. Engineering Cybernetics, NTNU, Trondheim, Norway, 2009.

[19]   F. Haglind, "A review on the use of gas and steam turbine combined cycles as prime movers for large ships. Part II: Previous work and implications," *Energy Conversion and Management,* vol. 49, pp. 3468-3475, 2008.

[20]   R. O'Rourke, "Navy Ship Propulsion Technologies: Options for Reducing Oil Use — Background for Congress," 2006.

[21]   A. J. Sørensen, "Structural issues in the design and operation of marine control systems," *Annual Reviews in Control,* vol. 29, pp. 125-149, 2005.

[22]   L. Zhang, "An energy-saving oil drilling rig for recovering potential energy and decreasing motor power," *Energy Conversion and Management,* vol. 52, pp. 359-365, 2011.

[23]   L. L. J. Mahon, *Diesel Generator Handbook*, 1992.

[24]   M. Kanogˇlu, S. Kazım Işık, and A. Abuşogˇlu, "Performance characteristics of a Diesel engine power plant," *Energy Conversion and Management,* vol. 46, pp. 1692-1702, 2005.

[25]   Wärtsilä-Italia, "Factory Test Report-Engine coupled with alternator," 2006.

[26]   D. Brown and L. Ekstrom, "Vessel thuster-thruster interactions during azimuthing operations," in *International Conference on Offshore Mechanics and Arctic Engineering (OMAE)*, Halkidiki, Greece, 2005, pp. 991-996.

[27]   M. Bodson, "Evaluation of optimization methods for control allocation," *Journal of Guidance, Control, and Dynamics,* vol. 25, pp. 703-711, 2002.

[28]   R. Jeyasenthil and J. Dasgupta, "Thrust allocation logic of dynamically positioned offshore vessel," *Ships and Offshore Structures,* vol. 5, pp. 243-251, 2010.

[29]   T. A. Johansen, T. I. Fossen, and S. P. Berge, "Constrained Nonlinear Control Allocation With Singularity Avoidance Using Sequential Quadratic Programming," *Ieee Transactions on*

Control Systems Technology, vol. 12, pp. 211-216, 2004.

[30]   C. C. Liang and W. H. Cheng, "The optimum control of thruster system for dynamically positioned vessels," *Ocean Engineering,* vol. 31, pp. 97-110, 2004.

[31]   K. P. Lindegaard and T. I. Fossen, "Fuel-efficient rudder and propeller control allocation for marine craft: Experiments with a model ship," *Ieee Transactions on Control Systems Technology,* vol. 11, pp. 850-862, 2003.

[32]   I. Lindfors, "Thrust allocation method for the dynamic positioning system," in *10th International Ship Control Systems Symposium*, Ottawa, Canada, 1993, pp. 93–106.

[33]   J. A. M. Petersen and M. Bodson, "Constrained quadratic programming techniques for control allocation," *Ieee Transactions on Control Systems Technology,* vol. 14, pp. 91-98, 2006.

[34]   E. Ruth, A. J. Sørensen, and T. Perez, "Thrust allocation with linear constrained quadratic cost function," in *Conference on Control Applications in Marine Systems*, Bol, Croatia, 2007.

[35]   P. Sinding and S. V. Anderson, "A force allocation strategy for dynamic positioning," in *Eight International Offshore and Polar Engineering Conference*, Montreal, Canada, 1998, pp. 346-353.

[36]   Y. Chen and J. Wang, "Fast and Global Optimal Energy-Efficient Control Allocation With Applications to Over-Actuated Electric Ground Vehicles," *Control Systems Technology, IEEE Transactions on,* vol. PP, pp. 1-10, 2011.

[37]   L. Joon-Woo, C. Byoung-Suk, and L. Ju-Jang, "Energy-Efficient Coverage of Wireless Sensor Networks Using Ant Colony Optimization With Three Types of Pheromones," *Industrial Informatics, IEEE Transactions on,* vol. 7, pp. 419-427, 2011.

[38]   M. Qiu, W. Gao, M. Chen, J. W. Niu, and L. Zhang, "Energy Efficient Security Algorithm for Power Grid Wide Area Monitoring System," *Smart Grid, IEEE Transactions on,* vol. PP, pp. 1-1, 2011.

[39]   C. Q. Xu, C. J. Xue, and E. H. M. Sha, "Energy-Efficient Joint Scheduling and Application-Specific Interconnection Design," *Very Large Scale Integration (VLSI) Systems, IEEE Transactions on,* vol. 19, pp. 1813-1822, 2011.

[40]   W. Zhong, R. Hui, W. Ho, and X. Liu, "Using Self-Driven AC-DC Synchronous Rectifier for Power Applications As A Direct Energy-Efficient Replacement for Traditional Diode Rectifier," *Industrial Electronics, IEEE Transactions on,* vol. PP, pp. 1-1, 2011.

[41] T. M. Chiwewe and G. P. Hancke, "A Distributed Topology Control Technique for Low Interference and Energy Efficiency in Wireless Sensor Networks," *Industrial Informatics, IEEE Transactions on,* vol. 8, pp. 11-19, 2012.

[42] K. Hahnsang and K. G. Shin, "DESA: Dependable, Efficient, Scalable Architecture for Management of Large-Scale Batteries," *Industrial Informatics, IEEE Transactions on,* vol. 8, pp. 406-417, 2012.

[43] W. M. Ng, D. Y. Lin, and S. Y. Hui, "Design of a Single Ultra-Low-Loss Magnetic Ballast for a Wide Range of T5 High-Efficiency Fluorescent Lamps," *Industrial Electronics, IEEE Transactions on,* vol. 59, pp. 1849-1858, 2012.

[44] T. Ericsen, N. Hingorani, and Y. Khersonsky, "Power electronics and future marine electrical systems," *Industry Applications, IEEE Transactions on,* vol. 42, pp. 155-163, 2006.

[45] T. Hoevenaars, I. Evans, and A. Lawson, "New marine harmonic standards," *Industry Applications Magazine, IEEE,* vol. 16, pp. 16-25, 2010.

[46] "ABS Guidance Notes on Control of Harmonics in Electrical Power Systems," American Bureau of Shipping 2006.

[47] J. P. Nelson, "A better understanding of harmonic distortion in the petrochemical industry," in *Petroleum and Chemical Industry Conference, 2002. Industry Applications Society 49th Annual*, 2002, pp. 237-250.

[48] H. M. Zubi, R. W. Dunn, F. V. P. Robinson, and M. H. El-werfelli, "Passive filter design using genetic algorthims for adjustable speed drives," in *Power and Energy Society General Meeting, 2010 IEEE*, 2010, pp. 1-7.

[49] M. S. M. Malinowski, "Sensorless control strategies for three-phase PWM rectifiers," *Ph.D. dissertation, Inst. Control Ind. Electron, Warsaw Univ. Technol.,* 2001.

[50] J. R. Rodriguez, J. Pontt, C. Silva, E. P. Wiechmann, P. W. Hammond, F. W. Santucci, R. Alvarez, R. Musalem, S. Kouro, and P. Lezana, "Large current rectifiers: State of the art and future trends," *Industrial Electronics, IEEE Transactions on,* vol. 52, pp. 738-746, 2005.

[51] D. A. Paice, *Power Electronic Converter Harmonics: Multipulse Methods for Clean Power*. New York: IEEE Press, 1996.

[52] A. Siebert, A. Troedson, and S. Ebner, "AC to DC power conversion now and in the future," *Industry Applications, IEEE Transactions on,* vol. 38, pp. 934-940, 2002.

[53] W. Lixiang, N. N. Guskov, R. A. Lukaszewski, and G. L. Skibinski, "Mitigation of Current Harmonics for Multipulse Diode Front-End Rectifier Systems," *Industry Applications, IEEE Transactions on,* vol. 43, pp. 787-797, 2007.

[54] P. Yadav, R. Kumar, S. K. Panda, and C. S. Chang, "Energy-Efficient Thrust allocation for Semi-submersible Oil Rig Platforms using Improved Harmony Search Algorithm," *IEEE Transactions on Industrial Informatics* 2012.

[55] P. Yadav, C. W. Cheah, A. S. Allana, T. Lye, C. S. Chang, S. K. Panda, and S. K. Sahoo, "Investigation of current harmonics in thruster AC drives in oil-rig platforms," in *Eighth International Conference on Power Electronics and Drive Systems, PEDS 2009*, Taipei, Taiwan, R.O.C, 2009, pp. 920-925.

[56] C. S. Chin, M. W. S. Lau, E. Low, and G. G. L. Seet, "Design of thrusters configuration and thrust allocation control for a remotely operated vehicle," 2006.

[57] M. G. Feemster and J. M. Esposito, "Comprehensive framework for tracking control and thrust allocation for a highly overactuated autonomous surface vessel," *Journal of Field Robotics,* vol. 28, pp. 80-100, 2011.

[58] J. A. Leavitt, "Optimal thrust allocation in a dynamic positioning system," *Transactions - Society of Naval Architects and Marine Engineers,* vol. 116, pp. 153-165, 2009.

[59] J. Spjøtvold and T. A. Johansen, "Fault tolerant control allocation for a thruster-controlled floating platform using parametric programming," in *Joint IEEE Conference on Decision and Control and Chinese Control Conference*, Shanghai, P.R. China, 2009, pp. 3311-3317.

[60] C. D. Wit, "Optimal Thrust Allocation Methodsfor Dynamic Positioning of Ships," Master of Science, Delft University of Technology, Delft, Netherlands, 2009.

[61] D. W. Zhao, F. G. Ding, J. F. Tan, Y. Q. Liu, and X. Q. Bian, "Optimal thrust allocation based GA for dynamic positioning ship," 2010, pp. 1254-1258.

[62] S. S. Rao, *Engineering Optimization: Theory and Practice*, Fourth ed. Hoboken, NJ, USA: John Wiley & Sons, Inc., 2009.

[63] E.-G. Talbi, *Metaheuristics: From Design to Implementation*. Hoboken, NJ, USA: John Wiley & Sons, Inc., 2009.

[64] K. Tang and X. Yao, "Special issue on "nature inspired problem-solving"," *Information Sciences,* vol. 178, pp. 2983-2984, Aug 1 2008.

[65]   X.-S. Yang, *Nature-inspired metaheuristic algorithms*. Frome, U.K.: Luniver Press, 2008.

[66]   Z. W. Geem, J. H. Kim, and G. V. Loganathan, "A new heuristic optimization algorithm: Harmony search," *Simulation,* vol. 76, pp. 60-68, Feb 2001.

[67]   A. Askarzadeh and A. Rezazadeh, "A grouping-based global harmony search algorithm for modeling of proton exchange membrane fuel cell," *International Journal of Hydrogen Energy,* vol. 36, pp. 5047-5053, Apr 2011.

[68]   H. Ceylan, S. HaIdenbilen, and O. Baskan, "Transport energy modeling with meta-heuristic harmony search algorithm, an application to Turkey," *Energy Policy,* vol. 36, pp. 2527-2535, Jul 2008.

[69]   Y. M. Cheng, L. Li, and S. S. Fang, "Improved Harmony Search Methods to Replace Variational Principle in Geotechnical Problems," *Journal of Mechanics,* vol. 27, pp. 107-119, Mar 2011.

[70]   Y. M. Cheng, L. Li, T. Lansivaara, S. C. Chi, and Y. J. Sun, "An improved harmony search minimization algorithm using different slip surface generation methods for slope stability analysis," *Engineering Optimization,* vol. 40, pp. 95-115, Feb 2008.

[71]   L. D. Coelho and D. L. D. Bernert, "An improved harmony search algorithm for synchronization of discrete-time chaotic systems," *Chaos Solitons & Fractals,* vol. 41, pp. 2526-2532, Sep 15 2009.

[72]   L. D. Coelho and V. C. Mariani, "An improved harmony search algorithm for power economic load dispatch," *Energy Conversion and Management,* vol. 50, pp. 2522-2526, Oct 2009.

[73]   K. Das Sharma, A. Chatterjee, and A. Rakshit, "Design of a Hybrid Stable Adaptive Fuzzy Controller Employing Lyapunov Theory and Harmony Search Algorithm," *IEEE Transactions on Control Systems Technology,* vol. 18, pp. 1440-1447, Nov 2010.

[74]   S. O. Degertekin and M. S. Hayalioglu, "Harmony search algorithm for minimum cost design of steel frames with semi-rigid connections and column bases," *Structural and Multidisciplinary Optimization,* vol. 42, pp. 755-768, Nov 2010.

[75]   F. Erdal, E. Dogan, and M. P. Saka, "Optimum design of cellular beams using harmony search and particle swarm optimizers," *Journal of Constructional Steel Research,* vol. 67, pp. 237-247, Feb 2011.

[76]   R. Forsati, M. Mahdavi, M. Kangavari, and B. Safarkhani, "Web page clustering using

Harmony Search optimization," in *Canadian Conference on Electrical and Computer Engineering, CCECE 2008*, Niagara Falls, ON, 2008, pp. 1601-1604.

[77]   J. Fourie, S. Mills, and R. Green, "Harmony filter: A robust visual tracking system using the improved harmony search algorithm," *Image and Vision Computing,* vol. 28, pp. 1702-1716, Dec 2010.

[78]   S. Ghosh, D. Kundu, K. Suresh, S. Das, and A. Abraham, "Design of Optimal Digital IIR Fillers by Using a Bandwidth Adaptive Harmony Search Algorithm," in *2009 World Congress on Nature & Biologically Inspired Computing (Nabic 2009)*, Coimbatore, India, 2009, pp. 480-485.

[79]   D. C. Hoang, P. Yadav, R. Kumar, and S. K. Panda, "A robust harmony search algorithm based clustering protocol for wireless sensor networks," in *2010 IEEE International Conference on Communications Workshops, ICC 2010* Cape Town, South Africa, 2010, pp. 1-5.

[80]   M. Jaberipour and E. Khorram, "Solving the sum-of-ratios problems by a harmony search algorithm," *Journal of Computational and Applied Mathematics,* vol. 234, pp. 733-742, Jun 1 2010.

[81]   A. Kattan, R. Abdullah, and R. A. Salam, "Harmony Search Based Supervised Training of Artificial Neural Networks," in *UKSim/AMSS 1st International Conference on Intelligent Systems, Modelling and Simulation, ISMS 2010*, Liverpool, 2010, pp. 105-110.

[82]   A. Kaveh and A. S. M. Abadi, "Harmony search based algorithms for the optimum cost design of reinforced concrete cantilever retaining walls," *International Journal of Civil Engineering,* vol. 9, pp. 1-8, Mar 2011.

[83]   A. H. Khazali and M. Kalantar, "Optimal reactive power dispatch based on harmony search algorithm," *International Journal of Electrical Power & Energy Systems,* vol. 33, pp. 684-692, Mar 2011.

[84]   A. H. Khazali, A. Parizad, and M. Kalantar, "Optimal Voltage/Reactive Control by an Improve Harmony Search Algorithm," *International Review of Electrical Engineering-Iree,* vol. 5, pp. 217-224, Jan-Feb 2010.

[85]   E. Khorram and M. Jaberipour, "Harmony search algorithm for solving combined heat and power economic dispatch problems," *Energy Conversion and Management,* vol. 52, pp. 1550-

1554, Feb 2011.

[86] M. Mahdavi and H. Abolhassani, "Harmony K-means algorithm for document clustering," *Data Mining and Knowledge Discovery,* vol. 18, pp. 370-391, Jun 2009.

[87] D. Mora-Melia, P. L. Iglesias-Rey, G. Lopez-Patino, and V. S. Fuertes-Miquel, "Application of the harmony search algorithm to water distribution networks design," *Environmental Hydraulics: Theoretical, Experimental and Computational Solutions,* pp. 265-271, 2010.

[88] S. Mun and Z. W. Geem, "Determination of viscoelastic and damage properties of hot mix asphalt concrete using a harmony search algorithm," *Mechanics of Materials,* vol. 41, pp. 339-353, Mar 2009.

[89] S. Mun and Z. W. Geem, "Determination of individual sound power levels of noise sources using a harmony search algorithm," *International Journal of Industrial Ergonomics,* vol. 39, pp. 366-370, Mar 2009.

[90] N. Nahas and D. Thien-My, "Harmony search algorithm: application to the redundancy optimization problem," *Engineering Optimization,* vol. 42, pp. 845-861, 2010.

[91] Q. K. Pan, P. N. Suganthan, J. J. Liang, and M. F. Tasgetiren, "A local-best harmony search algorithm with dynamic subpopulations," *Engineering Optimization,* vol. 42, pp. 101-117, 2010.

[92] Q. K. Pan, P. N. Suganthan, J. J. Liang, and M. F. Tasgetiren, "A local-best harmony search algorithm with dynamic sub-harmony memories for lot-streaming flow shop scheduling problem," *Expert Systems with Applications,* vol. 38, pp. 3252-3259, Apr 2011.

[93] Q. K. Pan, P. N. Suganthan, and M. F. Tasgetiren, "A Harmony Search Algorithm with Ensemble of Parameter Sets," in *2009 IEEE Congress on Evolutionary Computation, CEC 2009,* Trondheim, Norway, 2009, pp. 1815-1820.

[94] Q. K. Pan, P. N. Suganthan, M. F. Tasgetiren, and J. J. Liang, "A self-adaptive global best harmony search algorithm for continuous optimization problems," *Applied Mathematics and Computation,* vol. 216, pp. 830-848, Apr 1 2010.

[95] V. R. Pandi and B. K. Panigrahi, "Dynamic economic load dispatch using hybrid swarm intelligence based harmony search algorithm," *Expert Systems with Applications,* vol. 38, pp. 8509-8514, Jul 2011.

[96] B. K. Panigrahi, V. R. Pandi, S. Das, and A. Abraham, "A Bandwidth-Adaptive Harmony Search Algorithm to Solve Optimal power Flow Problems with Non-smooth Cost Functions,"

in *Recent Advances in Harmony Search Algorithm*, Z. W. Geem, Ed., ed Germany: Studies in Computational Intelligence, 2010.

[97]   A. Rami, A. Zeblah, and Y. Massim, "Cost optimization of power system structure subject to reliability constraints using harmony search," *Przeglad Elektrotechniczny,* vol. 85, pp. 169-172, 2009.

[98]   G. G. Roy, B. K. Panigrahi, P. Chakraborty, and M. K. Mallick, "On Optimal Feature Selection Using Modified Harmony Search for Power Quality Disturbance Classification," in *2009 World Congress on Nature & Biologically Inspired Computing (Nabic 2009)*, Coimbatore, India, 2009, pp. 1354-1359.

[99]   M. P. Saka, "Optimum design of steel sway frames to BS5950 using harmony search algorithm," *Journal of Constructional Steel Research,* vol. 65, pp. 36-43, Jan 2009.

[100]   V. Togan, A. T. Daloglu, and H. Karadeniz, "Optimization of trusses under uncertainties with harmony search," *Structural Engineering and Mechanics,* vol. 37, pp. 543-560, Mar 10 2011.

[101]   A. Verma, B. K. Panigrahi, and P. R. Bijwe, "Harmony search algorithm for transmission network expansion planning," *IET Generation Transmission & Distribution,* vol. 4, pp. 663-673, Jun 2010.

[102]   L. Wang, Q. K. Pan, and M. F. Tasgetiren, "Minimizing the total flow time in a flow shop with blocking by using hybrid harmony search algorithms," *Expert Systems with Applications,* vol. 37, pp. 7929-7936, Dec 2010.

[103]   L. Wei, W. Guo, F. Wen, G. Ledwich, Z. Liao, and J. Xin, "Waveform matching approach for fault diagnosis of a high-voltage transmission line employing harmony search algorithm," *Iet Generation Transmission & Distribution,* vol. 4, pp. 801-809, Jul 2010.

[104]   P. Yadav, R. Kumar, S. K. Panda, and C. S. Chang, "Improved harmony search algorithm based optimal design of the brushless DC wheel motor," in *2010 IEEE International Conference on Sustainable Energy Technologies, ICSET 2010*, Kandy, Srilanka, 2010, pp. 1-5.

[105]   O. Zarei, M. Fesanghary, B. Farshi, R. J. Saffar, and M. R. Razfar, "Optimization of multi-pass face-milling via harmony search algorithm," *Journal of Materials Processing Technology,* vol. 209, pp. 2386-2392, Mar 1 2009.

[106]   D. X. Zou, L. Q. Gao, S. Li, and J. H. Wu, "Solving 0-1 knapsack problem by a novel global harmony search algorithm," *Applied Soft Computing,* vol. 11, pp. 1556-1564, Mar 2011.

[107]   D. X. Zou, L. Q. Gao, J. H. Wu, S. Li, and Y. Li, "A novel global harmony search algorithm for reliability problems," *Computers & Industrial Engineering,* vol. 58, pp. 307-316, Mar 2010.

[108]   O. M. Alia and R. Mandava, "The variants of the harmony search algorithm: an overview," *Artificial Intelligence Review,* vol. 36, pp. 49-68, Jun 2011.

[109]   Z. W. Geem, *Harmony search algorithms for structural design optimization* Berlin Springer : Heidelberg, 2009.

[110]   Y. Wang, B. Li, T. Weise, J. Wang, B. Yuan, and Q. Tian, "Self-adaptive learning based particle swarm optimization," *Information Sciences,* vol. In Press, Corrected Proof.

[111]   Z. W. Geem, *Recent advances in harmony search algorithm* Berlin Springer-Verlag, 2010.

[112]   M. Mahdavi, M. Fesanghary, and E. Damangir, "An improved harmony search algorithm for solving optimization problems," *Applied Mathematics and Computation,* vol. 188, pp. 1567-1579, May 15 2007.

[113]   R. Eberhart and J. Kennedy, "A new optimizer using particle swarm theory," in *Proceedings of the Sixth International Symposium on Micro Machine and Human Science, MHS '95*, Nagoya, Japan, 1995, pp. 39-43.

[114]   M. G. H. Omran and M. Mahdavi, "Global-best harmony search," *Applied Mathematics and Computation,* vol. 198, pp. 643-656, May 1 2008.

[115]   C. M. Wang and Y. F. Huang, "Self-adaptive harmony search algorithm for optimization," *Expert Systems with Applications,* vol. 37, pp. 2826-2837, Apr 2010.

[116]   S. Das, A. Mukhopadhyay, A. Roy, A. Abraham, and B. K. Panigrahi, "Exploratory Power of the Harmony Search Algorithm: Analysis and Improvements for Global Numerical Optimization," *Ieee Transactions on Systems Man and Cybernetics Part B-Cybernetics,* vol. 41, pp. 89-106, Feb 2011.

[117]   R. Mallipeddi, S. Mallipeddi, and P. N. Suganthan, "Ensemble strategies with adaptive evolutionary programming," *Information Sciences,* vol. 180, pp. 1571-1581, May 1 2010.

[118]   Y. Shi, H. Liu, L. Gao, and G. Zhang, "Cellular particle swarm optimization," *Information Sciences,* vol. In Press, Corrected Proof.

[119]   F. van den Bergh and A. P. Engelbrecht, "A Cooperative approach to particle swarm optimization," *IEEE Transactions on Evolutionary Computation,* vol. 8, pp. 225-239, 2004.

[120]   A. M. Potter and K. A. D. Jong, "A cooperative coevolutionary approach to function

optimization," in *Proceeding in the Third International Conference on Parallel Problem Solving from Nature*, 1994, pp. 249–257.

[121] J. J. Liang and P. N. Suganthan, "Dynamic multi-swarm particle swarm optimizer," in *2005 IEEE Swarm Intelligence Symposium, SIS 2005*, Pasadena, CA, 2005, pp. 127-132.

[122] J. J. Liang and P. N. Suganthan, "Dynamic multi-swarm particle swarm optimizer with local search," in *2005 IEEE Congress on Evolutionary Computation, IEEE CEC 2005*, Edinburgh, Scotland, 2005, pp. 522-528.

[123] S. Z. Zhao, P. N. Suganthan, Q. K. Pan, and M. Fatih Tasgetiren, "Dynamic multi-swarm particle swarm optimizer with harmony search," *Expert Systems with Applications,* vol. 38, pp. 3735-3742, 2011.

[124] S. Z. Zhao, J. J. Liang, P. N. Suganthan, and M. F. Tasgetiren, "Dynamic multi-swarm particle swarm optimizer with local search for large scale global optimization," in *2008 IEEE Congress on Evolutionary Computation, CEC 2008*, Hong Kong, 2008, pp. 3845-3852.

[125] X. Yao, Y. Liu, and G. M. Lin, "Evolutionary programming made faster," *Ieee Transactions on Evolutionary Computation,* vol. 3, pp. 82-102, Jul 1999.

[126] P. N. Suganthan, N. Hansen, J. J. Liang, K. Deb, Y. P. Chen, A. Auger, and S. Tiwari, "Problem definitions and evaluation criteria for the CEC 2005 Special Session on Real Parameter Optimization," 2005.

[127] S. Garcia, D. Molina, M. Lozano, and F. Herrera, "A study on the use of non-parametric tests for analyzing the evolutionary algorithms' behaviour: a case study on the CEC'2005 Special Session on Real Parameter Optimization," *Journal of Heuristics,* vol. 15, pp. 617-644, Dec 2009.

[128] F. Wilcoxon, "Individual Comparisons by Ranking Methods," *Biometrics Bulletin,* vol. 1, pp. 80-83, 1945.

[129] A. Quarteroni, R. Sacco, and F. Saleri, *Numerial Mathematics*. NewYork: Springer, 2006.

[130] D. Radan, T. A. Johansen, A. J. Sørensen, and A. K. Ådnanes, "Optimization of Load Dependent Start Tables in Marine Power Management Systems with Blackout Prevention," *WSEAS Transactions on Circuits and Systems,* vol. 4, pp. 1861-1867, 2005.

[131] K. T. Chau and Y. S. Wong, "Overview of power management in hybrid electric vehicles," *Energy Conversion and Management,* vol. 43, pp. 1953-1968, 2002.

[132]   L. d. S. Coelho and V. C. Mariani, "An improved harmony search algorithm for power economic load dispatch," *Energy Conversion and Management,* vol. 50, pp. 2522-2526, 2009.

[133]   C. F. Matt, L. S. R. Vieira, G. F. W. Soares, and L. P. T. d. Faria, "Optimization of the Operation of Isolated Industrial Diesel Stations," presented at the 6th World Congress on Structural and Multidisciplinary Optimization, Rio de Janeiro, Brazil, 2005.

[134]   Wei Wu, K. Davey, and A. Arapostathis, "Dynamic Optimal Generation Scheduling of Shipboard Power Systems," presented at the ESRDC controls workshop, Purdue University, West Lafayette, 2006.

[135]   P. Yadav, R. Kumar, S. K. Panda, and C. S. Chang, "Optimization of the power generation scheduling in oil-rig platforms using genetic algorithm," Bari, 2010, pp. 2292-2297.

[136]   K. D. Jong, *Evolutionary computation: a unified approach*. Cambridge: MIT Press, 2006.

[137]   Siemens, "String Test Report, Thruster Drive System " 440-1018.120-R-005, 2006.

[138]   O. J. Sørdalen, "Optimal thrust allocation for marine vessels," *Control Engineering Practice,* vol. 5, pp. 1223-1231, 1997.

[139]   S. Boyd and L. Vandenberghe, "Convex Optimization," *Cambridge University Press,* 2004.

[140]   K. Deb, "An efficient constraint handling method for genetic algorithms," *Computer Methods in Applied Mechanics and Engineering,* vol. 186, pp. 311-338, 2000.

[141]   R. Mallipeddi and P. N. Suganthan, "Ensemble of Constraint Handling Techniques," *Evolutionary Computation, IEEE Transactions on,* vol. 14, pp. 561-579, 2010.

[142]   Z. Michalewicz, "A Survey of Constraint Handling Techniques in Evolutionary Computation Methods," in *Proceedings of the 4th Annual Conference on Evolutionary Programming*, Cambridge, Massachusetts, 1995, pp. 135-155.

[143]   Keppel-FELS, "General Arrangement View of Pontoons, Ultra Deepwater Development Semi-Submersible DSS21-DPS2," DEL.02.1001.004.101 ed, 2005.

[144]   Siemens, "Test Reports and Certificates, Thruster Transformers," 440-1067-140-R003, 2006.

[145]   B. K. Bose, *Power Electronics and Variable Frequency Drives: Technology and Applications*: Wiley-IEEE Press, 1996.

[146]   A. Muñoz-García, T. A. Lipo, and D. W. Novotny, "A New induction motor v/f control method capable of high-performance regulation at low speeds," *IEEE Transactions on Industry Applications,* vol. 34, pp. 813-821, 1998.

[147]   E. A. H. Abdelkarim, "Control and Measuring Method for Three Phase Induction Motor with Improved Efficiency," Ph.D, Department of Power Electronics and Control of Drives, Darmstadt University of Technology, Darmstadt, 2011.

[148]   I. Kioskeridis and N. Margaris, "Loss minimization in induction motor adjustable-speed drives," *Ieee Transactions on Industrial Electronics,* vol. 43, pp. 226-231, 1996.

[149]   "Rotating electrical machines – Part 2-1: Standard methods for determining losses and efficiency from tests (excluding machines for traction vehicles)," ed: IEC 60034-2-1, 2007.

[150]   M. Hiller, R. Sommer, and M. Beuermann, "Converter topologies and power semiconductors for industrial medium voltage converters," in *Conference Record - IAS Annual Meeting (IEEE Industry Applications Society)*, 2008.

[151]   S. S. Fazel, "Investigation and comparison of multi-level converters for medium voltage applications," Ph.D. dissertation, Technische Universität Berlin, Berlin, Germany, 2007.

[152]   F. Blaabjerg, J. K. Pedersen, S. Sigurjonsson, and A. Elkjaer, "Extended model of power losses in hard-switched IGBT-inverters," 1996, pp. 1454-1463.

[153]   S. Dieckerhoff, S. Bernet, and D. Krug, "Power loss-oriented evaluation of high voltage IGBTs and multilevel converters in transformerless traction applications," *IEEE Transactions on Power Electronics,* vol. 20, pp. 1328-1336, 2005.

[154]   T. Matsuo, S. Bernet, R. S. Colby, and T. A. Lipo, "Modeling and simulation of matrix converter/induction motor drive," *Mathematics and Computers in Simulation,* vol. 46, pp. 175-195, 1998.

[155]   Eupec.   Infineon   IGBT/Diode   module   data   sheets   [Online].   Available: www.infineon.com/eupec.

[156]   B. Wu, *High-Power Converters and ac Drives*. Hoboken, NJ, USA: John Wiley & Sons, Inc., 2005.